CHARLES UNIVERSITY, PRAGUE

2ND MEDICAL FACULTY

and

ACADEMY OF SCIENCES OF THE CZECH REPUBLIC

INSTITUTE OF EXPERIMENTAL MEDICINE

MUDr. Helena Pivoňková (born Neprašová)

Membrane Properties of Glial Cells after Ischemia *in vivo*

PhD thesis

Prague 2011

Acknowledgement

I would like to express my gratitude to my supervisor, Dr. Miroslava Anderova, for her advice and patient guidance from the very early beginning of my research experience. I would also like to thank my colleagues and the technicians in the laboratory who participated in these experiments.

I am particularly grateful to my husband Petr Pivonka for his endless support during the whole time of my doctoral studies.

This work was performed in the Laboratory of Neurobiology, Department of Cellular Neurophysiology, Institute of Experimental Medicine, v.v.i., Academy of Sciences of the Czech Republic, under the supervision of Dr. Miroslava Anderova.

This work is based on the results published in the following papers, which are attached at the end of this thesis:

1. **Pivonkova H.**, Benesova J., Butenko O., Chvatal A. and Anderova M. (2010) Impact of Global Cerebral Ischemia on K^+ Channel Expression and Membrane Properties of Glial Cells in the Rat Hippocampus. *Neurochemistry International. Dec;57(7):783-94*, IF 3.54
   (Contributions: experiment design – HP, MA; surgery – HP, JB, OB; patch-clamp – HP, OB, MA; western blot – JB; immunohistochemistry – HP; cell counts – MA, AC; writing – HP, MA)
2. **Neprasova H.**, Anderova M., Petrik D., Vargova L., Kubinova S., Chvatal A. and Sykova E. (2007) High extracellular K^+ evokes changes in voltage-dependent K^+ and Na^+ currents and volume regulation in astrocytes. *Pflugers Archiv – European Journal of Physiology. Mar;453(6):839-49*, IF 3.84
   (Contributions: experiment design – MA, HP, DP, ES; spinal cord isolation – HP, DP, MA, LV, SK; patch-clamp – HP, DP, MA; pH_e and $[K^+]_e$ measurement – LV, SK, ES; confocal microscopy and 3D volume measurements – HP, MA, AC; immunohistochemistry – MA, HP; writing – HP, MA)
3. Anderova M., Vorisek I., **Pivonkova H.**, Benesova J.,Vargova L., Cicanic M., Chvatal A. and Sykova E. (2011) Cell death/proliferation and alterations in glial morphology contribute to changes in diffusivity in the rat hippocampus after hypoxia-ischemia. *Journal of Cerebral Blood Flow and Metabolism. Mar;31(3):894-907*, IF 5.46
   (Contributions: experiment design – MA; surgery – HP, JB, IV; immunohistochemistry – MA, HP; confocal microscopy and 3D volume measurements – MA, HP, AC; cell counting – MA; diffusion measurements – LV, MC; MRI – IV, ES; writing – MA, IV, LV, HP)

Other impacted publications of the author:

1. Chvatal A., Anderova M., **Neprasova H.**, Prajerova I., Benesova J., Butenko O., Verkhratsky A (2008) Pathological Potential of Astroglia. *Physiol Res. 57 Suppl 3:S101-S110*, IF 1.65
2. Chvatal A., Anderova M., Hock M., Prajerova I., **Neprasova H.**, Chvatal V., Kirchhoff F. and Sykova E. (2007) Three-Dimensional Confocal Morphometry Reveals Structural Changes in Astrocyte Morphology *In Situ*. *J Neurosci Res. Feb 1;85(2):260-71*, IF 3.27
3. Anderova M., Kubinova S., Jelitai M., **Neprasova H.**, Glogarova K., Prajerova I., Urdzikova L., Chvatal A. and Sykova E. (2006) Transplantation of embryonic neuroectodermal progenitor cells into the site of a photochemical lesion: immunohistochemical and electrophysiological analysis. *J Neurobiol. Sep 1;66(10):1084-100*, IF 4.2
4. Anderova M., Antonova T., Petrik D., **Neprasova H.**, Chvatal A. and Sykova E. (2004) Voltage-dependent potassium currents in hypertrophied rat astrocytes after a cortical stab wound. *Glia. 48:311-326*, IF 4.7

Table of Contents

Abbreviations:

AA	arachidonic acid
aCSF	artificial cerebrospinal fluid
aCSF50	isotonic aCSF containing 50 mM K^+
AMPA	α-amino-3-hydroxyl-5-methyl-4-isoxazole-propionate
APC	adenomatous polyposis coli
ATP	adenosine-5'-triphosphate
CD	current density
C_M	membrane capacitance
CNS	central nervous system
Cx	connexin
DAPI	4',6-diamidino-2-phenylindole
DG	dentate gyrus
DTT	dithiothreitol
EGTA	ethylene glycol bis(2-aminoethylether)-N,N,N′N′-tetraacetic acid
E_K	K^+ equilibrium potential
FJB	Fluoro-Jade B
GABA	γ-aminobutyric acid
GCI	global cerebral ischemia
GFAP	glial fibrillary acidic protein
(E)GFP	(enhanced) green fluorescent protein
GluR	glutamate receptor
GluT	glutamate transporter
ΔK^+	K^+ accumulation in the vicinity of the cell membrane
$[K^+]_e$	extracellular K^+ concentration
$[K^+_m]_e$	extracellular K^+ concentration prior to a depolarizing prepulse
$[K^+_{rev}]_e$	extracellular K^+ concentration after a depolarizing prepulse
I_{Na}	fast activating Na^+ current
K_{2P}	two-pore domain K^+ channels
K_A	A-type K^+ current
K_{DR}	delayed outwardly rectifying K^+ current
K_{IR}	inwardly rectifying K^+ current
Kir	inwardly rectifying K^+ channels

Kv	voltage-gated K^+ channels
ISMs	ion-selective microelectrodes
MCAO	middle cerebral artery occlusion
NG2	neuronal-glial antigen 2
NGS	normal goat serum
NSCs	neural stem cells
NeuN	neuron-specific nuclear antigen
OGD	oxygen-glucose deprivation
OPCs	oligodendrocyte precursor cells
PARP	poly(ADP-ribose) polymerase
PB	phosphate buffer
PBS	phosphate buffered saline
PCNA	proliferating cell nuclear antigen
PDGFαR	platelet-derived growth factor alpha-receptor
PFA	paraformaldehyde
pH_e	extracellular pH
PTB	pentobarbital
PtdIns(4,5)P_2	phosphatidylinositol-4,5-bisphosphate
R_M	membrane resistance
RMP	resting membrane potential
RT	room temperature
RVD	regulatory volume decrease
SDS	sodium dodecyl sulphate
SGZ	subgranular zone
SVZ	subventricular zone
TREK	TWIK-related K^+ channel
TTX	tetrodotoxin
TUNEL	terminal deoxynucleotidyl transferase dUTP nick end labeling
TWIK	two-pore domain weak inwardly rectifying K^+ channel
VRACs	volume-regulated anion channels
V_{rev}	reversal potential
$V_{rev\ tail}$	reversal potential of the tail current

1. INTRODUCTION

Stroke is the third leading cause of death and a leading cause of adult disability in developed countries. In the United States, about 800,000 people suffer a new or recurrent stroke each year, from which about 150,000 people die and the rest require permanent or transient care (www.stroke.org). In the Czech Republic, about 30,000 strokes occur each year. The mortality and morbidity of stroke in the Czech Republic is one of the highest in Europe. This also makes stroke one of the most costly diseases.

After many years of effort, treatment possibilities for stroke still remain very poor. Within several hours after the onset of stroke, an intravenous application of recombinant tissue plasminogen activator (rt-PA) has beneficial effects, and this treatment has become the only causal standard therapy. Other therapeutic approaches are only symptomatic, such as anticoagulant therapy, blood pressure correction or early extensive rehabilitation (Adams et al., 2005). Calcium channel antagonists, free radical scavengers, glutamate receptor antagonists and many other promising drugs have been used in clinical trials without any amelioration of the neurological outcome of the patients. Interestingly, these compounds show beneficial effects in experimental research. This fact represents the major discrepancy in stroke research (Dirnagl, 2006). Therefore, to establish new therapeutic strategies, it is essential to understand in more detail the mechanisms involved in neuronal injury and repair during ischemia as well as during the early and late stages of reperfusion.

Ischemic injury of the central nervous system (CNS) affects both neurons and glial cells, which comprise astrocytes, oligodendrocytes, microglia and NG2 glia. Glial cells represent an integral part of the CNS cellular environment and perform a large number of important functions in the nervous tissue under physiological as well as pathological conditions. However, experimental therapeutic strategies after ischemia have been focused mainly on neurons, probably due to the relative delay of glial cell research compared to research on neurons. In the last two decades, much work has been done to show that glial cells and especially astrocytes or NG2 glia, thanks to their specific functional properties, might have beneficial effects after CNS injury. Nevertheless, the mechanisms involved in glial supportive functions are still not well understood.

In my PhD thesis, I aimed to characterize the membrane properties of astrocytes and NG2 glia in the acute and chronic phases of ischemic injury of the CNS with a

focus on the expression and activity of K^+ ion channels in these two cell types. In astrocytes, K^+ ion channels play an essential role in the maintenance of K^+ ion and glutamate homeostasis, which are impaired after CNS ischemia. In NG2 glia, K^+ ion channels are involved in cell cycle regulation and thus in the proliferative activity of these cells. Since K^+ ion channels in both astrocytes and NG2 glia profoundly influence cellular functions, their activity might consequently have a large impact on tissue survival or regeneration after ischemia.

1.1 ASTROCYTES

1.1.1 Basic characteristics of astrocytes

The up-to-date view of astrocytes as a diverse population of glial cells with numerous functions is based on increasing knowledge about their functional properties, studied with advanced morphological, electrophysiological, molecular and genetic tools (Kimelberg, 2007; Wang and Bordey, 2008). Two types of astrocytes were classically described within the CNS – protoplasmic astrocytes in the grey matter and fibrous astrocytes in the white matter. Fibrous astrocytes have fewer and longer processes compared to protoplasmic astrocytes, and they project to the pial surface and form the glia limitans. Similarly, in astrocyte primary cultures we also recognize two types of astroglial cells – type I and type II – although their relevance to astrocyte subtypes *in vivo* is not clear. Functionally specialized cells with astrocytic properties can be found in most CNS regions: Bergmann glia in the cerebellum, Muller glial cells in the retina, tanycytes in the periventricular organs, pituicytes in the neuro-hypophysis and ependymocytes lining the ventricles (Kettenmann and Ransom, 2005). Recently, neural stem cells in the two neurogenic regions of adult brain, the subventricular zone (SVZ) and the subgranular zone (SGZ) of the dentate gyrus (DG) in the hippocampus, have also been characterized as cells with astrocytic properties (Ganat et al., 2006).

In the human brain, glial cells, and among them especially astrocytes, comprise the largest cellular population. The glia-neuron ratio increases during phylogenesis, being about 0.3 in rodents and 1.65 in humans (Verkhratsky and Butt, 2007). Within the primate species, the glia-neuron ratio in the cerebral cortex is highest in Homo sapiens (1.65 versus, e.g., Pan troglodytes 1.20 or Macaca maura 0.84; layer II/III, Area 9L)

(Sherwood et al., 2006). Moreover, the morphology of protoplasmic astrocytes undergoes large alterations during phylogenesis. Human astrocytes comprise more elaborated processes, which connect to many more neuronal synapses compared to astrocytes in phylogenetically lower species (Oberheim et al., 2006). The human neocortex harbors several morphologically and anatomically defined subtypes of astrocytes not present in other species, such as interlaminar astrocytes (Oberheim et al., 2009). These findings suggest an important role of astrocytes for cognitive functions in phylogenetically higher species, above all in humans.

Astrocytes are commonly identified by the expression of an intermediate filament, glial fibrillary acidic protein (GFAP) (Eng et al., 2000), which is widely used as their specific antigenic marker. However, the immunohistochemical staining of astrocytes for GFAP may lead to confusing results because not all astrocytes appear GFAP-positive (Walz, 2000; Kimelberg, 2004). Other proteins used as specific markers for astrocytes include S100β calcium-binding protein and glutamine synthetase. Astrocytes also express the glutamate transporters EAAT1 (Excitatory Amino Acid Transporter 1, also called GLAST for GLutamate ASpartate Transporter) and EAAT2 (GLT-1), both of which show higher specificity for this cell type than other astrocytic markers. Using a transcriptome database approach in FACS-sorted S100β-green fluorescent protein (GFP)-expressing astrocytes, Cahoy et al. (2008) identified a new potential astrocyte-specific marker, aldehyde dehydrogenase 1 family, member L1 (A1dhL1).

Astrocytes are directly connected via gap junctions into a large functional syncytium. Gap junctions are close appositions of the cytoplasmic membranes of adjacent cells with concentrated channel proteins called connexons or hemichannels. Two hemichannels, one from each neighboring cell, form one gap junctional channel. Hemichannels are composed of six proteins called connexins (Cx). The prevailing connexin subtypes in astrocytes include Cx43, Cx30 and Cx26 (Theis et al., 2005). Gap junctions are permeable for small ions and molecules up to 1 kDa in molecular weight such as K^+, inositol 1,4,5-triphosphate (IP3), adenosine-5'-triphosphate (ATP) and some intracellular fluorescent dyes. The connection of astrocytes into a syncytium makes these cells well suited for K^+ buffering and enables them to communicate with each other by specific means described as the Ca^{2+} wave (see the following text).

1.1.2 Morphology of astrocytes and their respective anatomical domains

As proclaimed by their name, astrocytes in the grey matter of the CNS resemble stars in their morphology. Observations of this star-like shape were based on metallic impregnation methods, which were used at the beginning of glia research and which stained the main filaments in the cell body and large processes (Verkhratsky, 2006; Kettenmann and Verkhratsky, 2008). Newer histological techniques revealed a more elaborate shape of astrocytes nowadays often described as a bushy-like morphology (Pekny and Nilsson, 2005; Wilhelmsson et al., 2006). The astrocyte bushy-like or spongiform appearance comes from their peculiar process ramification – they possess a few primary processes, which branch into countless fine secondary processes (Fig. 1).

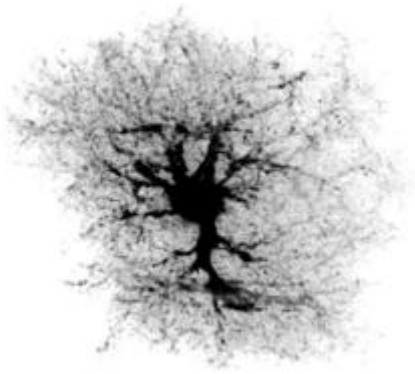

Fig. 1: Typical morphology of protoplasmic astrocytes. Astrocytes have several primary processes extending from their cell body, which divide into many fine secondary processes. From Wilhelmsson et al. (2006).

Recent experiments have shown that protoplasmic astrocytes establish distinct anatomical microdomains in the CNS (Bushong et al., 2002; Ogata and Kosaka, 2002). These microdomains are formed by an astrocyte with its processes enwrapping neuronal synapses and vasculature in its vicinity. Processes of neighboring astrocytes do not overlap (Fig. 2 left), and thus one microdomain is separated from another. This morphological feature might have important implications in CNS physiology as neuronal signals in one astrocytic microdomain might be synchronized by the corresponding astrocyte. Moreover, astrocytes are organized into higher non-overlapping anatomical domains, where astrocytes are interconnected via gap junctions (Fig. 2 right), but gap junctional connection between the two neighboring domains is very low (Houades et al., 2008).

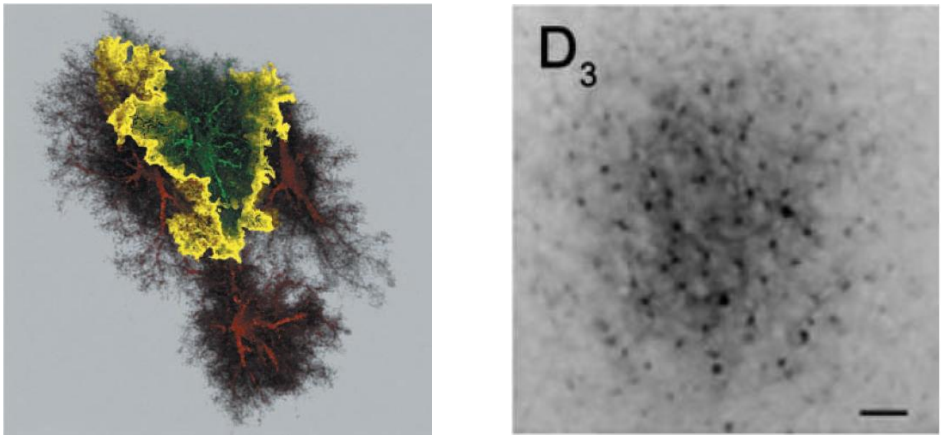

Fig. 2: Astrocytic microdomains and colocalization between adjacent astrocytes. Left: An image of a 3-dimensional reconstruction of four neighboring astrocytes with visualization of a sheet where astrocyte processes interact with each other. Each astrocyte forms a distinct morphological and functional microdomain. From Bushong et al. (2002). **Right**: Astrocyte syncytium labeled by biocytin diffusing into tens of adjacent astrocytes. From Houades et al. (2008).

1.1.3 Astrocytes and CNS development

Astrocytes are macroglial cells of neuroectodermal origin. Cells with astrocytic properties have been found to play a pivotal role during CNS development. Radial glia, which serve as neural and glial precursors during embryonic development, possess intrinsic properties of astrocytes including GFAP expression. In the postnatal CNS, radial glia evolve into GFAP-positive protoplasmic astrocytes. Cells with astrocytic properties, which serve as adult neural stem cells (NSCs), remain only in the two neurogenic zones in the adult brain – in the SVZ of the lateral ventricular wall and in the SGZ of the hippocampal DG region (Ganat et al., 2006). Recently, it has been shown that during astrocyte development, specific molecular cues might be used as markers of astrocytic maturation. The calcium-binding protein, S100β, is expressed only in mature astrocytes (Fig. 3), and its expression is restricted in the GFAP-positive NSCs of the adult neurogenic zones (Raponi et al., 2007).

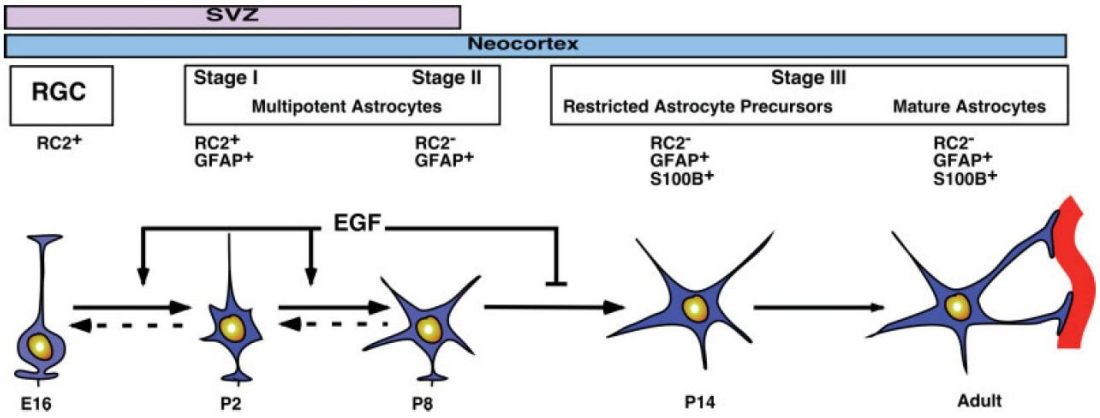

Fig. 3: Model of development of GFAP-positive astrocytes. EGF, epidermal growth factor; GFAP, glial fibrillary acidic protein; RC2, an antibody recognizing RGCs; RGC, radial glial cell; SVZ, subventricular zone. From Raponi et al. (2007).

1.1.4 Membrane properties of astrocytes

Since the pioneer electrophysiological experiments of Kuffler and his colleagues in the 1960s (Kuffler et al., 1966), it has been known that the glial cell membrane is highly permeable to K^+ ions. The first experiments conducted to characterize the membrane properties of glial cells more systematically were done on glial cell cultures in the 1980s after employing the newly invented patch-clamp method (Hamill et al., 1981). Later in the 1990s, the membrane properties of glial cells could also be studied in their natural environment in tissue slices (Edwards et al., 1989). However, measurements in tissue slices are accompanied by considerable problems, e.g. due to the space clamp problem, limited access to the cells or lack of precise cell identification. Thus, approaches to measure the membrane properties of glial cells using the patch-clamp method on acutely isolated glial cells have been employed as well.

Early experiments on primary glial cell cultures brought surprising results showing that glial cells express a large repertoire of voltage-gated ion channels and neurotransmitter receptors similarly as do neurons (Sontheimer, 1994; Verkhratsky and Steinhauser, 2000). Moreover, the expression of neurotransmitter receptors is controlled by the local environment, and astrocytes express specific receptors sensitive to neurotransmitters released in their vicinity, such as glycine receptors in the spinal cord (Pastor et al., 1995). These findings started a long-lasting debate about the physiological functions of these ion channels and receptors in glia. However, the expression of

specific ion channels and receptors was often not proven in glial cells *in situ*. Finally, it has been suggested that glial cells might be divided into more specialized groups of cells, which greatly differ with respect to ion channels and neurotransmitter receptor expression.

In acutely isolated hippocampal glial cells, which show substantial functional relevance to the native tissue environment compared to primary glial cell cultures, whole-cell patch-clamp experiments led to a rough differentiation between "complex" and "passive" glia based on the activation of voltage-gated Na^+ and K^+ channels elicited by depolarizing and hyperpolarizing pulses (Steinhauser et al., 1992; Tse et al., 1992; Steinhauser et al., 1994). Passive currents were characterized as time- and voltage-independent ohmic K^+ conductance, while complex currents represented passive K^+ conductance together with outwardly rectifying delayed and A-type K^+ (K_{DR} and K_A) currents, inwardly rectifying K^+ (K_{IR}) currents and fast-activating tetrodotoxin (TTX)-sensitive Na^+ (I_{Na}) currents. Later studies on hippocampal glial cells in transgenic mice expressing enhanced GFP under the control of the human GFAP promoter showed the presence of two types of glial cells derived from their electrophysiological properties. Hippocampal glia were recognized based on strong or weak GFP expression as brightly or weakly fluorescent cells, respectively. Brightly fluorescent cells had passive currents and expressed glutamate transporters (GluT); on the other hand, weakly fluorescent cells had complex currents and expressed glutamate receptors (GluR). Thus, glia were marked as GluT or GluR cells, respectively. GluT cells were further reported to express GFAP and to be extensively dye coupled. Conversely, GluR cells were never dye-coupled and could be stained with an antibody against S100β calcium-binding protein or NG2 chondroitin sulfate proteoglycan (Matthias et al., 2003; Wallraff et al., 2004). Interestingly, complex glial cells were shown to express GFAP mRNA but not the protein (Zhou and Kimelberg, 2000). The two reported groups of glia, passive GluT cells and complex GluR cells, were described in both the mouse and rat hippocampus or cortex; however, recent findings have put forward the idea that complex GluR cells might belong, at least in adult animals, to a distinct glial cell population characterized by the expression of NG2 chondroitin sulfate proteoglycan.

Until recently, considerable controversy existed surrounding the existence of passive currents in astrocytes (Walz, 2000). In the early patch-clamp studies on glial cells, passive currents were regarded as an artifact and were often discarded from the final data (Tse et al., 1992). Other studies showed that voltage-gated currents might be

masked during the whole-cell patch-clamp measurement due to poor cell access or due to the spillover of low Ca^{2+}/ethylene glycol bis(2-aminoethylether)-N,N,N′N′-tetraacetic acid (EGTA) solution from the patch pipette while approaching the cell (Bordey and Sontheimer, 1998a). Other authors have included glial cells with passive membrane currents in their studies, because these cells had a highly negative membrane potential and were thus regarded as healthy cells. Later, it became obvious from experiments in many laboratories that passive currents are an intrinsic property of glial cells and especially astrocytes, and several hypotheses were introduced about their nature. Originally, it was suggested that they are carried by weakly inwardly rectifying Kir4.1 channels, the expression of which is typical of astrocytes. The passive currents are also partially mediated by currents flowing through gap junctions (Wallraff et al., 2006; Adermark and Lovinger, 2008). Finally, it has been shown that the passive K^+ conductance in astrocytes is based on their combined expression of Kir4.1 channels together with the two-pore domain K^+ channels TWIK1 and TREK1, which are well suited for carrying passive K^+ conductance (Seifert et al., 2009; Zhou et al., 2009).

The expression of voltage-gated ion channels in astrocytes is developmentally regulated. Calcium and sodium ion channels are expressed in glial precursors and immature glial cells (Kressin et al., 1995). The development of the basic electrophysiological profile of rat hippocampal glial cells *in situ* was shown by Schools et al. (2006) and Zhou et al. (2006). In the immature rat hippocampus shortly after birth, astrocyte precursors with a complex current profile greatly outnumber passive astrocytes. Later during postnatal development, authors have observed a switch in the current profile of astrocytes, and starting from the fourth postnatal week (from P21), hippocampal astrocytes display mostly passive currents (Fig. 4).

From the above-mentioned studies, we can assume that mature gray matter astrocytes are electrophysiologically characterized as cells with passive currents, mostly carried by K^+ ions, while astrocyte precursors present in the rat CNS during the first 3 weeks of postnatal development display a complex current pattern. Moreover, both in the immature and mature CNS tissue, NG2 glial cells with a complex current pattern similar to the current pattern of astrocyte precursors can be found. From this point of view, it is important to characterize the cell type of glial cells measured *in situ* by immunohistochemistry. Finally, in the mature CNS tissue, we can clearly distinguish two types of glial cells – astrocytes characterized by passive K^+ currents and GFAP

expression, and NG2 glia characterized by a complex current pattern and the expression of NG2 chondroitin sulfate proteoglycan.

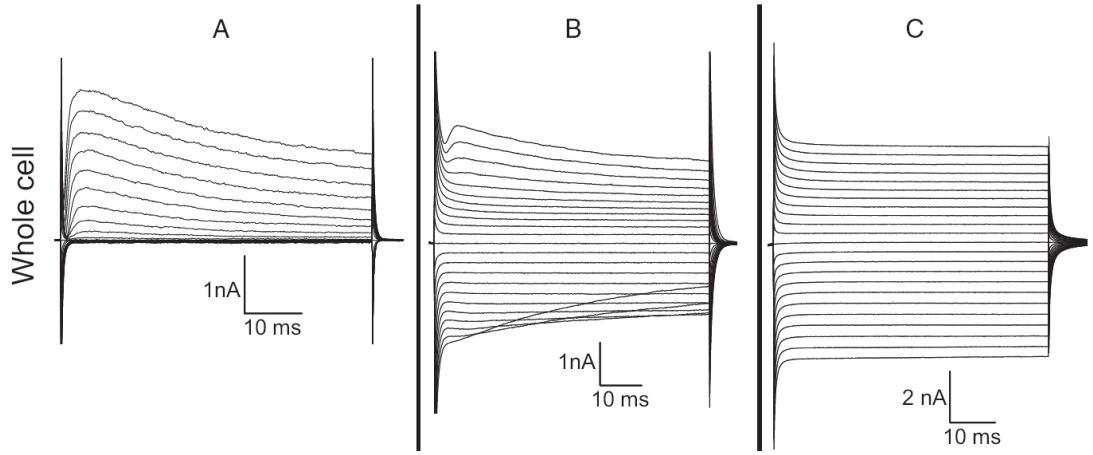

Fig. 4: Distinct electrophysiologically identified glial cells. A: Outwardly rectifying glia, presumably glial precursors. **B**: Variably rectifying glia, presumably NG2 glia or astrocyte precursors. **C**: Passive currents in mature astrocytes. From Schools et al. (2006).

1.1.5 Physiological functions of astrocytes

At the beginning of glia research, glial cells were believed to serve trophic functions for neurons by means of their processes connecting both neurons and blood vessels. Glia could also serve as a structural scaffold or insulators to prevent the undesirable spread of neuronal impulses. Throughout almost the entire 20^{th} century, glial cells were considered passive elements of the brain, completely devoid of any role in the integration and processing of information. In the last few decades, an increasing body of evidence has emerged demonstrating that glia are extremely interesting cells performing a number of important functions in the brain, under both physiological and pathological conditions.

The first well characterized astrocytic function was their maintenance of ionic homeostasis in the extracellular space of the CNS. In the 1960s in the laboratory of Stephen W. Kuffler at Harvard, Kuffler et al. (1966) and Orkand et al. (1966) performed seminal electrophysiological recordings from glial cells. They demonstrated the high K^+ permeability of the glial cell membrane and active neuronal-glial interactions by showing that stimulation of the amphibian optic nerve triggered depolarization of the

adjacent glia. Since astrocytes possess large K^+ conductance and thus their membrane potential lies close to the equilibrium potential for K^+ (E_K), astrocytes sense slight changes in the extracellular K^+ concentration ($[K^+]_e$) produced by firing neurons. Based on this finding, Kuffler and Orkand proposed a hypothesis of K^+ spatial buffering (Orkand, 1986), which was later elaborated in more detail by Neumann and Kofuji (Kofuji and Newman, 2004). Astrocytes, being perfect K^+ concentration sensors, follow changes in $[K^+]_e$, which increases during a higher rate of neuronal firing, by subtle changes in their membrane potential. Potassium ions are taken up into astrocytes at sites of high neuronal activity and are redistributed through the astrocyte syncytium. K^+ ions are then extruded at sites of relative low K^+ concentration (Fig. 5B). Other mechanisms contributing to K^+ ion homeostasis are net K^+ and Cl^- uptake by specific ion channels and/or transporters and K^+ uptake via Na^+K^+ATPase (Fig. 5A).

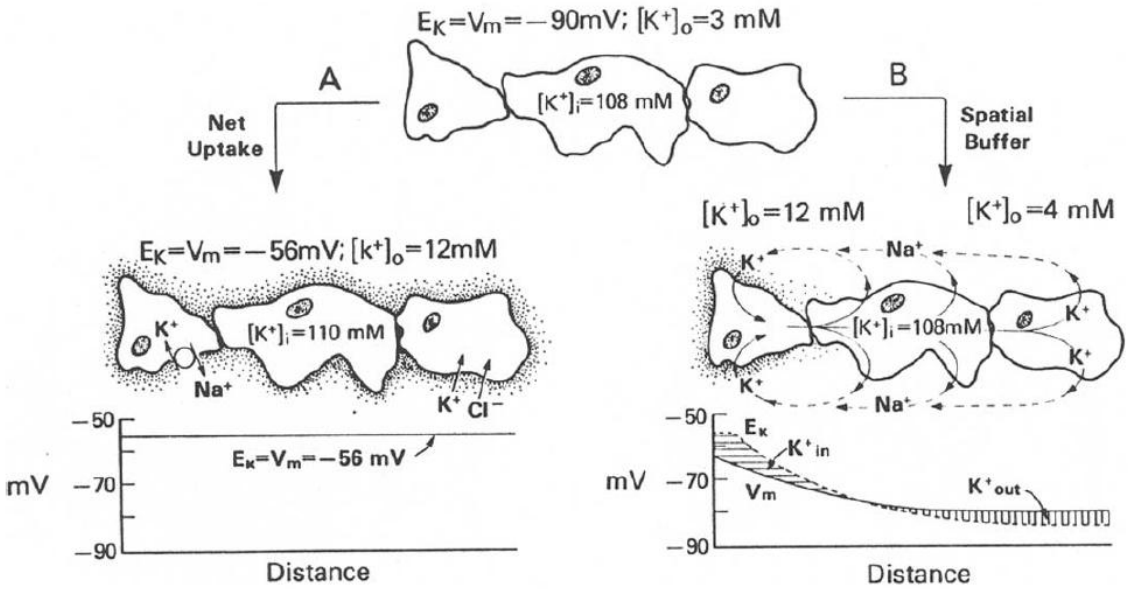

Fig. 5: Role of astrocytes in K^+ buffering. Glial cells are electrically coupled via gap junctions forming a functional syncytium. With extracellular K^+ concentration ($[K^+]_o$) equaling 3 mM, the glial syncytium has a membrane potential of approximately -90 mV. **A: Net K^+ uptake mechanism.** When $[K^+]_o$ is increased, glial cells accumulate K^+ either by the activity of Na^+K^+ATPase or by a pathway in which K^+ is cotransported with Cl^-. In this mechanism of $[K^+]_o$ regulation, the membrane potential in the glial syncytium is spatially uniform at -56mV. **B: K^+ spatial buffering mechanism.** Local increases of $[K^+]_o$ produce a glial depolarization that spreads through the glial syncytium. The local difference in the resting membrane potential (V_m) and E_K drives the K^+ uptake in regions of elevated $[K^+]_o$ and K^+ outflow at distant regions. The intracellular currents are carried by K^+ and extracellular currents are mediated by other ions such as Na^+. From Kofuji and Newman (2004).

The K^+ spatial buffering mechanism is based on the polarized expression of specific ion channels on the astrocytic membrane. The subcellular expression of the weakly inwardly rectifying K^+ channel, Kir4.1, has a distinct spatial pattern – Kir4.1 is expressed on astrocytic endfeet surrounding synapses and blood vessels. Since Kir4.1 is a weakly rectifying channel and may thus allow K^+ fluxes in both directions, it is perfectly suited for functioning in the K^+ buffering mechanism. On the other hand, Kir2.1 is expressed only on astrocyte membranes surrounding neuronal synapses. It is a strongly rectifying channel, and thus it allows only an inward flow of K^+ ions, which are further redistributed through the astrocytic syncytium. A similar mechanism to K^+ spatial buffering, K^+ siphoning, has been well described in retinal Muller cells. Potassium siphoning occurs within one Muller cell. Potassium is taken up by strongly rectifying Kir2.1 channels at processes close to neuronal synapses, then redistributed throughout the Muller cell and extruded by weakly rectifying Kir4.1 channels at processes near blood vessels.

The role of the Kir4.1 channel subunit and astrocytes in K^+ removal after neuronal activity has been extensively studied. It seems that Kir4.1 and astrocytes play a very specific role in this process. Neusch et al. (2006) have shown that a lack of Kir4.1 channel subunits in astrocytes in the ventral respiratory group of the brain stem does not influence the basic neuronal activity. However, the baseline of $[K^+]_e$ in Kir4.1$^{-/-}$ mice was higher and the decay of a stimulus-induced increase of $[K^+]_e$ was slower and exhibited an undershoot. This result is in line with the results shown by D'Ambrosio et al. (2002), who demonstrated that the stimulus-induced increase in $[K^+]_e$ is cleared by neuronal and glial Na^+K^+ATPase together with glial Kir channels. The observed undershoot is due to prolonged activity of the pump, and in normal conditions this decrease in $[K^+]_e$ is replenished by the release of K^+ through Kir channels. Although the K^+ buffering theory is widely accepted, some data indicate controversial results for the physiologically relevant spatial K^+ buffering during brief bursts of presynaptic activity (Meeks and Mennerick, 2007). Recently, the pivotal role of Kir4.1 channels for efficient K^+ spatial buffering has been confirmed by *in vivo* data obtained in transgenic animals lacking astrocytic Kir4.1 expression (Chever et al., 2010). Additionally, since it has been shown that astrocytes also express two-pore domain K^+ channels, these channels might play a role in K^+ buffering as well. Nevertheless, this hypothesis has to be confirmed.

Astrocytes participate in glutamate clearance from the synaptic cleft, preventing undesirable prolongation of glutamate's action on its postsynaptic receptors. Glutamate removal occurs via the glutamate-glutamine cycle (Daikhin and Yudkoff, 2000). Glutamate released from presynaptic terminals is transported primarily to astrocytes, where it is converted to glutamine via the glutamine synthetase pathway: Glutamate + NH_3 + ATP → Glutamine + ADP + P_i. Glutamine is released back to the neurons, where glutamate is regenerated by glutamine hydrolysis to glutamate and ammonia via phosphate-dependent glutaminase, a mitochondrial enzyme: Glutamine → Glutamate + NH_3.

Another basic function of astrocytes was already proposed by Cajal in the 19th century based on his histological observations showing that astrocyte processes contact both neurons and blood vessels. He speculated that astrocytes might provide energetic substrates, such as glucose, to neurons. Astrocytes use two sources of glucose for their energetic metabolism - they take up glucose from blood vessels by their endfeet or convert glycogen stored in their vesicles into glucose by glycogenolysis, which is active mainly in the absence of external glucose. Glycolysis then converts glucose into pyruvate, utilized either in the astrocyte mitochondria in the tricarboxylic acid cycle to produce energy or converted to lactate and transported to neurons using lactate as one of the energy sources (Fig. 6). Neurons may use lactate and ketone bodies as metabolic substrates, especially in the immature brain. Lactate is provided to neurons from astrocytes via the neuronal-glial lactate shuttle (Pellerin, 2003). Recently, it has been shown that the gap-junctional proteins Cx43 and Cx30 allow intercellular trafficking of glucose and its metabolites through the astrocytic syncytium from blood vessels to neurons (Rouach et al., 2008). Interestingly, energetic metabolism in astrocytes can be stimulated by increased neuronal activity (Pellerin et al., 2007).

During increased neuronal activity, the higher energy demands might be compensated for by capillary vasodilation and the subsequent augmented blood supply to the active neurons. Recently, astrocytes have been discovered to be key players during this process. The regulation of microcirculation is achieved in so-called neuro-glio-vascular units. Increased intracellular Ca^{2+} triggered by neuronal activity in astrocytes may cause both the constriction as well as the dilation of neighboring blood vessels. The production of arachidonic acid (AA) in astrocytes by Ca^{2+}-sensitive phospholipase A2 has been shown to be common for both the constriction and the dilation mechanisms. Constriction results from the conversion of AA to 20-

hydroxyeicosatetraenoic acid (20-HETE) and dilation from the production of prostaglandin E2 (PGE2) or epoxyeicosatrienoic acid (EET). The ability of astrocytes to induce vasodilation over vasoconstriction relies on the metabolic state of the brain tissue (Gordon et al., 2008). In addition, the activation of Ca^{2+} activated K^+ channels in astrocyte endfeet and the subsequent efflux of K^+ have also been suggested to modify vascular tone by the hyperpolarization and relaxation of smooth muscle cells (Gordon et al., 2007).

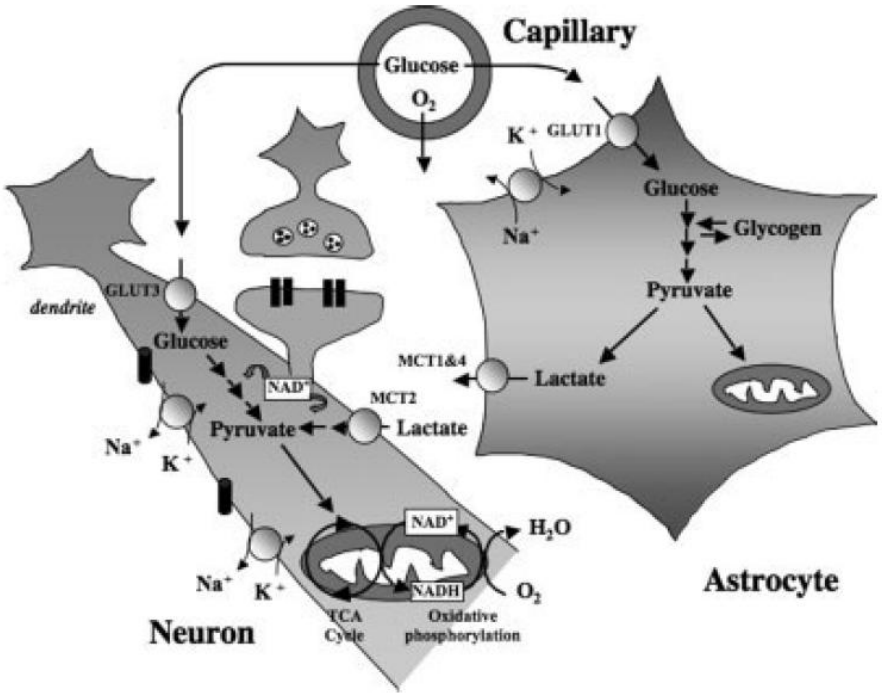

Fig. 6: Basal neuroenergetics in the absence of glutamatergic activation. Glucose, the main cerebral energy substrate in the adult brain under normal conditions, and O_2 are supplied via the blood circulation to parenchymal cells. In astrocytes, glucose is taken up via the glucose transporter GLUT1. Part of it is processed oxidatively via the tricarboxylic acid cycle in mitochondria while the remaining part is converted to lactate, which is released via the monocarboxylate MCT1 and MCT4 transporters into the extracellular space. In neurons, glucose is transported via the glucose transporter GLUT3. In parallel, lactate from the extracellular space is taken up via MCT2. Pyruvate arising from both glucose and lactate is used oxidatively in mitochondria to satisfy neuronal resting energy needs. It cannot be ruled out that neurons could produce a certain amount of lactate, but it is thought that they have a net lactate consumption. Overall, glucose is almost entirely oxidized to CO_2 and H_2O within the brain, yielding a net O_2/glucose consumption ratio close to six. From Pellerin et al. (2007).

Astrocytes have long been considered as non-excitable cells. In the early 1990s, Cornell-Bell et al. (1990) first reported that astrocytes are able to respond to neuronal activity via Ca^{2+} oscillations and that these oscillations may serve as transmitters of activity to neighboring cells. Propagating intercellular Ca^{2+} waves in astrocytes may comprise an extraneuronal pathway for long-distance signal transmission in the CNS. In response to an elevated intracellular Ca^{2+} concentration, astrocytes release "gliotransmitters" by regulated exocytosis. These transmitters used by astrocytes include glutamate, ATP and D-serine (Bezzi et al., 2004; Hamilton and Attwell, 2010). Gliotransmitters released by astrocytes near the synaptic cleft act on adjacent neurons by modulating their synaptic activity. This cooperation between neurons and astrocytes based on feedback modulation of interneuronal communication by astrocytes at the synaptic cleft is called the tripartite synapse (Araque et al., 1999). These findings led to the current view of astrocytes as excitable cells, which may generate, receive and propagate signals by means of Ca^{2+} waves (Haydon, 2001; Fiacco and McCarthy, 2006).

1.1.6 Astrocytes in CNS pathology – reactive astrogliosis

Upon CNS injury, astrocytes undergo rapid morphological and physiological changes. Within several days, they transform into a reactive state forming a gliotic scar. Reactive astrocytes in the gliotic scar are characterized by hypertrophied morphology, increased GFAP expression, *de novo* expression of nestin and proliferation. The functions of reactive astrocytes are wide and diverse. They modulate the tissue inflammatory response by releasing cytokines, mainly tumor necrosis factor-alpha (TNFα) and interleukins, and produce molecules of the extracellular matrix (Ridet et al., 1997). The gliotic scar might separate healthy tissue from the core of the injury, thus preventing the propagation of seizure activity from the injured to the healthy tissue. After mild spinal cord injury, reactive astrocytes may protect the tissue and preserve neuronal functions (Faulkner et al., 2004). On the other hand, the glial scar produces diffusion barriers for many substances such as neurotransmitters and cytokines as well as therapeutic compounds (Roitbak and Sykova, 1999). Moreover, the gliotic scar represents a prohibitive milieu for eventual neuronal regeneration (Qiu et al., 2000; Silver and Miller, 2004).

It is already quite well established which signaling pathways play a role in the activation of astrocytes upon injury; however, it is not understood what signal is the initiating one or whether more specific signals might trigger astrocyte activation. The activation of the epidermal growth factor receptor and the subsequent intracellular signaling cascade have been shown to be crucial for astrocytic activation in the optic nerve (Liu et al., 2006). Another signaling pathway involves endothelin-1, which is upregulated in CNS tissue upon injury, and activation of its receptor, ET_B (Gadea et al., 2008). Signal transducer and activator of transcription 3 (STAT3) has been demonstrated to be a critical regulator of astrogliosis and scar formation after spinal cord injury (Herrmann et al., 2008).

Although it has been hypothesized for a long time that reactive astrocytes might separate the healthy from the injured tissue, the significance of this effect is not clear. The harmful effects of reactive astrocytes comprise provoking inflammation, mediating toxic edema, releasing cytotoxins and/or inhibiting axonal regeneration by the glial scar (Sofroniew, 2005). Bush et al. (1999) have clearly shown many important aspects of glial scar formation. Since ablation of scar-forming reactive astrocytes in transgenic mice led to the spreading of inflammation into a larger area and a longer inflammatory response, it was speculated that reactive astrocytes, which release many cytokines modulating the inflammatory response and influencing leukocyte infiltration, may demarcate the inflammatory zone. The ablation of reactive astrocytes also led to a pronounced secondary tissue degeneration and neuronal and oligodendrocyte cell death, demyelination, higher glutamate accumulation, impaired blood brain barrier repair after injury, massive local tissue edema and pronounced dilation of capillaries. This is in good agreement with the studies of Mulligan and MacVicar (2004), who showed that astrocytes regulate small blood vessel diameter by the release of vasoconstrictors.

Glial scar formation appeared normal after spinal cord or brain lesions in $GFAP^{-/-}$ or $vimentin^{-/-}$ mice, but was impaired in transgenic animals lacking both GFAP and vimentin intermediate filaments. These data suggest that GFAP and vimentin are required for proper glial scar formation (Pekny et al., 1999). In $GFAP^{-/-}vimentin^{-/-}$ double knock-out mice, an entorhinal cortex lesion led to limited astrocytic hypertrophy and glial scar formation compared to wild type mice. This was accompanied by a remarkable synaptic regeneration in the hippocampus (Wilhelmsson et al., 2004). Cell transplantation into injured retinas in $GFAP^{-/-}vimentin^{-/-}$ mice led to a robust integration of the graft and subsequent tissue regeneration compared to wild type mice (Kinouchi et

al., 2003). Moreover, Larsson et al. (2004) have shown increased proliferation and neurogenesis in the adult hippocampus in GFAP$^{-/-}$vimentin$^{-/-}$ mice compared to wild type controls, suggesting an important role for these intermediate filaments in astrocyte functions.

1.1.7 Astrocyte membrane properties after CNS injury

Because many astrocytic functions directly depend on the activity of their ion channels, it is obvious that changes in astrocyte membrane properties after CNS injury might influence astrocyte function and consequently the impact of the injury on the neuronal tissue. The membrane properties of astrocytes have been extensively studied after many types of CNS injuries, and they largely depend on the type, extent and localization of the injury. Three days after a kainic acid lesion of the hippocampus in adult rats, Jabs et al. (1997) found no differences in the membrane properties of passive glial cells compared to controls; however, complex glial cells displayed a lack of sodium currents, decreased K_{DR} currents and increased input resistance. Koller et al. (2000) observed a decrease in K_{IR} currents in glial cells acutely dissociated from the brains of adult rats 3 days after a permanent middle cerebral artery occlusion (MCAO). Schroder et al. (1999) found a decrease in the number of passive astrocytes in the hippocampus of adult rats after an entorhinal cortex lesion. The remaining astrocytes did not differ from those in controls. On the other hand, complex astrocytes displayed increased input resistance, depolarization and a decrease in K_{IR} currents. D'Ambrosio et al. (1999) recognized three types of glial cells in the CA3 hippocampal region 2 days after a midline fluid percussion injury in adult rats - complex glial cells, inwardly rectifying glial cells and glial cells with a linear current/voltage relationship. The authors found a decrease in K_{IR} currents in complex and inwardly rectifying glial cells, while they excluded the linear glial cells from their final data because of their small number. In astrocytes isolated from a gelatin sponge implanted into a cortical stab wound, Perillan et al. (1999) found strongly inwardly rectifying K^+ currents, which were later recognized as being based on the expression of Kir2.3 channel subunits (Perillan et al., 2000). Hippocampal astrocytes from patients operated on for intractable temporal lobe epilepsy displayed a decrease in K_{IR} currents and an increase in sodium currents (Bordey and Sontheimer, 1998b; Hinterkeuser et al., 2000). An increase in K^+ inward conductance was found in astrocytes in the hyperexcitable zone surrounding the core of a neonatal freeze lesion

filled with proliferating astrocytes, which showed no K_{IR} currents (Bordey et al., 2000; Bordey et al., 2001). Our previous experiments demonstrated an upregulation of K_{DR} currents in passive astrocytes and a downregulation of K_{IR} currents in complex astrocytes after a cortical stab wound injury (Anderova et al., 2004). A decrease in K_{IR} currents accompanied by a concomitant increase in outwardly rectifying K^+ currents was clearly shown to be associated with astrocytic proliferation (MacFarlane and Sontheimer, 2000; Bordey et al., 2001).

Wang et al. (2008) used EGFP-GFAP mice for studying the membrane properties of striatal astrocytes after a transient MCAO. In controls, brightly fluorescent cells had passive currents and were GFAP-positive, while weakly fluorescent cells had a complex current pattern, as reported previously. After MCAO, the number of glial cells with a complex current pattern greatly increased, and these cells displayed stronger responses to kainic acid.

Several investigators focused on identifying the changes in the expression of specific Kir subunits in glial cells after a CNS lesion. The expression of Kir2.1 channel subunits in astrocytes was increased 3 and 5 days after a kainic acid lesion in the rat hippocampus (Kang et al., 2008). Gene expression profiling in astrocytes from hyperammonemic mice revealed decreased mRNA expression of both Kir4.1 and Kir5.1 channels together with a decreased expression of AQP4 and Cx43 (Lichter-Konecki et al., 2008). Recently, Olsen et al. (2010) found a decrease in Kir4.1 expression 7 days after a crush spinal cord injury in adult male rats, while Stewart et al. (2010) showed a decrease in Kir4.1 channel expression in the rat neocortex after a fluid percussion injury connected with the chronic impairment of K_{IR} currents in astrocytes in the epileptic focus. Reduced Kir4.1 channel activity in astrocytes associated with deficits in K^+ and glutamate buffering was also found in the hippocampus of seizure-susceptible mice (Inyushin et al., 2010).

Changes in the electrophysiological properties and Kir channel expression profile were shown in radial Muller cells of the ischemic retina. At first, retinal Muller cells after transient ischemia showed a reduction of K_{IR} currents together with increased input resistance and depolarization (Pannicke et al., 2005). In retinal glial cells, proliferative gliosis caused the mislocation of Kir4.1 and Kir2.1 followed by the inactivation of K_{IR} currents (Ulbricht et al., 2008), and ischemia led to decreased Kir4.1 protein expression after 7 days of reperfusion (Iandiev et al., 2006).

Other experiments revealed a novel non-specific cation channel regulated by internal Ca^{2+} and ATP, expressed in reactive astrocytes. The molecular candidate for this channel is not known; however, its properties suggest that this channels might play an important role during pathological swelling (Chen and Simard, 2001; Chen et al., 2003). Indeed, it is crucially involved in the development of brain edema after ischemia (Simard et al., 2006).

From the above-mentioned studies, it is obvious that the common response of astrocytes to CNS injury with respect to their membrane properties is still not well understood. Nevertheless, changes in the membrane properties, and especially changes in the function of K^+ ion channels in astrocytes, might have great functional consequences for the outcome of the affected tissue.

1.2 NG2 GLIA

1.2.1 Basic properties of NG2 glia

NG2 glial cells have been recently recognized as the fourth CNS glial cell type, distinct from astrocytes, oligodendrocytes and microglia. Their specific marker, NG2 (which stands for neuronal-glial antigen 2) chondroitin sulfate proteoglycan, was first isolated in the late 1970s in the laboratory of W. Stallcup (Stallcup, 1981). These researchers found this antigen being expressed in a distinct class of cells in the CNS that did not show either neuronal or glial properties (Nishiyama et al., 2009). Later during the 1980s and 1990s, NG2 glia were recognized as a fourth glial cell type residing in the CNS and constituting about 5% of the total glial cell number (Dawson et al., 2003). Nowadays, NG2 glia are considered an important cellular element of the CNS with specific properties and functions.

NG2 glia, also called polydendrocytes (Nishiyama et al., 2002) or synantocytes (Butt et al., 2002), are morphologically characterized by a small cell body with several radially extending processes that branch into many secondary processes. Apart from the NG2 antigen, NG2 glia express the alpha receptor for platelet-derived growth factor (PDGFαR), also used as their specific marker. Moreover, NG2 glia, or at least a subpopulation of these cells, belong to the oligodendrocyte lineage and as such, during

distinct phases of their development, they express markers for oligodendrocytes such as Olig2 or O4 (Fig. 7).

Concerning their electrophysiological properties, NG2 glia display the "complex" type of membrane currents, i.e. passive K^+ conductance, K_{IR}, K_{DR} and K_A currents and, in some cells, I_{Na} currents (Lin and Bergles, 2002; Chittajallu et al., 2004). Moreover, NG2 glia possess ionotropic $GABA_A$ receptors and glutamate receptors of the AMPA subtype.

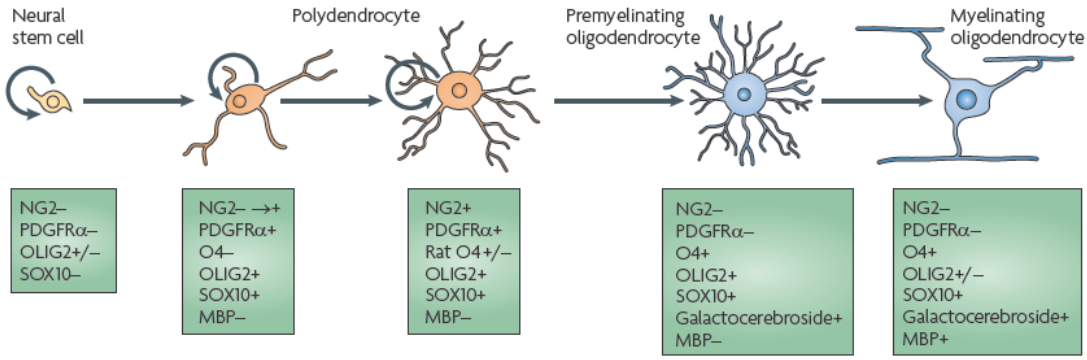

Fig. 7: The oligodendrocyte development lineage. A scheme showing NG2 glia in the oligodendrocyte lineage. The two markers for NG2 glia, NG2 chondroitin sulfate proteoglycane and platelet-derived growth factor receptor-α (PDGFRα), are not expressed by neural stem cells but are expressed by proliferating progenitor cells (proliferation is indicated by the semicircular arrows) of the oligodendrocyte lineage. As NG2 glia undergo terminal differentiation into mature oligodendrocytes they lose the expression of NG2 and PDGFRα and begin to express the immature oligodendrocyte antigen O4, followed by galactocerebroside and subsequently myelin basic protein (MBP). SOX10 is expressed throughout development whereas OLIG2 seems to be downregulated in the mature oligodendrocytes. Most NG2 glia express OLIG2, but there are many OLIG2+ cells in the germinal zones and elsewhere that are NG2– (and therefore not NG2 glia). From Nishiyama et al. (2009).

1.2.2 Physiological functions of NG2 glia

NG2 glia give rise to myelinating oligodendrocytes during the development of the CNS, largely upon signals from maturing neurons. Thus, these cells are often referred to as oligodendrocyte precursor cells (OPCs). In some brain regions, NG2 glia might also give rise to astrocytes (Zhu et al., 2008) or neurons (Rivers et al., 2008; Guo et al., 2010). However, NG2 glia survive to a great extent in the mature CNS, and here their physiological role is still unknown. Lately it has been shown that NG2 glia divide

extensively in the adult CNS (Ge et al., 2009), yet their subsequent fate remains a matter of debate.

The seminal experiments conducted in the laboratory of Dwight E. Bergles have shown that NG2 glia are synaptically connected with neurons in the hippocampus and the cerebellum. They receive GABAergic inputs from interneurons and glutamatergic inputs from Schaffer collaterals in the hippocampus. NG2 glia then respond to glutamatergic stimulation by Ca^{2+} entry through AMPA receptors and subsequent elevation of the intracellular Ca^{2+} concentration (Bergles et al., 2000; Lin and Bergles, 2004; Lin et al., 2005). During oligodendrocyte development, NG2 glia may thus monitor the firing patterns of the surrounding neurons, which acts as a signal to differentiate into oligodendrocytes (De Biase et al., 2010; Kukley et al., 2010). The excitatory synapses between neurons and NG2 glia in the hippocampus may undergo activity-dependent modifications similar to long term potentiation (Ge et al., 2006). On the other hand, the way in which NG2 glia reciprocally signal to neurons is still unknown.

In the rat CNS white matter, Karadottir et al. (2008) have shown two types of OPCs or NG2 glia. One type expresses voltage-gated sodium and potassium channels, generates action potentials when depolarized and senses its environment by receiving excitatory and inhibitory synaptic input from axons. The other type lacks action potentials and synaptic input. Action-potential generating OPCs are preferentially damaged during white matter ischemia and thus can not help remyelinate the tissue.

1.2.3 NG2 glia in CNS pathology

NG2 glia respond promptly to an acute CNS injury contributing to the development of the glial scar. The responses of NG2 glia to CNS disorders have been extensively studied in animal models of stab wound (Levine, 1994; Alonso, 2005), experimental autoimmune encephalomyelitis (Nishiyama et al., 1997; Reynolds et al., 2002), demyelination (Keirstead et al., 1998), axonal degeneration (Nielsen et al., 2006), amyotrophic lateral sclerosis (Magnus et al., 2008) and, most extensively, in contusive spinal cord injury (Lytle et al., 2006; Lytle and Wrathall, 2007; Rabchevsky et al., 2007; Tripathi and McTigue, 2007; Lytle et al., 2009). An increasing amount of evidence has been put forward showing that in the injured CNS white matter, NG2 glia proliferate and newly derived NG2 glial cells differentiate into myelinating oligodendrocytes. This

is an important finding because NG2 glia might thus promote tissue regeneration. Some authors claim that proliferating NG2 glia, especially in the injured grey matter, might also give rise to reactive astrocytes (Alonso, 2005; Magnus et al., 2008); however, this hypothesis has to be proven by further studies. Tripathi et al. (2010) have recently shown that the number of astrocytes generated from NG2 glia in a murine model of demyelinating disease is very low (about 2%). Special care has to be taken when evaluating the contribution of NG2 glia to glial scar formation since NG2 chondroitin sulfate proteoglycan is also expressed by activated microglia in acute CNS injury (Gao et al., 2010). The role of NG2 chondroitin sulfate proteoglycan in the glial scar with respect to axonal growth still remains controversial. Early studies showed that NG2 chondroitin sulfate proteoglycan impedes axonal growth, but newer studies have come to different conclusions (Fidler et al., 1999; Yang et al., 2006).

Up to now, the membrane properties of NG2 glia after CNS injury have been demonstrated only in two studies by the same authors. Lytle et al. (2006) found an increase in membrane capacitance, a decrease in K_{DR} and K_A current densities and an increase in K_{IR} current density in NG2 glia isolated from the spinal cord 3 days after a contusion injury. Recently the same authors (Lytle et al., 2009) have shown an increase in K_{DR} currents in proliferative NG2 glia *in situ* 3 days after a spinal cord contusion injury performed in CNP-EGFP transgenic mice.

1.3 ISCHEMIA

1.3.1 Ischemic injury of the CNS

Ischemic injury is caused by the partial or complete blockage of blood flow to the affected tissue. In humans, the whole brain might be affected by transient global ischemia after a heart attack, drowning, cardiopulmonary resuscitation or some other rare circumstances. More frequently, focal cerebral ischemia (commonly called stroke) occurs in the vicinity of an occluded blood vessel. Stroke can occur in two ways: embolic or thrombotic. In an embolic stroke, a blood clot formed in the heart or carotid arteries travels to the brain and closes an artery. In a thrombotic stroke, a thrombus develops on an atherosclerotic blood vessel deposit in one of the CNS arteries. Most

frequently, stroke occurs in the vicinity of the middle cerebral artery, which determines the symptoms of stroke in humans.

On the macroscopic level, stroke leads to the development of an ischemic core with a surrounding penumbra zone. In the ischemic core, all cells die by a phenomenon called pannecrosis. In the penumbra, the cell outcome depends on many circumstances, especially on the duration and severity of the ischemia. Without any treatment or spontaneous reperfusion, the necrotic core extends into the penumbral region. Potential therapeutic approaches are thus focused on the possibility of preventing the extension of the ischemic core into the penumbral region and to help the cells in the penumbra to survive (Lo et al., 2003). Transient global cerebral ischemia, both in animals and humans, leads to selective neuronal loss and reactive gliosis in the CA1 region of the hippocampus followed by functional impairments in learning and memory tasks (Block, 1999).

1.3.2 Cellular and molecular mechanisms of ischemic injury

The basic factor that stands at the onset of the cellular injury triggered by ischemia is energy depletion. Low oxygen and glucose supply leads to diminished ATP production in mitochondria, followed by functional impairment of the cellular processes ultimately dependent on ATP. The first affected is Na^+/K^+ATPase in neurons, which maintains the physiological ion gradients through the plasma membrane. Impaired function of this pump leads to ionic imbalance, depolarization, and neurons immediately losing their ability to trigger an action potential. Depolarization leads to the opening of voltage-dependent ion channels, thus allowing an influx of Na^+ and Ca^{2+} into the cells. Increased intracellular Ca^{2+} concentration leads to the release of glutamate from neurons and additional depolarization caused by the activation of ionotropic glutamate receptors. This process is called glutamate excitotoxicity. Glutamate receptors allow a further influx of Ca^{2+} ions into the cell, which promotes the activation of Ca^{2+} dependent enzymes, starting proteolysis and pro-apoptotic pathways (Fig. 8) (Dirnagl et al., 1999; Lipton, 1999). Moreover, the increase in the intracellular Na^+ concentration leads to the reversal of the Na^+/Ca^{2+} exchanger and further Ca^{2+} influx (Kiedrowski, 2007).

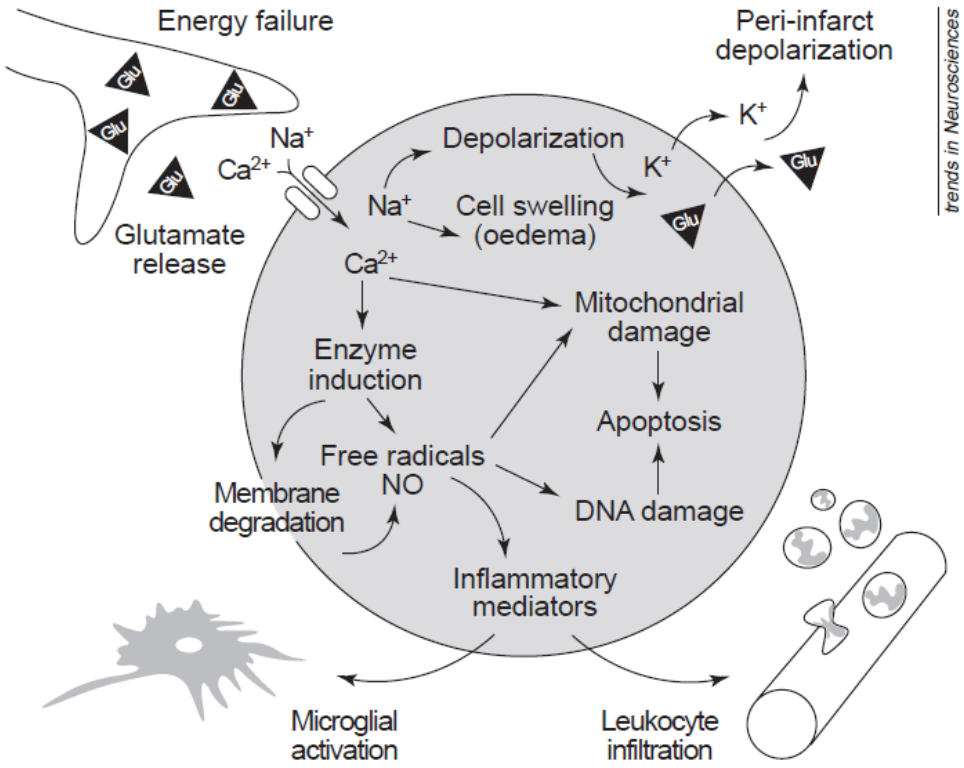

Fig. 8: Simplified overview of the pathophysiological mechanisms in the focally ischemic brain. Energy failure leads to the depolarization of neurons. Activation of specific glutamate receptors dramatically increases intracellular Ca^{2+}, Na^{+} and Cl^{-} levels while K^{+} is released into the extracellular space. Diffusion of glutamate (Glu) and K^{+} in the extracellular space can propagate a series of spreading waves of depolarization (peri-infarct depolarizations). Water shifts to the intracellular space via osmotic gradients and cells swell (edema). The universal intracellular messenger Ca^{2+} overactivates numerous enzyme systems (proteases, lipases, endonucleases, etc.). Free radicals are generated, which damage membranes (lipolysis), mitochondria and DNA, in turn triggering caspase-mediated cell death (apoptosis). Free radicals also induce the formation of inflammatory mediators, which activate microglia and lead to the invasion of blood-born inflammatory cells (leukocyte infiltration) via upregulation of endothelial adhesion molecules. From Dirnagl et al. (1999).

Many other molecules and mechanisms contribute to the tissue damage during ischemia and reperfusion, such as the accumulation of free AA after activation of phospholipase A2 (Taylor and Hewett, 2002), the accumulation of reactive oxygen species and NO leading to oxidative/nitrosative stress followed by lipid peroxidation and membrane damage, the reduction of protein synthesis, the inhibition of growth factor signals, and the activation of pro-apoptotic signals (White et al., 2000; Doyle et al., 2008). As demonstrated, the cellular mechanisms involved in ischemic tissue injury

are complex, and thus a single treatment directed at one specific process appears to be ineffective.

1.3.3 Hypoxia/ischemia models *in vitro* and *in vivo*

For studying the impact of hypoxia/ischemia on CNS tissue and neural cells, many *in vitro* models mimicking these conditions have been established. One might speculate about the real significance of using *in vitro* models for studying hypoxic/ischemic conditions because of the lack of tissue complexity. On the other hand, this is an appropriate way to distinguish the impact of distinct conditions on the tissue or cell outcome. The most widely used model is that of oxygen/glucose deprivation (OGD), when the cells are exposed to low or zero levels of oxygen and/or glucose. This model can be modified by using an additional pH shift and shifts in ion concentrations (Bondarenko and Chesler, 2001). Another model of *in vitro* ischemia is based on ATP depletion, e.g. by blocking glycolysis and mitochondrial oxidative phosphorylation (Rose et al., 1998). Since ischemia is generally accompanied by a substantial increase in $[K^+]_e$, some *in vitro* studies use the application of a solution with high K^+ concentration on cells or tissue segments to mimic the ischemic conditions (Kimelberg et al., 1995).

To imitate clinically relevant ischemic injury in animals, many approaches have been established (for review see Hossmann, 2008). Global cerebral ischemia (GCI) is most commonly induced by cardiac arrest or 4-vessel occlusion. This model requires the occlusion of both common carotid arteries and vertebral arteries in rats or mice. In gerbils, where the circle of Willis is incomplete, occlusion of only the common carotid arteries is sufficient to induce complete brain ischemia. A new model of GCI was introduced by Dijkhuizen et al. (1998) and Zoremba et al. (2008). In this model, only the common carotids are occluded, and the animal is concurrently ventilated with a low oxygen concentration.

The most common and most clinically relevant model of brain ischemic injury is focal cerebral ischemia induced by MCAO. By its pathophysiology, MCAO closely resembles common stroke in humans. In this model, the basal ganglia consistently suffer a severe reduction in blood flow, whereas the cerebral cortex exhibits a gradient of blood flow decreasing from the peripheral towards the central parts of the occluded vascular area (Kawamura et al., 1991).

1.3.4 Programmed cell death

Programmed cell death, together with necrosis, plays a critical role in nervous system pathologies such as ischemia. The global cerebral ischemia used in our experiments is characterized by delayed selective neuronal death in the CA1 region of the hippocampus, preferentially by programmed cell death (Lo et al., 2003). Programmed cell death is an active process requiring protein synthesis and leading to cellular loss. According to morphological criteria, two forms are classically distinguished – apoptosis and autophagy. Moreover, several atypical forms, such as paraptosis, oncosis and poly(ADP-ribose) polymerase (PARP)-mediated have been described (Bredesen et al., 2006). Cell death might be triggered by various factors following CNS injury such as DNA damage, reactive oxygen or nitrogen species, calcium entry, mitochondrial-complex inhibition, excitotoxicity, death-receptor activation or misfolded protein accumulation.

Apoptosis is morphologically characterized by membrane blebbing, chromatin condensation, nuclear fragmentation and the formation of apoptotic bodies. The activation of apoptosis occurs through two classical pathways (Fig. 9). The extrinsic pathway originates through the activation of cell-surface death-receptors and leads to the activation of initiator caspase-8 or -10. The intrinsic pathway starts with the mitochondrial release of cytochrom-c and the subsequent activation of initiator caspase-9 (MacFarlane and Williams, 2004; Nakka et al., 2008). The intrinsic pathway is regulated by the balance between pro- and anti-apoptotic members of the Bcl-2 family. Apoptosis is initiated when this balance is shifted towards the pro-apoptotic members. Caspases are cysteine-aspartyl-specific proteases, which act in two ways during apoptosis: as initiators or effectors. The initiator caspases cleave inactive forms of effector caspases (such as caspase-3 or -7), thereby activating them. The effector caspases in turn cleave other protein substrates in the affected cell resulting in its apoptotic death by the activation of proteolytic cascades, the inactivation of repair mechanisms, DNA cleavage, mitochondrial permeabilization and the initiation of the process of phagocytosis to clean up the dying cells and debris.

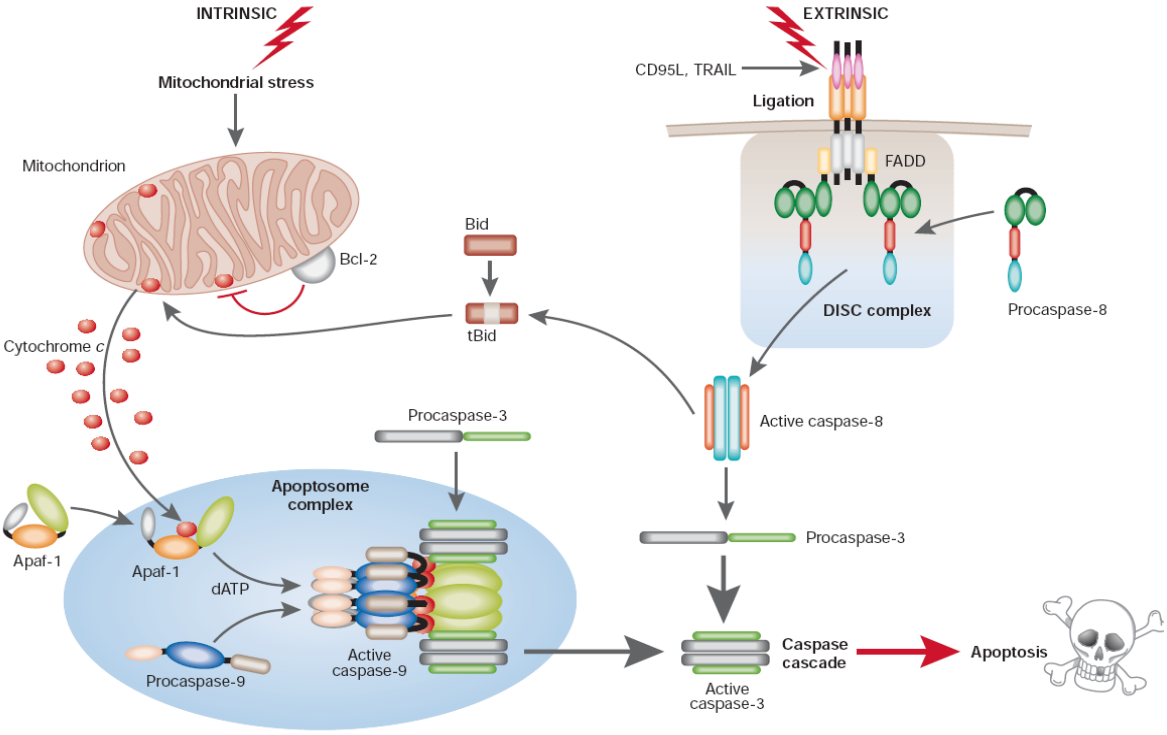

Fig. 9: Apoptosis: the 'extrinsic' and 'intrinsic' pathways to caspase activation. Two major apoptotic pathways are illustrated: one activated via death receptor activation ('extrinsic') and the other by stress-inducing stimuli ('intrinsic'). Triggering of cell surface death receptors of the tumour necrosis factor (TNF) receptor superfamily, including CD95 and TNF-related apoptosis-inducing ligand (TRAIL)-R1/-R2, results in rapid activation of the initiator caspase 8 after its recruitment to a trimerized receptor-ligand complex (DISC) through the adaptor molecule Fas-associated death domain protein (FADD). In the intrinsic pathway, stress-induced apoptosis results in perturbation of mitochondria and the ensuing release of proteins, such as cytochrome *c*, from the inter-mitochondrial membrane space. The release of cytochrome *c* from mitochondria is regulated in part by Bcl2 family members, with anti-apoptotic (Bcl2/Bcl-XL/Mcl1) and proapoptotic (Bax, Bak and tBid) members inhibiting or promoting the release, respectively. Once released, cytochrome *c* binds to apoptotic protease-activating factor 1 (Apaf1), which results in the formation of the Apaf1–caspase 9 apoptosome complex and activation of the initiator caspase 9. The activated initiator caspases 8 and 9 then activate the effector caspases 3, 6 and 7, which are responsible for the cleavage of important cellular substrates resulting in the classical biochemical and morphological changes associated with the apoptotic phenotype. From MacFarlane and Williams (2004).

Autophagic cell death is mostly triggered by nutrient starvation. Essentially, it is an intracellular form of phagocytosis targeting, e.g., damaged mitochondria or aggregates of misfolded proteins. An autophagosome fuses with a lysosome resulting in the degradation of its contents (Assuncao Guimaraes and Linden, 2004). The degradation of molecules and organelles by autophagy leads to the production of energy

and amino acids for new protein synthesis. This process is constitutively active at low levels and can be upregulated by starvation.

1.3.5 The role of astrocytes during ischemia and reperfusion

Astrocytes may play both beneficial and detrimental roles during ischemia and reperfusion (Nedergaard and Dirnagl, 2005), depending on the severity of the injury. During mild insults, under incomplete ischemia or in the penumbral zone, astrocytes may help neurons to survive by maintaining ion homeostasis or by preventing glutamate excitotoxicity by glutamate uptake into astrocytes. On the other hand, at the onset of severe ischemia, glutamate neurotoxicity might even be exacerbated by astrocytes by their release of glutamate via GluT reversal and/or glutamate efflux through volume-regulated anion channels (VRACs) (Li et al., 1999; Feustel et al., 2004; Kosugi and Kawahara, 2006). The interconnection of astrocytes into a large syncytium might have two different effects during ischemia and reperfusion. Either gap junctions may help buffer the excess of extracellular K^+ or molecules promoting cell death may spread through them into neighboring healthy cells and extend the borders of the injury.

During reperfusion, astrocytes provide neurons with glutathione to scavenge reactive oxygen species (Raps et al., 1989; Griffin et al., 2005). Later after ischemia, astrocytes are the source of growth factors for neurons; they also promote neovascularization, neurogenesis and synaptogenesis and modulate the inflammatory response in the affected tissue (Ullian et al., 2004; Panickar and Norenberg, 2005). In particular, activated astrocytes may produce many neuroprotective factors; however, the exact effect depends on the degree of activation as influenced by the stimulus severity, duration, or some other unknown factors.

Astrocytes are well known to increase their volume under many acute pathological or experimental conditions, such as hypotonic challenge, hypoxia/ischemia, exposure to high K^+ or traumatic brain injury. Astrocytic swelling represents a hallmark of post-ischemic brain edema. The swelling of astrocytes activates K^+ and Cl^- ion channels, which permit active ion efflux and concomitant water release leading to a compensatory phenomenon called regulatory volume decrease (RVD). The anion channels involved in RVD are VRACs, permeable for Cl^- and excitatory amino acids such as glutamate and taurine (Kimelberg, 2005). During brain ischemia, the release of glutamate through VRACs might contribute to excitotoxic neuronal injury

(Feustel et al., 2004). The cation channels opened by cell swelling and responsible for RVD in astrocytes still remain to be elucidated. Astrocyte swelling might contribute to postischemic hypoperfusion, which causes the closure of small blood vessels and capillaries during reperfusion. However, this process is not likely to be involved in neuronal death after ischemia/reperfusion (White et al., 2000).

Neurons in some particular brain regions appear to be selectively vulnerable during GCI. This phenomenon occurs in the CA1 pyramidal neurons, cortical projection neurons in layer 3, subsets of neurons in dorsolateral striatum and Purkinje cells (Lo et al., 2003). The selective vulnerability of these particular neuronal populations might be explained by several hypothesis. In the CA1 region of the hippocampus, astrocytes play an active role in selective neuronal loss (Ouyang et al., 2007). Moreover, it has been shown in an *in vitro* OGD model on brain slices that the CA1 region of the hippocampus is the most susceptible to increases in $[K^+]_e$ evoked by OGD compared to the CA3 region or to the cortex (Perez-Pinzon et al., 1995), which might be caused by an ineffective astrocyte K^+ buffering capacity.

Noxious stimuli below the threshold of damage are able to induce protection (‘‘tolerance’’) against a subsequent deleterious stimulus of the same or even another modality (‘‘cross-tolerance’’). This phenomenon is termed ischemic preconditioning and it might change the cellular response to ischemia. This process requires protein synthesis and influences many metabolical and biochemical pathways in the affected cells. It may reduce the deleterious inflammatory response, adapt energy metabolism as well as enhance various neuroprotective mechanisms. Ischemic preconditioning can be induced in both neurons and astrocytes; however, since astrocytes have a better ability to survive ischemia and since they possess specific properties that might help neurons to survive during energy depletion, the processes of ischemic tolerance have been widely studied particularly in these cells (Trendelenburg and Dirnagl, 2005).

1.4 POTASSIUM ION CHANNELS

1.4.1 Inwardly rectifying K^+ channels

Inwardly rectifying K^+ (Kir) channels are widely expressed in many cell types and play an important role in diverse physiological functions in the brain, retina, ears, heart,

kidney and endocrine cells. The 15 known members of the Kir channel family are divided based on their electrophysiological and molecular characteristics into 7 subfamilies (Kir1-7) (Kubo et al., 2005; Hibino et al., 2010). The primary function of Kir channels is maintaining the cell resting membrane potential (RMP) close to E_K. In excitable cells, such as cardiomyocytes or neurons, Kir channels contribute to the modulation of cell excitability and action potential repolarization. The determining feature of Kir channels is their ability to conduct K^+ better in the inward than in the outward direction.

Kir channels form tetrameric structures, which can be co-assembled by heteromeric or homomeric Kir subunits (Fig. 10). Each subunit has two transmembrane segments called M1 and M2, a pore loop (P), and amino (N)- and carboxy (C)-terminal cytoplasmic domains (Bichet et al., 2003).

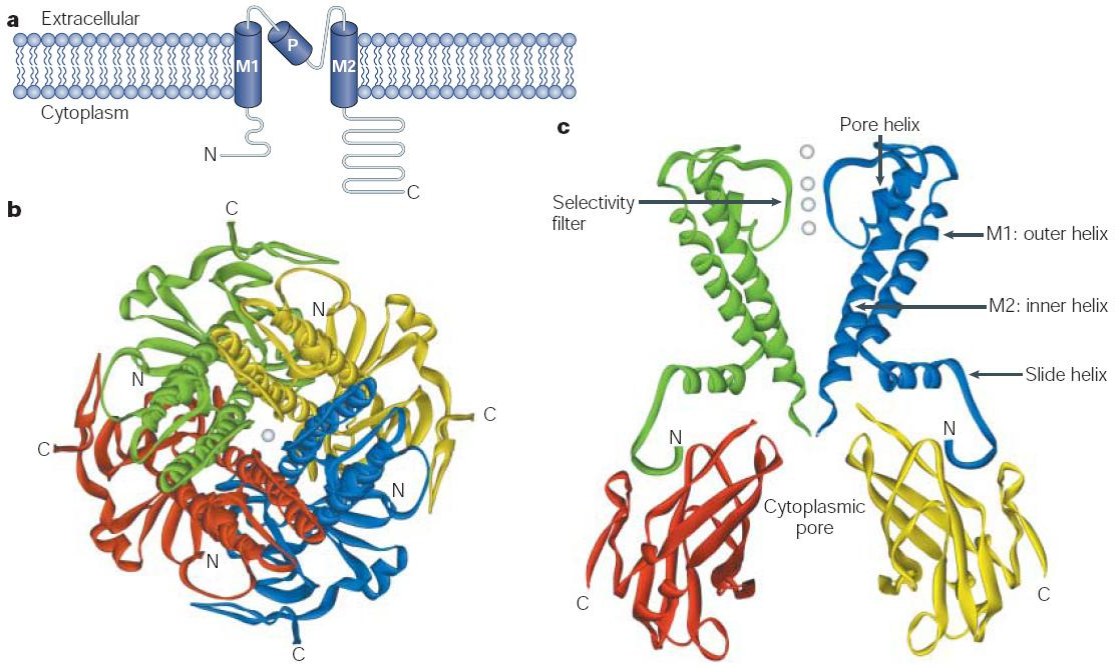

Fig. 10: Architecture of the inwardly rectifying K^+ (Kir) channels. a: Schematic drawing of a Kir channel subunit. Each subunit comprises two transmembrane helices (M1 and M2), a pore-forming region containing the pore-helix (P), and a cytoplasmic domain formed by the amino (N) and carboxy (C) termini. **b**: View of the tetrameric structure of the KirBac1.1 channel4 (PDB ID:1P7B) from the extracellular side. Monomers are individually colored red, green, yellow and blue. A K^+ ion (white) indicates the conduction pathway. **c**: Side view of the KirBac1.1 structure showing the transmembrane domain of two subunits (green and blue) and the C-terminal domains of their neighboring subunits (red and yellow). White spheres represent K^+ ions in the selectivity filter. From Bichet et al. (2003).

The inward rectification of Kir channels is caused by blocking the channel by intracellular Mg^{2+} and/or polyamines (e.g. putrescine, spermine, spermidine) at potentials positive to the cell RMP, thus impeding the outward flow of K^+ ions. Based on the degree of rectification correlating with the binding affinity of the channel for blocking cations, we can distinguish weak (Kir1, Kir4, Kir6) and strong (Kir2, Kir3) rectifiers (Fig. 11). Another characteristic feature of inward rectification is its strong voltage dependence. The selectivity filter of the Kir channel, defined as the narrowest part of the conduction pathway, primarily discriminates between K^+ and Na^+ ions. The activity of Kir channels might be modulated by several cytoplasmic factors, such as phosphatidylinositol-4,5-bisphosphate (PtdIns(4,5)P_2), AA, Na^+ and Mg^{2+} ions, pH, G proteins, ATP, phosphorylation or oxidation/reduction. PtdIns(4,5)P_2 enhances the currents through Kir channels; on the other hand, its depletion during patch-clamp measurements, similarly to ATP, causes the channel to rundown (Bichet et al., 2003).

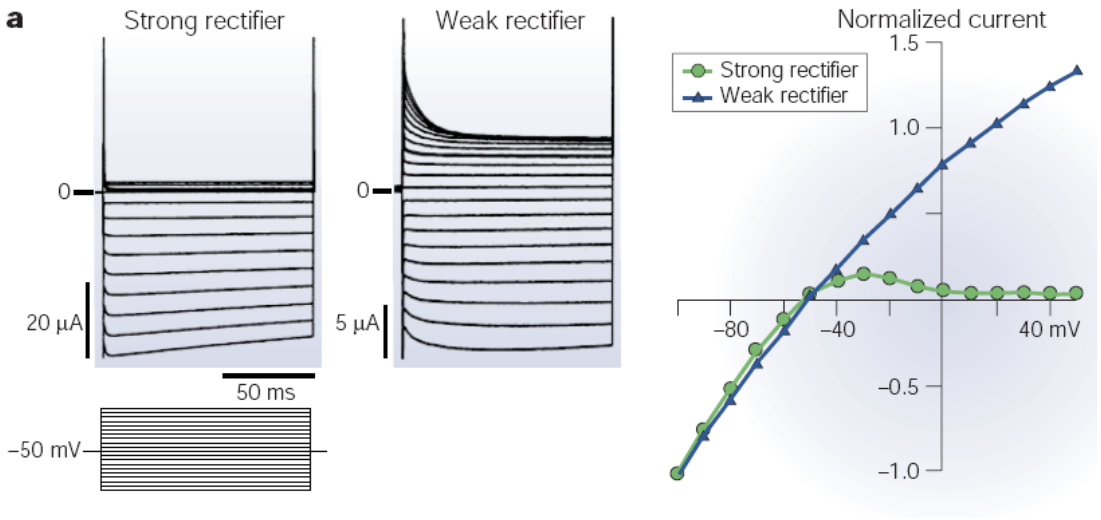

Fig. 11: Strong and weak inward rectification of Kir channels. a: Macroscopic current traces and current–voltage curves of a strong and a weak inward rectifier. The examples shown were obtained under a two-electrode voltage clamp of Xenopus oocytes expressing wild-type (left) Kir2.1 and E224G/E299S mutant (right) channels. The protocol of stimulation shown below the current traces consists of voltage steps of 10-mV increments from –140 mV to +50 mV from a holding potential of –50 mV. From Bichet et al. (2003).

Glial cells express a wide range of Kir channels (Butt and Kalsi, 2006). Astrocytes show a predominant and specific expression of the Kir4.1 isoform

(Poopalasundaram et al., 2000; Seifert et al., 2009), which is believed to represent the prerequisite for the high K^+ conductance in astrocytes, setting their RMP close to E_K and allowing the K^+ buffering mechanism. Moreover, the currents through Kir channels are modulated by $[K^+]_e$, which permits greater K^+ uptake when $[K^+]_e$ is raised. Temporal, astrocyte-specific Kir4.1 gene knockout in adult mice was shown to abolish K^+ spatial buffering (Neusch et al., 2006). Conditional knock-out of the Kir4.1 gene in adult astrocytes led to their depolarization, the inhibition of K^+ and glutamate uptake and subsequent K^+ accumulation in the extracellular space (Djukic et al., 2007; Kucheryavykh et al., 2007). In oligodendrocytes, Kir4.1 channels play an important role during development, and the genetic deletion of this channel subtype leads to spinal cord white matter hypomyelination and axonal degeneration, followed by motor function impairment and early death (Neusch et al., 2001). Kir4.1 forms functional channels with Kir2.1 and Kir5.1 subunits in astrocytes (Hibino et al., 2004). Such heteromeric channels display specific features such as higher sensitivity to changes in pH_i (Cui et al., 2001) and stronger rectification compared to homomeric Kir4.1 channels. The specific Kir channel subtype expressed in NG2 glia is not known; however, Tang et al. (2009) have recently shown that NG2 glia might express Kir4.1 channel subunits as well.

Kir4.1 channels are coexpressed with aquaporin-4 water channels on astroglial endfeet surrounding blood vessels (Nagelhus et al., 2004). Since the ion movement through Kir channels is facilitated by water movement through the aquaporins, this co-localization has great functional consequences. This feature seems to be essential for K^+ buffering, because it has been shown that aquaporin-4 mislocation in α-syntrophin knockout mice leads to impaired K^+ uptake (Amiry-Moghaddam et al., 2003).

1.4.2 Two-pore domain K^+ channels

The last family of K^+ channels, discovered only in the 1990s, is called two-pore domain K^+ (K_{2P}) channels. As their name suggests, these channels are characterized by a specific subunit topology, i.e. two P loops and four transmembrane segments. Biophysical experiments on K_{2P} channels revealed that they are K^+ selective with voltage-independent conductance, which obeys Goldman-Hodgkin-Katz (open) rectification. Thus, these channels were suggested to be responsible for the background K^+ conductance in many cell types. When the K^+ concentration is symmetrical across

the membrane, K_{2P} channels conduct K^+ currents in a linear manner, while under physiological K^+ concentrations they pass greater outward then inward currents (Fig. 12d). These properties give K_{2P} channels significant physiological functions – they maintain the RMP of many cell types and regulate the activity of neurons and other excitable cells (Goldstein et al., 2001). Many members of the K_{2P} channel family display polymodal characteristics, i.e. they are activated and/or modulated by different stimuli, such as volatile anesthetics, AA, temperature, pH or mechanical stress, which might be important during many pathological processes (Honore, 2007).

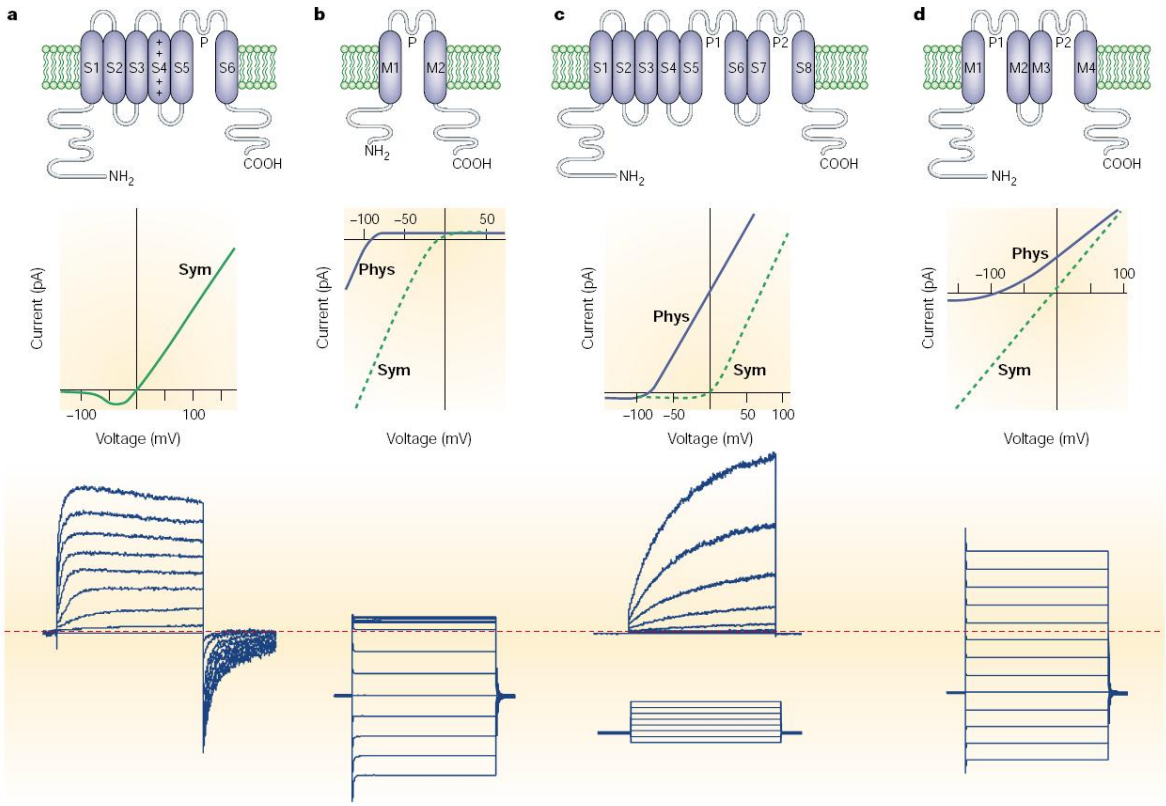

Fig. 12: Potassium channels: membrane topology and current–voltage relationships. Subunits are drawn with the external solution upwards. Graphs represent ideal examples. If the relationship is sensitive to changes in E_K, two conditions have been drawn: symmetric (sym, dashed) and physiological (phys, solid) K^+ concentration. Currents are drawn based on channels studied in symmetric conditions with 500 ms pulses to voltages of −80 to 60 mV (**c**, bottom panel); the dashed line corresponds to 0 mV. **(a)** Voltage-gated K^+ channel (Kv) subunits have a one-P/six transmembrane domain (1P/6TM) predicted topology and are noted for their positively charged fourth transmembrane segment (S4) that acts as a sensor for changes in membrane potential. Some Kv channels are activated by depolarization (as shown here), whereas others open in response to hyperpolarizing stimuli. The current trace is based on KCNQ1 and reveals a delay before current begins to flow, which reflects the time it takes for the channels to enter into the open state after the voltage change. **(b)** Inwardly rectifying K^+ channel (Kir) subunits have one P

domain and two transmembrane segments (1P/2TM). Kir channels pass small outward currents owing to chronic blockade by intracellular cations; large inward currents pass when voltage is negative to E_K and the pore is unblocked. The current trace is based on Kir4.2 and reveals no delay before current begins to flow because unblock kinetics are faster than the resolution of the recording. **(c)** TOK1, a non-voltage-gated, outwardly rectifying K^+ channel from Saccharomyces cerevisiae that has a 2P/8TM predicted topology. The channel passes outward current when membrane voltage is positive relative to E_K. The trace reveals a fast and a slow phase to current development after a change in voltage. **(d)** KCNK channels have a predicted 2P/4TM-subunit topology. The channels are open rectifiers and allow the passage of large outward currents under conditions of high internal and low external K^+ (BOX 2). The current trace is based on KCNK0. It shows a nearly linear current-voltage relationship under symmetrical K^+, and reveals no delay before current starts to flow because the channels are open before the voltage step. From Goldstein et al. (2001).

Since astrocytes *in situ* display passive, i.e. voltage-independent, K^+ currents it has been speculated that these currents might be based on constitutive opening of K_{2P} channels. Indeed, the expression of this type of K^+ channel has been shown recently both in cultured astrocytes as well as in astrocytes *in situ*. In cultured cortical astrocytes, Ferroni et al. (2003) have shown the expression of an open rectifier K^+ channel activated by AA, presumably being of the TREK family. Similar results were published by Gnatenco et al. (2002) using single-channel patch-clamp recording. Moreover, Skatchkov et al. (2006) have reported the expression of K_{2P} channels of the TASK family in retinal Muller cells. These preliminary results have been recently proven by two groups who have demonstrated the expression of K_{2P} channels in hippocampal astrocytes *in situ*. They demonstrated that passive K^+ conductance in astrocytes *in situ* is largely mediated by K_{2P} channels (Seifert et al., 2009; Zhou et al., 2009).

The link of K_{2P} channels with the pathogenesis of some diseases and the potential use of K_{2P} channel activators or inhibitors in therapy has been reviewed in Es-Salah-Lamoureux et al. (2010). TREK-1-deficient mice display higher sensitivity to ischemia and epilepsy than wild type animals (Heurteaux et al., 2004). The same authors have also shown that the deteriorating effect of ischemia was reduced by TREK-1 activators such as linolenic acid or lysophosphatidylcholine in wild type mice compared to the knock-out animals, where no such effect was observed. This phenomenon might be explained in a way that TREK-1 channels maintain a hyperpolarized membrane potential and thus a lower activity of neurons, resulting in their decreased vulnerability. In astrocytes, the overexpression of TREK-2 channels together with an increased ability to take up glutamate from the extracellular space,

which belongs to astrocytic neuroprotective mechanisms, has been shown under experimental ischemic conditions *in vitro* (Kucheryavykh et al., 2009). This enhanced neuroprotective effect was explained by better maintaining the RMP and astrocyte functions in ischemic conditions by increased TREK expression.

1.4.3 Voltage-gated K^+ channels

The diverse family of voltage-gated K^+ (Kv) channels plays an important role in many different cellular functions. It comprises 40 known members divided into 12 subfamilies (Gutman et al., 2005). Kv channels contain two subunits – the main alpha subunit and the auxiliary beta subunit. Alpha subunits form tetramers of four identical subunits arranged as a ring, each contributing to the wall of the trans-membrane K^+ pore. Each subunit is composed of six membrane spanning hydrophobic α-helical sequences (Fig. 12a) (Yellen, 2002). Functionally, Kv channels are membrane proteins conducting K_A and K_{DR} currents. The primary function of Kv channels is to repolarize the neuronal membrane after an action potential and thus setting the action potential frequency and neurotransmitter release in neurons.

In adult rat hippocampal and cerebellar slices, as well as in cultured spinal cord astrocytes, the *Shaker* type potassium channel Kv1.5 protein has been found (Roy et al., 1996). In cultured hippocampal astrocytes, K_A currents have been shown to be mediated by *Shaw* Kv3.4 and *Shal* Kv4.3 channels (Bekar et al., 2005). NG2 glia or OPCs express several subunits of the *Shaker* type Kv1 family (Chittajallu et al., 2002; Vautier et al., 2004).

Since neither astrocytes nor NG2 glia conduct action potentials, the presence and function of Kv channels in these cells remains enigmatic. However, some hypotheses have been proposed, such as the role of K_{DR} and K_A currents during cell division (Pardo, 2004) or in the apoptotic process (Burg et al., 2006). In certain pathological conditions characterized by an almost total loss of inward rectifier conductance, K_{DR} currents mediated by Kv channels might maintain the negative RMP of glial cells (Pannicke et al., 2000).

2. AIMS OF THE STUDY

The primary goal of my doctoral studies was to characterize the changes in the membrane properties of astrocytes and NG2 glia after an ischemic injury of the CNS using two models – global cerebral ischemia and incubation of rat spinal cord segments in a solution with high [K^+]. While the exposure of the rat spinal cord to high [K^+] represents an acute, *in vitro*, injury model, global cerebral ischemia is performed in animals *in vivo* and provides an opportunity to study the morphological, immunohistochemical and electrophysiological properties of glial cells during both the acute and chronic stages of recovery. Before starting the electrophysiological experiments, we determined the extent of the tissue injury in both ischemia models, which enabled us to assess their reproducibility and to correlate the time-dependent changes in the membrane properties of glial cells with the development of reactive astrogliosis, changes in glial cell morphology and the apoptotic and proliferative activity of astrocytes and NG2 glia.

The specific aims of the experiments were:

1. To elucidate the effect of global cerebral ischemia on the membrane properties of hippocampal astrocytes and NG2 glia with the main focus on the activity and expression of K^+ ion channels, such as inwardly rectifying K^+ channels and two-pore domain K^+ channels, in these glial cells.
2. To reveal the changes in the membrane properties of astrocytes prior to the onset of reactive astrogliosis formation in the rat spinal cord exposed to a solution with high [K^+].
3. To clarify, based on the obtained data, the role of K^+ ion channels in astrocytes and NG2 glia in the acute and chronic phases of the development of reactive astrogliosis after CNS ischemic injury.

3. METHODS

3.1 CNS INJURY MODELS

3.1.1 Induction of global cerebral ischemia in adult rats

All experiments involving the use of animals were performed in accordance with the European Communities Council Directive of 24 November 1986 (86/609/EEC) and animal care guidelines approved by the Institute of Experimental Medicine ASCR Animal Care Committee. All efforts were made to minimize animal suffering and to reduce the number of animals used. Wistar rats (male, 7-9 weeks old, 220-260 g) were premedicated with atropin (100 μg/kg, s.c.; Biotika, Slovak Republic) and anesthetized with sodium pentobarbital (PTB; 65 mg/kg, i.p.). The rats were intubated using a cannula tube (Abbocath-T 16G, Abbott, Sligo, Ireland) and held on mechanical ventilation (33.3% O_2 and 66.6% N_2; rate 60 cycles/min; Animal ventilator CIV-101, Columbus Instruments, Columbus, Ohio). GCI was induced by a bilateral, 15-minute common carotid arteries occlusion performed using aneurism clips. During occlusion, rats were ventilated with 6% O_2 and 94% N_2 (Linde Gas, Prague) as described previously (Dijkhuizen et al., 1998; Zoremba et al., 2008). The core temperature was maintained at 37°C with a heating pad throughout the procedure and recovery period until the animals awoke. After occlusion, the rats were left to survive (reperfusion period) for 2 hours, 6 hours, 1 day, 3 days, 7 days, 1 month, 3 months and 6 months (2H, 6H, 1D, 3D, 7D, 1M, 3M, 6M) prior to sacrifice. The animals were housed individually and allowed food and water *ad libitum*. Sham-operated animals receiving exactly the same surgical procedure without artery occlusion were used as controls for each reperfusion period.

3.1.2 Exposure of the rat spinal cord to high [K^+]

Wistar rats were sacrificed under Isoflurane anesthesia at postnatal days 9 to 11 (P9-11) by decapitation. Spinal cords were dissected out at 6-8°C, and 5-7-mm-long segments of the lumbar part of the spinal cord were isolated and incubated for 3 hours in either artificial cerebrospinal fluid (aCSF, as a control) or in aCSF containing 50 mM K^+

(aCSF50). To keep the solution iso-osmolar, aCSF50 had a reciprocally reduced Na^+ concentration.

3.2 ELECTROPHYSIOLOGICAL RECORDINGS

3.2.1 Preparation of acute tissue slices from brain or spinal cord

Acute CNS tissue slices were prepared basically as described by Edwards et al. (1989). After the reperfusion period, the rats were deeply anesthetized with PTB (100 mg/kg, i.p.) and perfused transcardially with cold (4°C) isolation solution containing (in mM): 110 NMDG-Cl, 3 KCl, 23 $NaHCO_3$, 1.25 Na_2HPO_4, 0.5 $CaCl_2$, 7 $MgCl_2$, 20 glucose, osmolality 290 mOsm/kg. The rats were decapitated, the brains were quickly dissected out and transversal 220-µm-thick slices were cut using a vibration microtome (HM 650V, Thermo Scientific Microm, Walldorf, Germany). The slices were incubated for 30 minutes at 34°C in the isolation solution and then held at room temperature (RT) in aCSF containing (in mM): 122 NaCl, 3 KCl, 28 $NaHCO_3$, 1.25 Na_2HPO_4, 1.5 $CaCl_2$, 1.3 $MgCl_2$, 10 glucose, osmolality 305 mOsm/kg. Solutions were equilibrated with 95% O_2/5% CO_2 to a final pH of 7.4. Osmolality was measured using a vapor pressure osmometer (Vapro 5520, Wescor, Logan, UT).

Acute spinal cord slices were prepared after rat spinal cord incubation in aCSF or aCSF50. The spinal cords were embedded in 2% agar cooled to ~ 37°C in the correct orientation to cut transversal slices. The agar block with the embedded spinal cord was glued on the stage of the tissue slicer. Transverse 220-µm-thick slices were made using an EMS-4000 automatic oscillating tissue slicer (Electron Microscopy Science, Hartfield, PA) in cooled aCSF. After sectioning, the slices were kept up to 6 hours in aCSF before the experiments.

3.2.2 Patch-clamp recordings

Acute brain or spinal cord slices were transferred to a recording chamber mounted on the stage of an upright microscope (Axioscop, Zeiss, Gottingen, Germany) equipped with a high-resolution digital camera (AxioCam HRc, Zeiss) and electronic micromanipulators (Luigs&Neumann, Ratingen, Germany). The slices were fixed using

a U-shaped platinum wire with a grid of nylon threads. The chamber was continuously perfused with oxygenated aCSF at a rate of 5 ml/min, at 27°C. Patch-clamp recordings in the whole-cell configuration (Hamill et al., 1981) were performed using an EPC-9 patch-clamp amplifier in combination with TIDA software (HEKA Elektronik, Lambrecht/Pfalz, Germany). Current signals were lowpass-filtered at 3 kHz and sampled at 5 kHz. Patch pipettes were pulled (P-97 Flaming/Brown Micropipette Puller, Sutter Instruments, Novato, CA) from borosilicate capillaries (Sutter Instruments) and filled with a solution containing (in mM): 130 KCl, 0.5 $CaCl_2$, 2 $MgCl_2$, 5 EGTA, 10 4-2-hydroxyethyl-1-piperazineethanesulfonic acid (HEPES); the final pH was adjusted to 7.2 with KOH. The pipette resistances were 7-10 MOhms.

The RMP was measured by switching the EPC-9 amplifier to the current-clamp mode. The membrane resistance (R_M) was calculated from the current elicited by a 10-mV test pulse depolarizing the cell membrane from the holding potential of -70 mV to -60 mV for 50 ms, at the end of the pulse. Membrane capacitance (C_M) was determined from the initial current transients elicited by the same test pulse, using the following equation: $\tau = R_M \times C_M$, as described previously (Schroder et al., 1999). Membrane currents were evoked by clamping the cell membrane from the holding potential of -70 mV to values ranging from -160 mV to +20 mV for 50 ms at 10-mV intervals. The outward-to-inward ratio of the currents in astrocytes was measured from the +20 mV and -160 mV voltage steps after offline offset correction of the currents to avoid shifts in the current amplitudes caused by the variable RMP.

The reversal potential (V_{rev}) was determined from the current/voltage (I/V) relationship plotted 45 ms after the onset of de- and hyperpolarizing pulses (duration 50 ms) ranging from -160 mV to +20 mV in 10-mV increments. The reversal potential of the tail current ($V_{rev\ tail}$) was determined from the I/V relationship measured 5 ms after the offset of a 20-ms depolarizing (+20 mV) prepulse followed by a series of 20-ms de- and hyperpolarizing pulses ranging from -130 mV to +20 mV. The K^+ accumulation in the vicinity of the cell membrane after a depolarizing prepulse (ΔK^+) was determined by subtracting the values of the extracellular K^+ concentration prior to ($[K^+_m]_e$) and after the depolarizing prepulse ($[K^+_{rev}]_e$) (Chvatal et al., 1999; Chvatal et al., 2004). Since the astrocytic membrane is almost exclusively permeable to K^+, $[K^+_m]_e$ and $[K^+_{rev}]_e$ can be calculated using the Nernst equation from the corresponding values of RMP and $V_{rev\ tail}$, respectively, i.e., $RMP = (RT/F)\ln([K^+_m]_e/[K^+]_i)$ and $V_{rev\ tail} = (RT/F)\ln([K^+_{rev}]_e/[K^+]_i)$.

Measurement of ΔK^+ was performed in aCSF and in hypotonic solution (200 mOsm/kg), which had a reduced concentration of NaCl (to 69 mM).

To isolate the K_{DR} current from the K_A current, voltage steps were preceded by a 100-ms prepulse depolarizing the membrane to -50 mV to inactivate the K_A current. K_{DR} current amplitudes were subsequently measured at +20 mV at the end of the pulse after subtracting offline the passive currents (the time- and voltage-independent current between -70 mV and -80 mV multiplied by the relative potential jumps) from the corresponding current traces. For maximal activation of the K_A current, a -110-mV prepulse of 170 ms duration was applied. The K_A current component was isolated by subtracting the current traces pre-clamped at -50 mV from those pre-clamped at -110 mV, and its amplitude was measured at +20 mV at the peak value, at the beginning of the pulse. K_{IR} currents were determined at -160 mV at the end of the pulse.

I_{Na} currents were activated by depolarizing steps from -70 mV to +20 mV following a 170-msec prepulse of -110 mV, and the corresponding current amplitudes were determined by passive current subtraction, as shown previously (Bordey and Sontheimer, 2000). The TTX-sensitivity of I_{Na} currents was confirmed in 15 cells in control spinal cord tissue and after spinal cord incubation in aCSF50.

Current densities (CDs) were calculated by dividing the maximum current amplitudes by the corresponding C_M for each individual cell. The patch-clamp data analyses were performed using software developed for our laboratory by Mgr. P. Pivonka.

3.3 IMMUNOHISTOCHEMISTRY

3.3.1 Post-recording cell identification

For cell identification after patch-clamp recording, the measured cells were filled with Alexa Fluor 488 or 594 hydrazide (0.1 mM; Molecular Probes, Invitrogen, CA) or by Lucifer Yellow dilithium salt (1 mg/ml) by dialyzing the cytoplasm with the patch pipette solution. Post-recording, the slices were fixed with 4% paraformaldehyde (PFA) in 0.1M phosphate buffer (PB) for 1 hour and then kept at 4°C in phosphate-buffered saline (PBS). The slices were incubated 2 hours at RT in a blocking solution containing 5% normal goat serum (NGS) or Chemiblocker (both Millipore, MA) and 0.5% Triton

in PBS. This blocking solution was also used as the diluent for the antisera. The slices were incubated with the primary antibodies at 4°C overnight. For astrocyte and NG2 glia identification, primary antibodies directed against GFAP, S100β or NG2 chondroitin sulfate proteoglycan were used (Table 1). The stained cells were visualized using appropriate secondary antibodies conjugated with a fluorochrome (Table 1). The secondary antibodies were applied for 2 hours at RT. After immunostaining, the slices were mounted using Vectashield mounting medium (Vector Laboratories, Burlingame, CA) and analyzed under a confocal microscope.

3.3.2 Immunohistochemical staining of fixed tissue sections

Animals were deeply anesthetized with PTB (100 mg/kg, i.p.) and perfused transcardially with 100 ml of saline followed by 200 ml of cooled 4% PFA in 0.1M PB. Brains were dissected out, post-fixed 3 hours and placed stepwise in solutions with gradually increasing sucrose concentrations (10%, 20%, 30%) for cryoprotection. Coronal, 20 μm or 40 μm thick slices were prepared using a cryostat (Leica CM1850, Leica Microsystems, Wetzlar, Germany) or a microtome (HM400, Thermo Scientific Microm), respectively. The slices were incubated with 5% NGS or Chemiblocker and 0.2% Triton in PBS. This blocking solution was also used as the diluent for the antisera. The primary antibodies (Table 1) were applied overnight at 4°C, and the secondary antibodies (Table 1) were applied for 2 hours at RT. Negative controls were performed using the same protocol omitting the primary antibodies. Slices were mounted with Vectashield alone or containing DAPI (to visualize cell nuclei; Vector Laboratories, Burlingame, CA) or Aqua PolyMount (Polysciences, Warrington, PA). All chemicals were purchased from Sigma-Aldrich (St. Louis, MO), unless otherwise stated.

A Leica TCS SP spectral confocal microscope or Zeiss 510DUO LSM equipped with Arg/HeNe lasers and 40x or 63x oil objectives were used for immunohistochemical analysis. Stacks of consecutive confocal images taken at intervals of 1 μm or 0.5 μm were acquired sequentially with the 2 lasers to avoid cross-talk between fluorescent labels. The background noise of each confocal image was reduced by averaging four image inputs. For each image stack the gain and detector offset were adjusted to minimize saturated pixels, yet still permit the detection of weakly stained cell processes. In all cases, the pinhole was set to 1 Airy unit. Colocalization images and

maximum *z* projection images were made using Leica confocal software or Zeiss LSM Image Browser.

Table 1: Primary and secondary antibodies used for immunohistochemistry

Antigen	dilution	type	manufacturer	sec. antibody
glia				
GFAP-Cy3	1:800	mouse IgG	Sigma-Aldrich	n/a
S100β	1:200	mouse IgG	Sigma-Aldrich	GAM 488/594
vimentin-Cy3	1:800	mouse IgG	Sigma-Aldrich	n/a
NG2	1:400	rabbit IgG	Millipore	GAR 488/594
CD11b	1:200	mouse IgG	Millipore	GAM 594
APC	1:100	mouse IgG	Calbiochem	GAM 488
neurons				
DCX	1:500	goat IgG	Santa-Cruz	DAG 594
NeuN	1:100	mouse IgG	Millipore	GAM 488/594
proliferation				
PCNA	1:200	mouse IgG	Millipore	GAM 594
nestin	1:1000	mouse IgG	Millipore	GAM 488/594
apoptosis/autophagy				
cleaved casp-3	1:50	rabbit IgG	Cell Signalling	GAR 488/594
cleaved PARP-1	1:200	mouse IgG	Cell Signalling	GAM 488/594
LC3-phospholipid	1:200	rat IgG	Novus Biological	CAR 488
Ion channels				
Kir2.1	1:200	rabbit IgG	Alomone Labs	GAR 488
Kir4.1	1:200	rabbit IgG	Alomone Labs	GAR 488
Kir5.1	1:200	rabbit IgG	Abcam	GAR 488
TREK1	1:200	rabbit IgG	Alomone Labs	GAR 488
TWIK1	1:200	rabbit IgG	Alomone Labs	GAR 488

GAR 488/594: goat anti-rabbit IgG conjugated with Alexa Fluor 488 or 594; GAM488/594: goat anti-mouse IgG conjugated with Alexa Fluor 488 or 594; DAG 594: donkey anti-goat IgG conjugated with Alexa Fluor 594; CAR 488: chicken anti-rat IgG conjugated with Alexa Fluor 488 (all from Molecular Probes). Anti-GFAP and vimentin antibodies were conjugated with Cy3.

GFAP, glial fibrillary acidic protein; CD11b, integrin Mac-1; APC, adenomatous polyposis coli; DCX, doublecortin; NeuN, neuron-specific nuclear antigen; PCNA, proliferating cell nuclear antigen; PARP, poly(ADP-ribose) polymerase; TREK, TWIK-related K^+ channel; TWIK, two-pore domain weak inwardly rectifying K^+ channel

3.4 CELL MORPHOMETRY AND CELL NUMBER QUANTIFICATION

3.4.1 Confocal 3D-morphometry

Dynamic changes in astrocyte morphology were quantified by estimating the cell volume from astrocyte images obtained by a LEICA TCS SP confocal microscope prior to and during the application of hypotonic solution (Fig. 13). Four hundred-micrometer-thick slices from mice expressing enhanced green fluorescent protein (EGFP) under the control of the human GFAP promoter (EGFP/GFAP mice, P10-12) (Nolte et al., 2001) were prepared in the same way as described above for rat spinal cord slices.

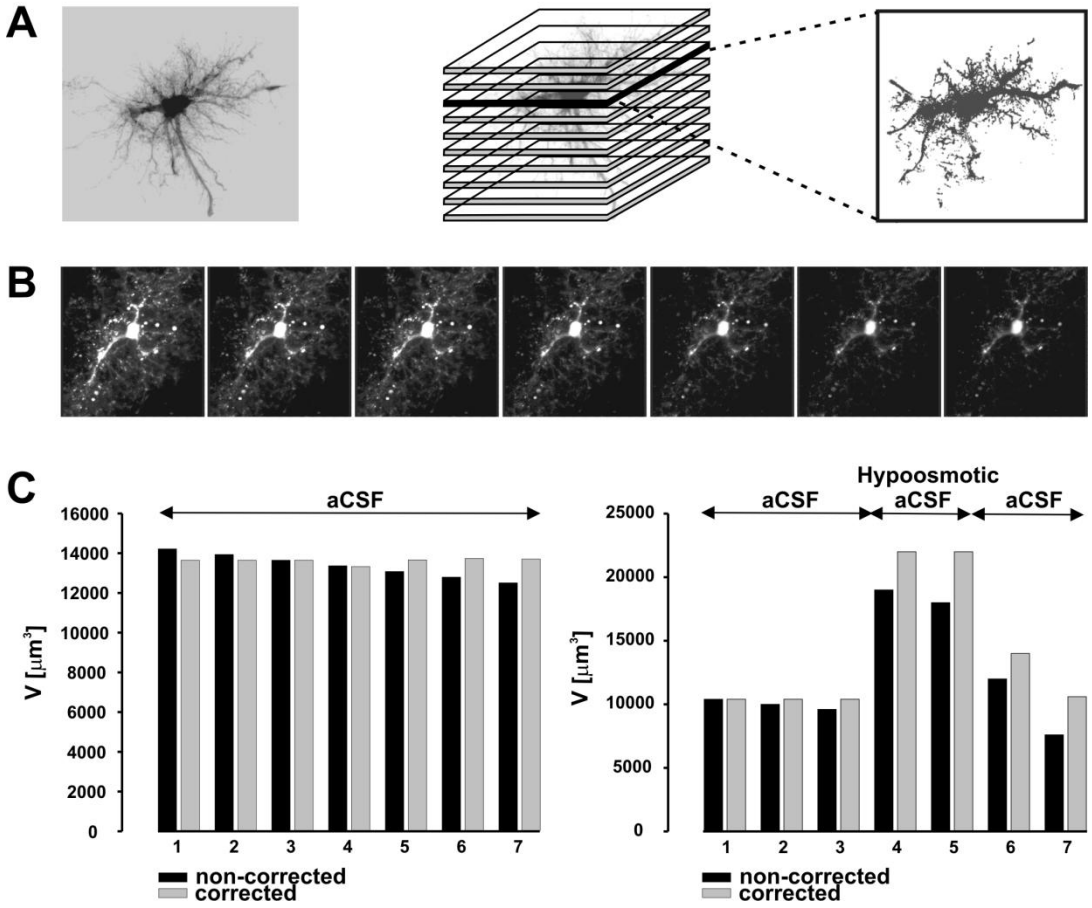

Fig. 13: 3D-confocal morphometry of EGFP/GFAP astrocytes and correction for photobleaching. **A**: The image of a brightly fluorescent EGFP-labeled cell (left) sectioned into a uniformly spaced (0.12 μm) set of 2D parallel images (middle). The cell surface was found in each image using an edge-detecting algorithm, and the area of the image surrounded by the edge was calculated for each image (right). **B**: The decrease in fluorescence intensity (photobleaching) of EGFP in a cell after exposure to the excitatory laser beam during confocal scanning. **C left**: A time-independent and linear decrease in cell volume was observed during 7 measurements in artificial cerebrospinal fluid (aCSF) (determined for the cell shown in

B). The black columns show the cell volume without correction for photobleaching, while the gray columns show the cell volume corrected for photobleaching. **C right**: Cell volume during 7 measurements (3 measurements in aCSF – used for photobleaching correction, 2 measurements during the application of hypotonic solution and 2 measurements during aCSF-washout). The black columns show the cell volume without correction for photobleaching, while the gray columns show the cell volume corrected for photobleaching.

The images of brightly fluorescent EGFP-labeled cells were sectioned into a uniformly spaced set of 2-dimensional parallel images (Fig. 13A). The cell surface was found in each image using an edge-detecting algorithm, and the area of the image surrounded by the edge was calculated for each image. The values of cell volume for individual cells were obtained by integrating the values of the edge length and area from all images in a set. Since the fluorescence intensity of the EGFP-labeled cells decreases due to their exposure to the excitatory laser beam, the estimated volume of the cells was corrected for the effect of photobleaching (Fig. 13B, C) (Chvatal et al., 2007a; Chvatal et al., 2007b; Benesova et al., 2009).

3.4.2 Cell counts

Changes in cell number due to cell death/proliferation were quantified by analyzing the number of cells in the hippocampal CA1 region in rats after GCI and comparing that to the number of cells in the same region in sham-operated animals. Brain slices from sham-operated animals were analyzed at 3 different time points – 7D, 1M and 6M after GCI. We used 2 rats for each time-point of reperfusion, and 4 consecutive coronal sections (40 μm thick) of a hippocampal segment (from bregma- caudally 3.3 – 3.6 mm) were analyzed from each rat. From each coronal brain section, 8 images (225 x 225 x 20 μm, step size 1 μm) of the hippocampal CA1 region covering the stratum radiatum, pyramidal cell layer and stratum oriens were taken from both hemispheres using a Zeiss 510 DUO laser scanning microscope. The regions selected for quantifying changes in cell number are shown in the insets of Figure 19A. The number of cells was estimated from superimposed images using GSA Image Analyzer v3.0.5 (Digital River, Eden Prairie, MN, USA). The changes in cell number were expressed either as the number of cells per section of 225 x 225 x 20 μm, or as the percentage of NG2/proliferating cell nuclear antigen (PCNA)-, S100β/PCNA- or NG2/nestin-positive cells from the total number of NG2- or S100β-positive cells.

3.5 MEASUREMENT OF $[K^+]_e$ AND pH_e

3.5.1 Measurement of $[K^+]_e$ and pH_e in the rat spinal cord

The $[K^+]_e$ and extracellular pH (pH_e) were measured using ion-selective microelectrodes (ISMs) as described previously (Sykova et al., 1992). Microelectrodes were inserted into a spinal cord segment from its dorsal surface. Double-barreled K^+-ISMs were filled with a liquid ion-exchanger (Corning 477317) and with 150 mM NaCl in the reference channel and calibrated in solutions containing 2, 3, 4, 6, 12 or 20 mM KCl in 150 mM NaCl. The same procedure was adopted to prepare double-barreled pH-sensitive microelectrodes. The reference channel was filled with 150 mM NaCl while the pH-sensitive channel contained liquid Hydrogen Ion Ionophore II-Coctail A (Sigma-Aldrich). The backfilling solution was composed of: 40 KH_2PO_4, 23 NaOH and 15 NaCl (mM, pH 7.0). The electrodes were calibrated in standard solutions of pH 7.0, 7.2, 7.4, 7.6, 7.8 and 8.0 with a background of 150 mM NaCl and 3 mM KCl.

3.6 WESTERN BLOT

3.6.1 Western blots of rat hippocampal tissue

Hippocampal tissue samples for Western blot analysis were isolated from rats after GCI (6H, 1D, 3D, 7D, 1M), sham operated animals (6Hs, 3Ds, 1Ms) or intact animals (controls). Rats were deeply anesthetized with PTB (100 mg/kg, i.p.), perfused transcardially with chilled isolation solution and decapitated. The brains were dissected out and cut into 500 μm thick slices. The CA1 region of the hippocampus was excised from each slice and homogenized using an ultrasound homogenizator in Tris buffer (pH 6.8) containing 10% glycerol and 1% sodium dodecyl sulphate (SDS). Total protein content in the homogenates was determined by the Micro BCA™ protein assay kit (Thermo Fisher Scientific, Rockford, IL, USA). Tissue homogenates were heated at 100°C for 5 min with 0.5% dithiothreitol (DTT). Equal amounts of proteins were separated on a 10% SDS-polyacrylamide gel and subsequently electrotransferred to a nitrocellulose membrane with a TE 70XP Semi-Dry Transfer unit (Hoefer, Holliston, MA, USA). Membranes were blocked with 5% non-fat dry milk in PBS-Tween buffer

(0.05% Tween) for 1 hour at RT. The incubation with the primary antibodies diluted in PBS containing 1% non-fat dry milk, 0.05% Tween and 0.1% NaN_3 was performed at 4°C overnight, followed by a 2 hour incubation with secondary anti-rabbit IgG antibody conjugated with peroxidase (Sigma-Aldrich) at RT. The following primary antibodies were used: rabbit anti-GFAP (1:600; Sigma-Aldrich), rabbit anti-Kir2.1 (1:200; Alomone Labs), rabbit anti-Kir4.1 (1:400; Alomone Labs), rabbit anti-Kir5.1 (1:600; Abcam), rabbit anti-TREK1 (1:200; Alomone Labs) and rabbit anti-TWIK1 (1:200; Alomone Labs). Finally, SuperSignal West Pico Chemiluminiscent Substrate (Thermo Fisher Scientific) was used to develop the Western blots.

3.6.2 GFAP quantification in the rat spinal cord

Segments of spinal cords were solubilized twice in SDS-polyacrylamide gel electrophoresis (PAGE) loading buffer (200 mM Tris-HCl, pH 6.8, 2% SDS, 10% glycerol, 50 mM DTT), extensively sonicated, boiled for 3 min, and loaded into the wells of a 10% SDS polyacrylamide gel. Denatured proteins were separated by electrophoresis at a constant current of 20 mA per gel and transferred to a nitrocellulose membrane by Western blotting. The membrane with transferred proteins was washed with PBS plus 0.01% Tween-20 (PBS-T), and incubated in PBS-T with 5% skim milk for 40 min at RT. The membrane was then incubated at RT with the primary mouse anti-GFAP antibody, diluted in PBS-T containing 1% skim milk to a final concentration of 1μg/ml, for 1 hour, then washed (3x10 min) and incubated with the secondary antibody (peroxidase conjugated goat anti-mouse IgG) for 1 hour. The proteins with bound antibody were visualized using an enhanced cytoluminiscent kit (Pierce, Rockford, IL) and then scanned to quantify the amount of GFAP in the spinal cord segments. All chemicals were purchased from Sigma-Aldrich.

3.7 STATISTICS

The results are expressed as the mean ± SEM. Statistical analyses of the differences between groups were performed using one-way ANOVA for multiple comparisons with Dunnett's post-hoc test or Student's *t* test, when appropriate. Values of $p<0.05$ were considered significant, $p<0.01$ very significant and $p<0.001$ extremely significant.

4. RESULTS

4.1 HIPPOCAMPAL DAMAGE AFTER GLOBAL CEREBRAL ISCHEMIA IN RATS

4.1.1 Cellular response

GCI induced by a bilateral, 15-minute common carotid artery occlusion and concurrent hypoxia triggered pyramidal cell damage and the formation of a gliotic scar, preferentially in the CA1 region of the hippocampus (Fig. 14, 15, 16). Neuron-specific nuclear antigen (NeuN) immunoreactivity markedly decreased within the first 3D after GCI, and no recovery of NeuN staining was detected within the next 3 - 6 months (Fig. 14A-F). A distinct time-dependent pattern of GFAP immunoreactivity was observed in the hippocampal CA1 region, similar to that described previously (Schmidt-Kastner et al., 1990; Petito and Halaby, 1993). In the acute phases of reperfusion (6H and 1D after GCI), hippocampal astrocytes had long, thin processes, while starting 3D after GCI typical reactive astrocytes with hypertrophied cell bodies and thickened processes appeared in the hippocampi (Fig. 14). Moreover, the reactive astrocytes displayed increased GFAP and *de novo* nestin expression (Fig. 14C-F right) (Frisen et al., 1995). The majority of nestin-positive astrocytes also expressed vimentin (Fig. 16A), another marker of reactive astrocytes (Schiffer et al., 1993). This pattern of reactive gliosis persisted in the CA1 region of the hippocampus up to several months after GCI.

An antibody against NG2 chondroitin sulfate proteoglycan was used to visualize the changes in NG2 glia morphology in response to GCI. Increased NG2 immunoreactivity was observed in the CA1 region of the hippocampus; however, this increase in NG2 staining was partially due to the enhanced expression of NG2 chondroitin sulfate proteoglycan in reactive microglia (Fig. 15). In addition, nestin-positive NG2 glia were detected in all regions of the CA1 hippocampus starting 1D after GCI (Fig. 16B).

Based on CD11b immunoreactivity, activated microglia could be detected in the CA1 region of the hippocampus from 1D after GCI onwards. Increased CD11b immunoreactivity persisted in the hippocampal CA1 region up to 1M after GCI, while later it declined (Fig. 15).

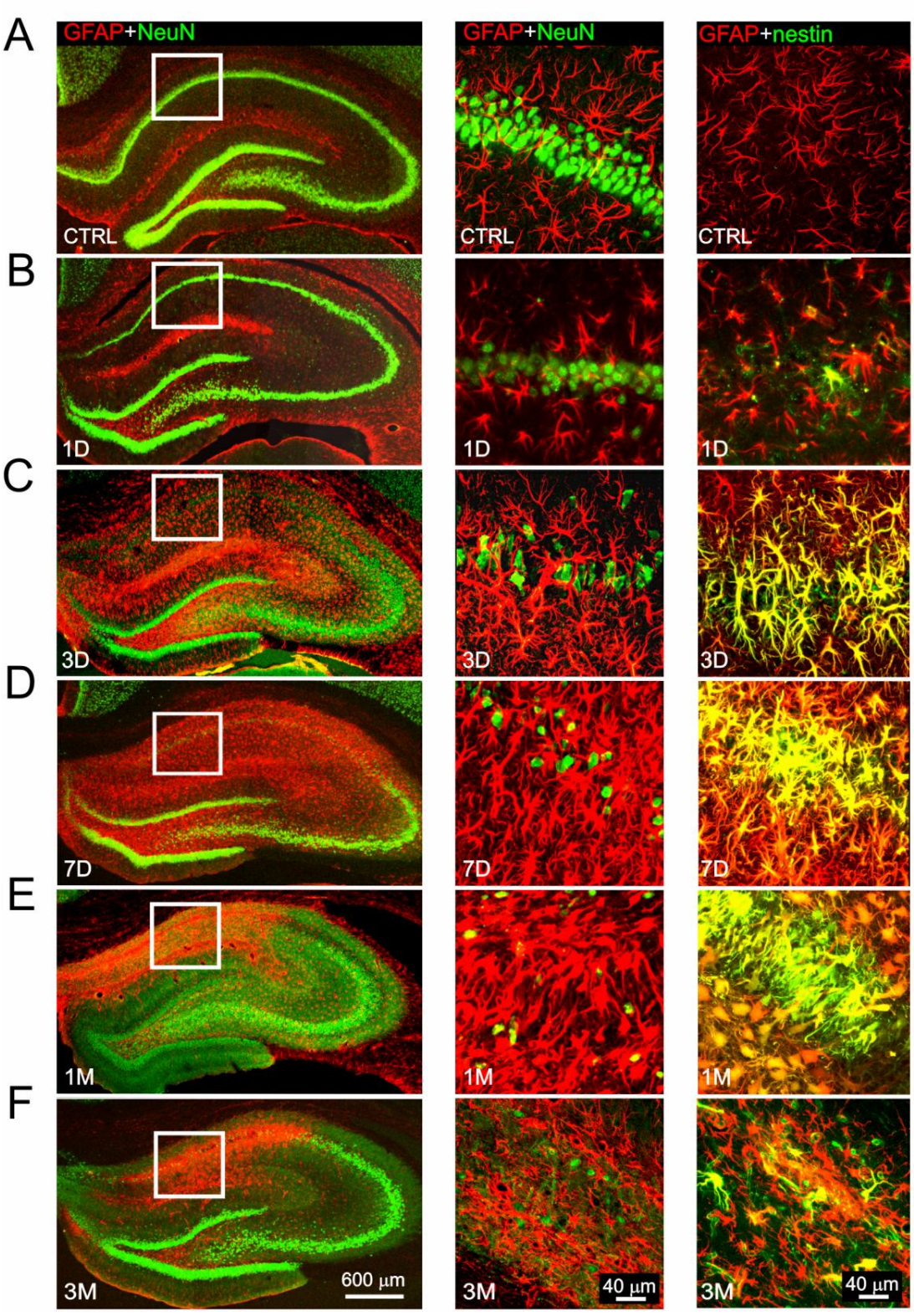

Fig. 14: **Immunohistochemical analyses of the rat hippocampus after GCI followed by reperfusion.** Coronal sections of the rat hippocampus (**left**) immunostained for NeuN and GFAP in controls (**A**) and 1 day (**B**), 3 days (**C**), 7 days (**D**) 1 month (**E**) and 3 months after GCI (**F**). Enlargements of the tissue section shown on the **right** illustrate changes in immunoreactivity for NeuN, GFAP and nestin in the hippocampal CA1 region. Yellow color indicates double-stained GFAP/nestin-positive cells.

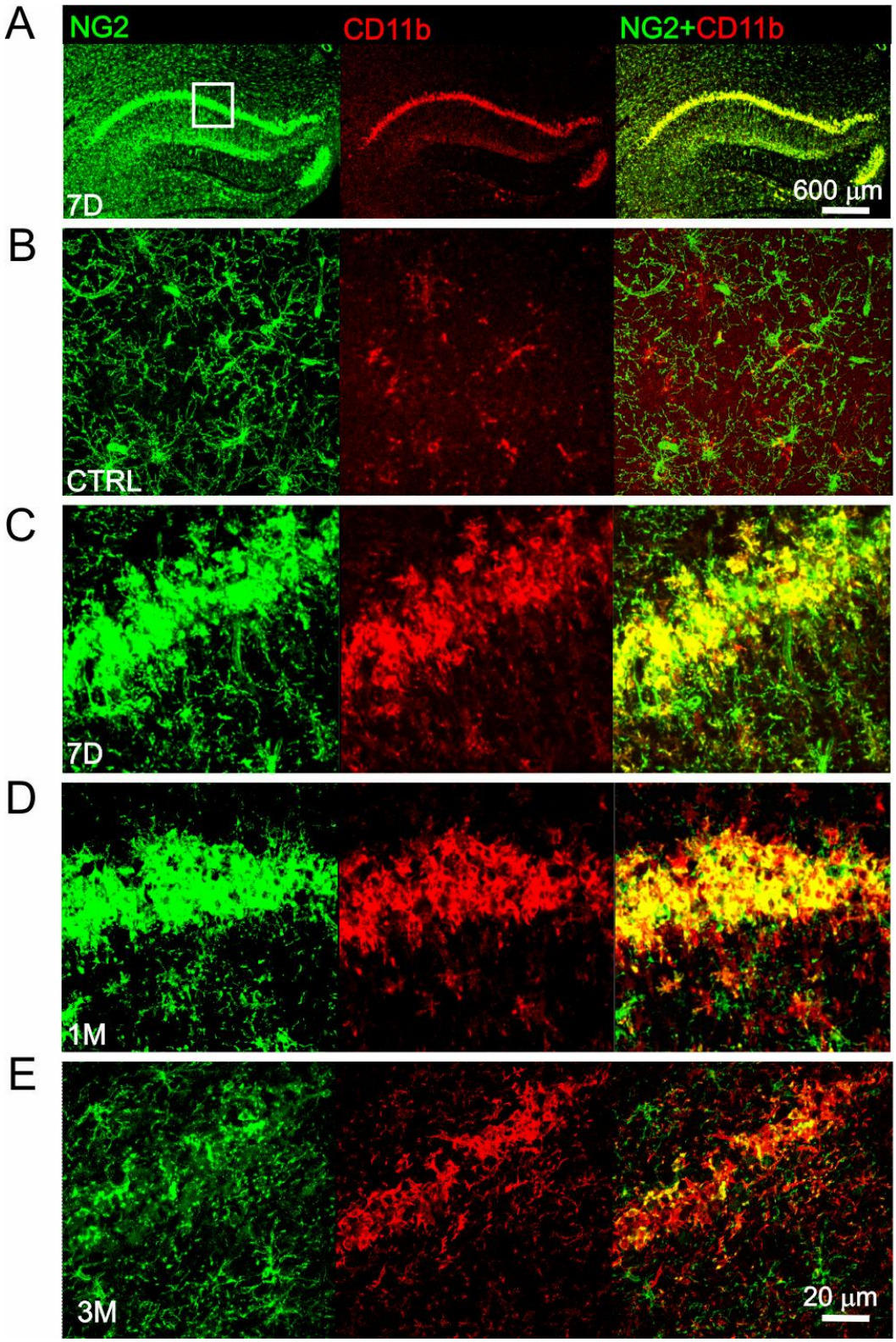

Fig. 15: Microglia activation and changes in NG2 immunoreactivity in the rat hippocampus after GCI. Coronal sections of the rat hippocampus 7 days after GCI immunostained for NG2 and CD11b (**A**). Enlargements of the tissue sections shown in **B-E** illustrate changes in immunoreactivity for NG2 and CD11b in the hippocampal CA1 region in controls (**B**) and 7 days (**C**), 1 month (**D**) and 3 months (**E**) after GCI. Yellow color indicates double-stained NG2/CD11b-positive cells.

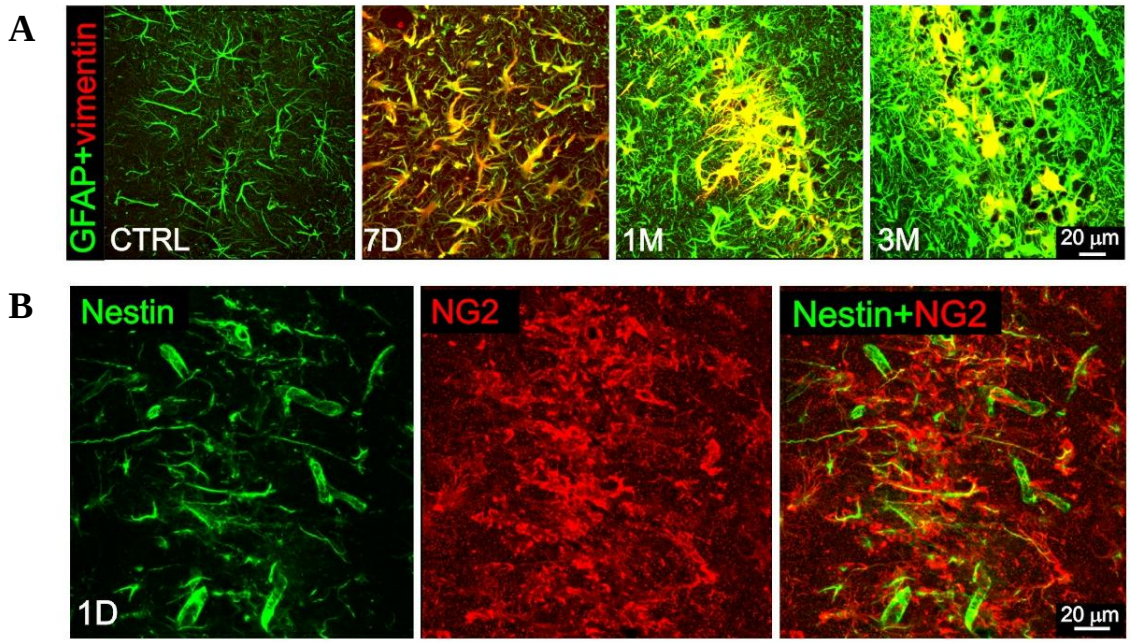

Fig. 16: Staining of hippocampal glial cells for vimentin and nestin after transient GCI. (**A**) The changes in immunoreactivity for vimentin and GFAP in the hippocampal CA1 region 7 days, 1 and 3 months after GCI. Yellow color indicates double-stained GFAP/vimentin-positive cells. (**B**) Nestin-positive NG2 glia were detected in the hippocampal CA1 region starting 1 day after GCI.

4.1.2 Cell death/proliferation induced by GCI in the rat hippocampal CA1 region

Cell death occurs in the post-ischemic brain and affects neurons as well as glial cells, namely astrocytes and oligodendrocytes (Giffard and Swanson, 2005; Adhami et al., 2007). Six hours after GCI, cleaved caspase-3 was detected in pyramidal neurons of the CA1 hippocampal region followed by the appearance of cleaved PARP-1, resulting in neuronal death 7D after GCI as visualized by Fluoro-Jade B (FJB) staining and the terminal deoxynucleotidyl transferase dUTP nick end labeling (TUNEL) assay (Fig. 17A-D). Despite the fact that astrocytes displayed increased immunoreactivity for cleaved caspase-3 in the early stages of reperfusion, FJB- or TUNEL-positive astrocytes were not detected within 7D of reperfusion. However, FJB- and TUNEL-positive hippocampal astrocytes were found 1M and 3M after GCI. As has been shown, autophagy, another type of cell death, is more pronounced in adult brains (Rami et al., 2008), therefore the autophagosome-related marker LC-3 was used to visualize cells undergoing autophagy (Fig. 17E). We did not find any adenomatous polyposis coli (APC)/TUNEL- or APC/LC3-positive oligodendrocytes within the hippocampal CA1

region; however, several LC3-positive or TUNEL-positive astrocytes were detected 1M after GCI, but only in the vicinity of the damaged CA1 pyramidal layer. Thus, we can conclude that neurons undergo apoptosis during the early phases of reperfusion, while astrocytes in the vicinity of the CA1 pyramidal cell layer undergo apoptosis/autophagy only in the late phases of reperfusion.

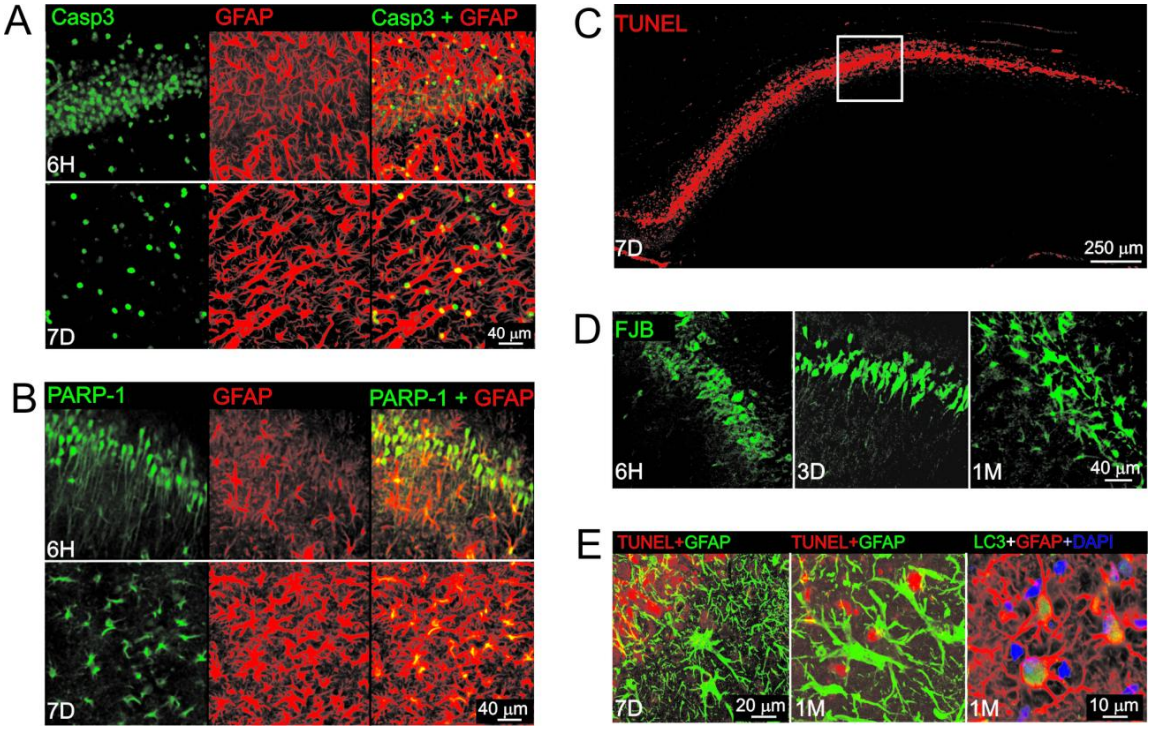

Fig. 17: Apoptosis/autophagy of neurons and astrocytes in the hippocampal CA1 region after GCI. The brain tissue sections illustrate changes in immunoreactivity for cleaved caspase-3 (Casp3, **A**) and the cleaved form of PARP-1 (**B**) in the hippocampal CA1 region 6 hours and 7 days after GCI. Note that 6 hours after GCI, mainly the pyramidal neurons are Casp3- and PARP-1-positive, while after 7 days astrocytes are positive for both apoptotic markers. A coronal section of the rat hippocampus 7 days after GCI immunostained for apoptotic cells using the TUNEL assay (**C**). Enlargements of the tissue shown in **D** demonstrate the time-dependent changes in FJB staining after GCI: from the left, damaged neurons after 6 hours and 3 days of reperfusion and FJB-positive astrocytes in the vicinity of the pyramidal layer 1 month after GCI. Higher magnification of TUNEL labeling in the CA1 region and GFAP illustrates apoptotic pyramidal neurons 7 days after GCI, while TUNEL/GFAP-positive or LC3/GFAP-positive astrocytes that appeared 1 month after GCI are shown in **E**.

Based on PCNA immunoreactivity, extensive proliferation was detected in the CA1 region 3-7D after GCI, and the majority of PCNA-positive cells were CD11b-positive microglia (Fig. 18A, B). Besides proliferating microglia, also PCNA-positive

NG2 glia and PCNA-positive astrocytes were detected during the acute as well as the late stages of reperfusion (Fig. 18C).

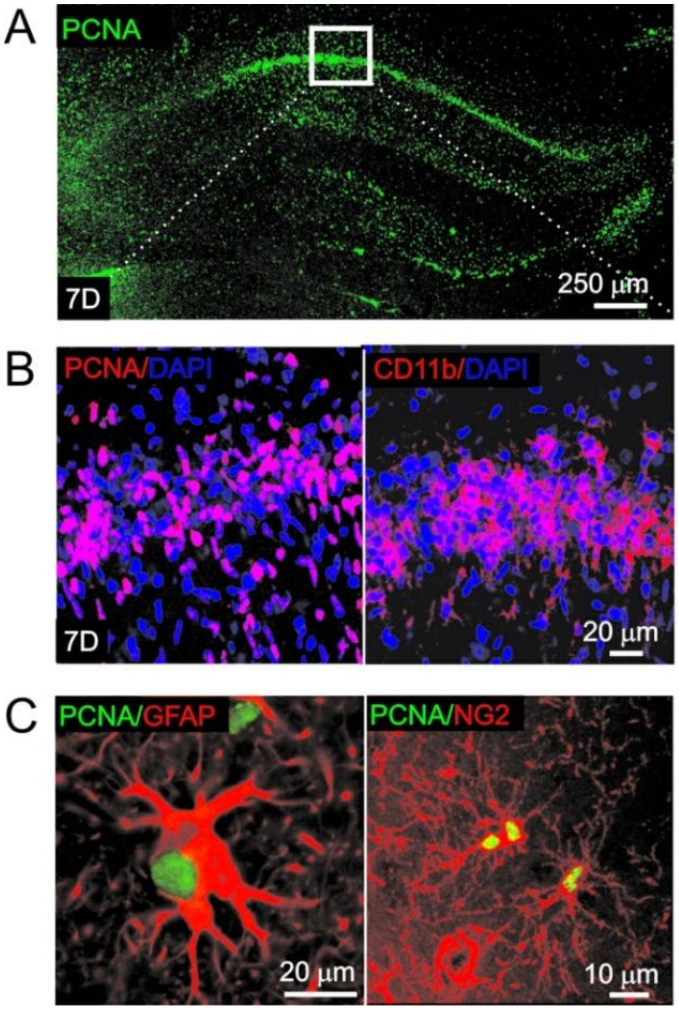

Fig. 18: Glial cell proliferation in the rat hippocampus induced by GCI. A coronal section of the rat hippocampus 7 days after GCI immunostained for PCNA (**A**). Enlargement of the tissue sections illustrate increased immunoreactivity for PCNA (**B**, **left**) and CD11b (**B**, **right**) in the CA1 region of the hippocampus 7 days after global cerebral ischemia. **C**: A detailed image of a PCNA-positive astrocyte (left) and PCNA-positive NG2 glia (right).

4.1.3 Time-dependent changes in the cellular composition of the hippocampal CA1 region during reperfusion after GCI

DAPI (4'6-diamidino-2-phenylindole)-, PCNA-, NeuN-, S100β-, NG2-, ACP- and CD11b-positive cells were counted in the stratum pyramidale and the adjacent stratum radiatum and stratum oriens of the CA1 region in order to quantify the changes in cell number after GCI (Fig. 19A-D). Since we found no significant differences between the numbers of DAPI-, PCNA-, GFAP-, NG2-, CD11b- and APC-positive cells in the hippocampus of sham-operated rats at different time points after GCI (1D, 1M, 6M), all sham-operated animals were pooled and used as controls. Counting DAPI-positive cells revealed a marked increase in total cell number in the CA1 region of the hippocampus

3D, 7D and 1M after GCI, caused mainly by the massive proliferation of microglia. The number of microglia was increased from 1D onwards, reaching a maximal number 3-7D after GCI, then started to decline after 1M of reperfusion, but still remained elevated above the control values 6M after GCI (Fig. 19B).

On the other hand, the number of NeuN-positive cells decreased within the first 7D of reperfusion, approximately by ~75%, and additional decreases after 1M and 3M resulted in a ~90% neuronal reduction when compared to control rats (Fig. 19B). The number of astrocytes decreased 6H after GCI, while 1, 3 and 6M after GCI it was noticeably increased. The number of oligodendrocytes (APC-positive cells) declined 6H and 1D after GCI, while after 7D it first increased and then decreased below the numbers found in controls. A decrease in the number of NG2 glia was observed only 7D after GCI, coinciding with an increased number of APC-positive cells (Fig. 19C).

Besides microglia, which significantly contributed to increased cell numbers in the CA1 region, NG2 glia were also found to increasingly proliferate. Approximately ~20% of the total number of NG2-positive cells were proliferating 1D after GCI, and this proportion raised to ~40% after 3D of reperfusion. Later, NG2 glia proliferation started to decline, but still remained increased above the control values (Fig. 19D). Increased proliferation of astrocytes was detected 3D, 7D and 1M after GCI, but only 5-7% of the total number of astroglia were PCNA-positive (Fig. 19C, D). Taken together, within 6M of reperfusion, neuronal cell death and glial cell proliferation resulted in a marked cellular re-organization of the hippocampal CA1 region, where astrocytes and microglia were the most prevalent cell types.

Fig. 19: (see the next page) Time–dependent changes in the cellular composition of the hippocampal CA1 region after GCI due to increased cell death/proliferation. A: Time-dependent changes in the number of DAPI- and PCNA-positive cells per section (225 x 225 x 20 µm). Selected regions, where the cell counting was carried out, are shown in the inset. Two rats were used for each time point, two slices were taken for analysis from each animal (from bregma- caudally 3.3 – 3.6 mm) and 8 selected regions (225 x 225 x 20µm) were analyzed from each slice. All together, for each time point 32 hippocampal regions were analyzed. The following abbreviations were used: CTRL (control), 6H (6 hours), 1D (1 day), 3D (3 days), 7D (7 days), 1M (1 month), 3M (3 months) and 6M (6 months). **B**: Time-dependent changes in NeuN- (neurons) and CD11b-(microglia) positive cells. **C**: Changes in the number of NG2-, GFAP- and APC- (oligodendrocytes) positive cells. **D**: Time-dependent changes in the number of PCNA/S100β- and PCNA/NG2-positive cells expressed as a percentage of the total number of astrocytes or NG2 glia counted in the CA1 region. Note that almost 40% of NG2 glia and only 6% of astrocytes in the CA1 region proliferated 3 days after GCI.

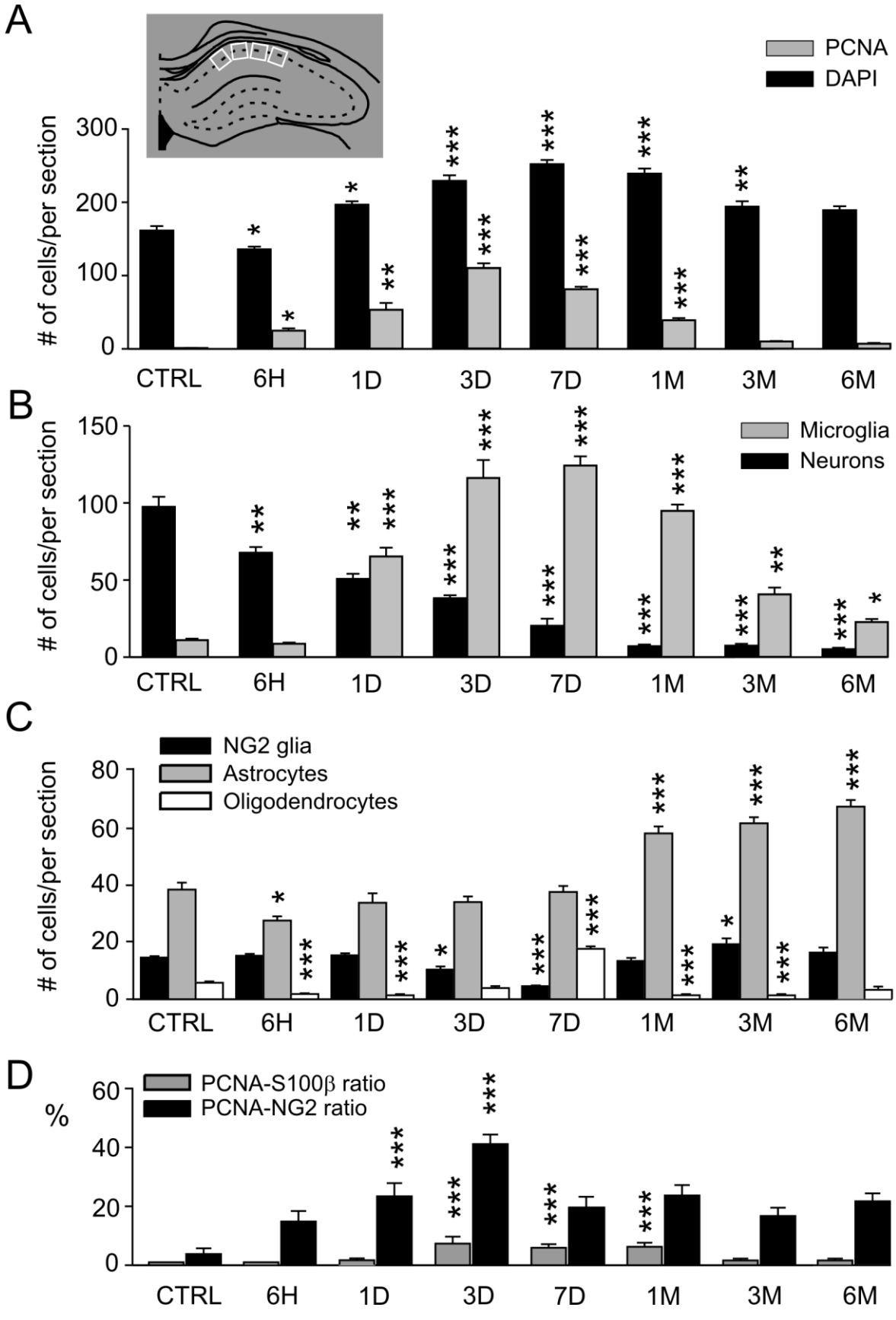
A
PCNA
DAPI
# of cells/per section
300
200
100
0
CTRL
6H
1D
3D
7D
1M
3M
6M
B
Microglia
Neurons
# of cells/per section
150
100
50
0
C
NG2 glia
Astrocytes
Oligodendrocytes
# of cells/per section
80
60
40
20
0
D
PCNA-S100β ratio
PCNA-NG2 ratio
%
60
40
20
0

4.1.4 Morphological changes of hippocampal astrocytes and NG2 glia after GCI

Morphological changes of astrocytes and NG2 glia represent a part of the functional alterations in glial cells after ischemia. In order to quantify their total cell volume changes induced by ischemia, and also to compare the contribution of the cell soma and cell processes to the total cell volume in astrocytes or NG2 glia of control rats and those 3D and 1M after GCI, we generated 3-dimensional images of Alexa-Fluor-hydrazide-labeled astrocytes and NG2 glia (Fig. 20, 21). Three days after GCI, the average values of total astrocyte volume (V), the volume of the processes (V_p) and the volume of the cell soma (V_s) were not significantly different from those obtained in the CA1 region of

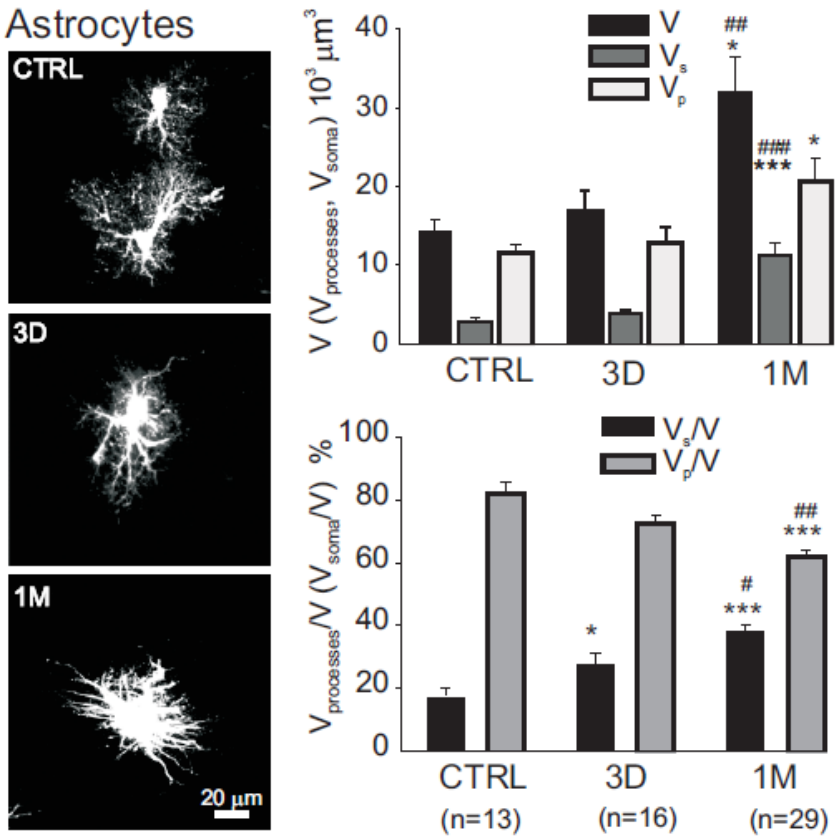

Fig. 20: Changes in morphology evoked by GCI in the hippocampal CA1 region. left: Superimposed confocal mages of CA1-hippocampal astrocytes in control rats (top), 3 days (middle) and 1 month after GCI (bottom). **right-top:** The time-dependent changes in total astrocyte volume (V) and the volumes of the astrocyte soma (V_s) and processes (V_p). **right-bottom:** The V_s and V_p expressed as a percentage of total cell volume. Asterisks (*) indicate significant differences between astrocytes from control and ischemic rats, while crosshatches (#) indicate significant differences between astrocytes 3 days and 1 month after GCI.

control animals. On the other hand, there was a marked increase in V, V_p and V_s after 1M of reperfusion. In addition, the differences in reactive astrocytes between the acute and late phases of reperfusion became more obvious when their compartments, i.e. the V_p and V_s, were compared and expressed as a percentage of V. In controls, an astrocytic cell soma occupied ~20% of the total cell volume and ~80% was taken up by the cell processes; however, 1M after GCI the astrocytic cell soma comprised ~40% of the total cell volume and 60% consisted of the cell processes (Fig. 20).

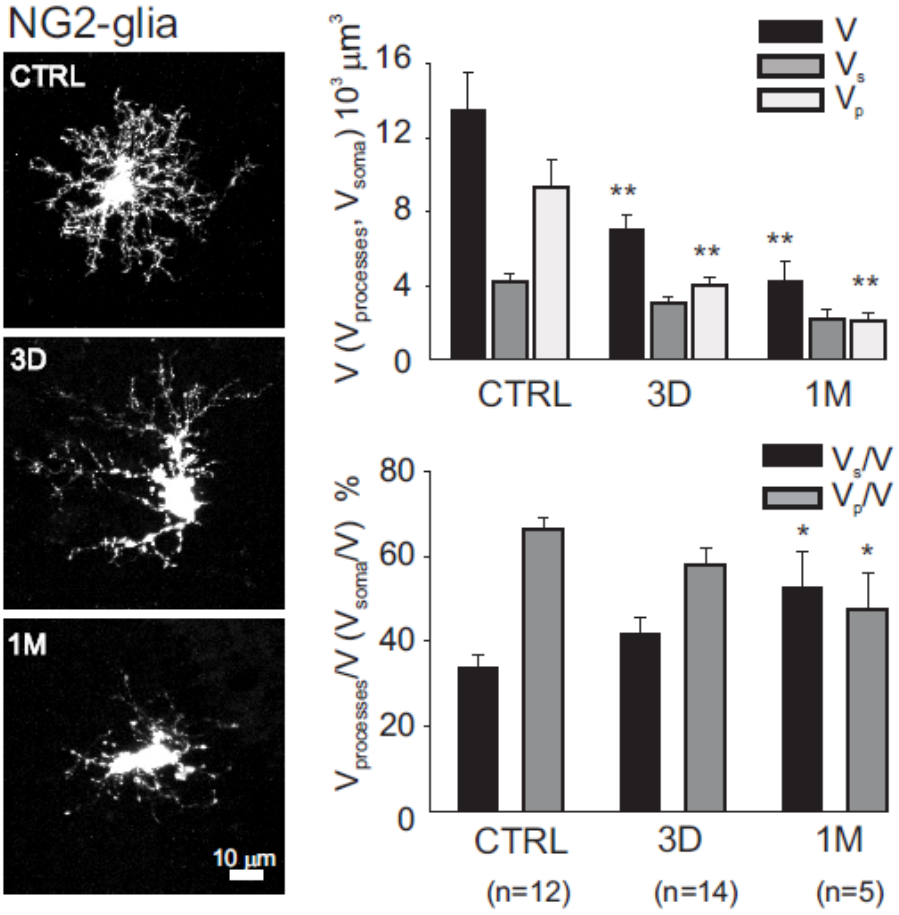

Fig. 21: Changes in NG2 glia morphology evoked by GCI in the hippocampal CA1 region. left: Superimposed confocal images of CA1-hippocampal NG2 glia in control rats (top), 3 days (middle) and 1 month after GCI (bottom). **right-top:** The time-dependent changes in total NG2 glia volume and the volumes of the cell soma (V_s) and processes (V_p). **right-bottom:** The volumes of the soma and processes of NG2 glia cells expressed as a percentage of total cell volume. Asterisks (*) indicate significant differences between NG2 glia from control and ischemic rats, while crosshatches (#) indicate significant differences between NG2 glia 3 days and 1 month after GCI.

Compared to NG2 glia from control rats, the average V and V_p of NG2 glia were reduced 3D and 1M after GCI, while V_s remained unchanged. Similarly to astrocytes, the contribution of V_s to V in NG2 glia increased as the cell processes retracted (Fig. 21). In controls, the cell soma occupied ~30% of the total cell volume and ~70% was taken up by cell processes, while 1M after GCI the cell soma of NG2 glia made up ~55% of the total cell volume and the cell processes 45% (Fig. 21).

In summary, 1M after GCI, the reactive astrocytes were significantly enlarged, while NG2 glia showed a reduced total cell volume during reperfusion. In both cell types, the percentage contribution of the cell soma markedly increased.

4.2 MEMBRANE PROPERTIES OF HIPPOCAMPAL GLIAL CELLS AFTER GLOBAL CEREBRAL ISCHEMIA

4.2.1 Astrocyte membrane properties after GCI

Membrane currents were recorded from astrocytes in the CA1 region (stratum radiatum) of adult rat hippocampi in sham operated rats (controls) and rats 2H, 6H, 1D, 3D, 7D and 1M after GCI using the patch-clamp technique in the whole-cell configuration. Cells with small (~10 μm) irregularly shaped cell bodies were selected as putative astrocytes in slices of control rats and those 2H, 6H and 1D after ischemia. Starting 3D after ischemia, hippocampal astrocytes displayed a reactive phenotype with large (~20-30 μm), spindle-shaped cell bodies. Dialyzing the cytoplasm of measured astrocytes with fluorescent dye from the patch pipette revealed a "bushy" appearance, i.e. the astrocytes had several primary processes, which densely ramified into many fine secondary processes (Fig. 22A). Astrocytes were extensively dye-coupled both in controls and at any studied time point after ischemia, and they stained positively for GFAP (Fig. 22A). In hippocampal astrocytes of control rats and those after GCI, clamping the cell membrane from the holding potential of -70 mV to values ranging from -160 mV to +20 mV elicited predominantly time- and voltage-independent currents with a linear current/voltage relationship (Fig. 22B, C). This type of membrane current, carried primarily by K^+ ions, has been shown to be typical of mature astrocytes (Wallraff et al., 2004; Zhou et al., 2006). Since we did not find any significant differences in any of the studied parameters in astrocytes among the control animals

(sham-operated rats with different reperfusion periods), the control astrocytes were combined into a single control group for the statistical analysis.

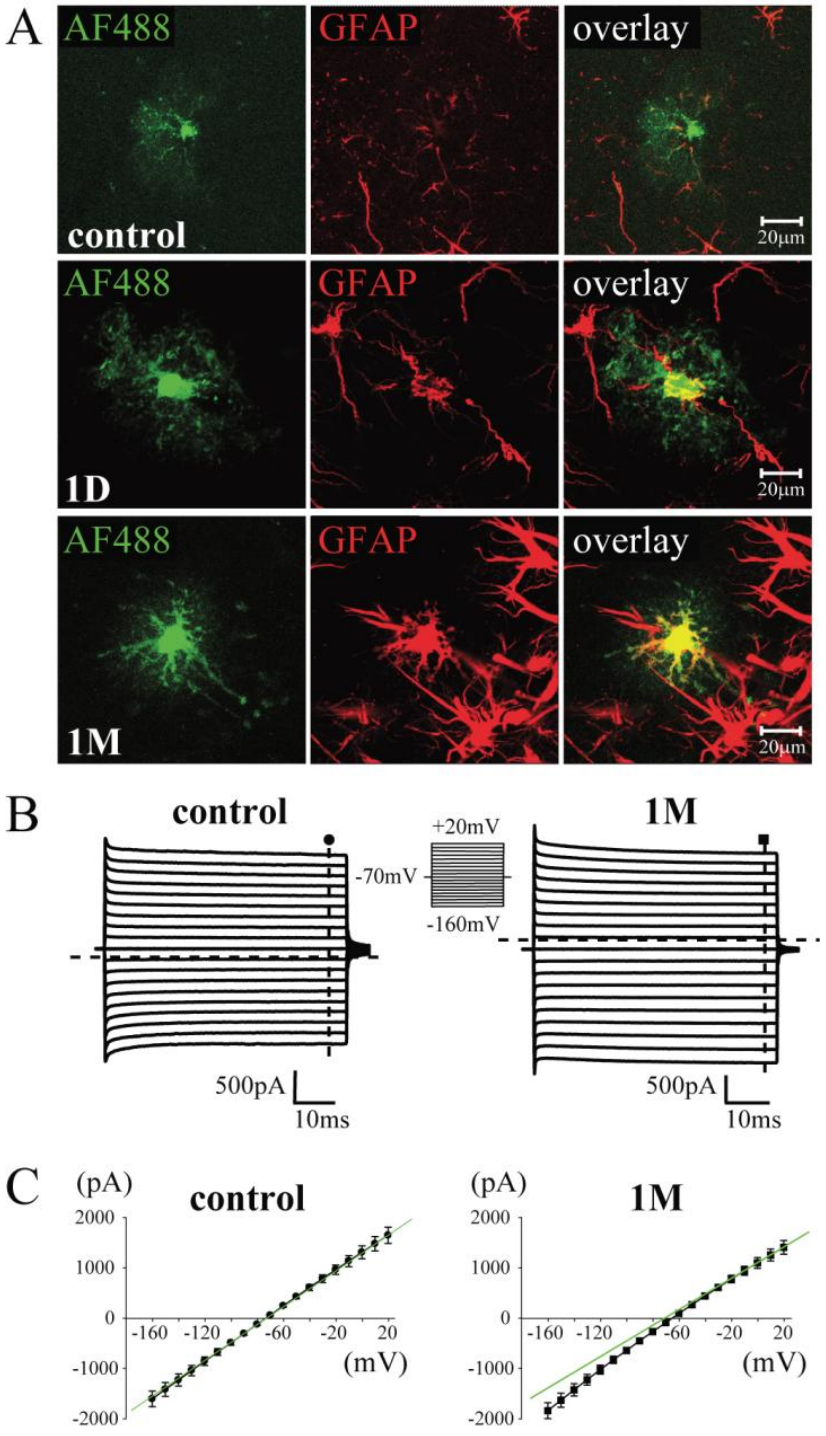

Fig. 22: The morphology and current pattern of hippocampal astrocytes after GCI. A: Astrocytes in control hippocampus, 1 day and 1 month after GCI, loaded with Alexa Fluor 488 hydrazid (AF488) during patch-clamp measurement and stained post-recording with an antibody directed against GFAP. Note that the reactive astrocytes 1 month after ischemia display a hypertrophied morphology compared to astrocytes in controls or 1 day after ischemia. **B:** Astrocyte currents in controls (left) and 1 month (right)

after ischemia revealed by membrane depolarization from a holding potential of -70 mV to +20 mV and hyperpolarization to -160 mV for 50 ms (see the inset in the middle). Zero current is marked by the dashed-line. **C:** Astrocytes, both in controls and 1 month after ischemia, display predominant time- and voltage- independent conductance with a linear I/V relationship. Moreover, astrocytes 1 month after ischemia show a higher degree of inward rectification compared to controls, as visualized by the green line interlaid through the mean I/V plots. The I/V plots were constructed from the currents elicited by membrane depolarization from a holding potential of -70 mV to +20 mV and hyperpolarization to -160 mV in control astrocytes (n=61) and those 1 month after ischemia (n=71).

The RMP of hippocampal astrocytes did not significantly change at 2H, 6H or 1D after ischemia compared to controls; however, starting 3D after ischemia, astrocytes displayed a progressive depolarization (Table 2). In controls, the average RMP of astrocytes was -75.7 ± 0.7 mV (n=61), and it shifted to -66.6 ± 0.8 mV (n=71; $p<0.001$) 1M after GCI. Astrocytes showed a significant increase in R_M only 7D after GCI and a decrease in their C_M 1D and 7D after ischemia (Table 2). Moreover, by calculating the ratio between the total outward and inward (out/in) currents in astrocytes we found an increase in the inward rectification of the currents in astrocytes 1M after ischemia compared to controls (Table 2; Fig. 22B, C). The out/in current ratio was 0.98 ± 0.02 (n=61) in controls, while it significantly decreased in astrocytes 1M after ischemia (0.90 ± 0.02; n=71; $p<0.05$).

4.2.2 Expression of K^+ channels in the hippocampus after GCI

Since the astrocyte membrane potential is maintained by inwardly rectifying K^+ channels, namely the Kir4.1 channel (Neusch et al., 2006; Djukic et al., 2007), changes in its expression might contribute to the depolarized RMP in astrocytes after GCI. Therefore, we evaluated Kir4.1 expression in the CA1 region of the hippocampus in control rats and in those subjected to GCI followed by different periods of reperfusion, using the Western blot technique. We found a decrease in Kir4.1 protein expression starting 3D after ischemia compared to controls (Fig. 23A).

Table 2: Membrane properties of hippocampal astrocytes in controls and after GCI

	RMP (mV)	R_M (MOhms)	C_M (pF)	out/in	n
CONTROLS	-75.7±0.7	64.1±6.3	26.6±2.5	0.98±0.02	61
2H	-74.8±1.3	54.1±8.6	23.9±3.6	1.01±0.02	25
6H	-72.9±0.7	67.5±5.1	19.7±2.7	0.94±0.02	43
1D	-74.2±0.7	80.2±4.0	14.6±1.0**	0.97±0.02	69
3D	-70.9±1.0**	71.9±7.0	19.7±2.4	1.0±0.02	38
7D	-66.5±1.3***	100.2±10.1**	12.8±1.8**	0.93±0.01	25
1M	-66.6±0.8***	74.6±4.8	19.5±2.4	0.9±0.02*	71

RMP, resting membrane potential; R_M, membrane resistance; C_M, membrane capacitance; out/in, outward/inward current ratio. The values are presented as mean ± S.E.M. Statistical significance was calculated using one-way ANOVA with Dunnett's post-hoc test; * $p<0.05$, significant; ** $p<0.01$, very significant; *** $p<0.001$, extremely significant.

In addition to Kir4.1, hippocampal astrocytes have been shown previously to express other K^+ ion channels, such as Kir2.1, Kir5.1, two-pore domain weak inwardly rectifying K^+ channel-1 (TWIK1) and TWIK-related K^+ channel-1 (TREK1) (Schroder et al., 2002; Kang et al., 2008; Seifert et al., 2009; Zhou et al., 2009). Western blot analysis revealed no differences in the expression of Kir2.1 and Kir5.1 channel subunits in the CA1 region of the hippocampus after GCI compared to controls (Fig. 23A). Concerning K_{2P} channels, we found no marked differences in the expression of TREK2 or TWIK1 in the CA1 region of the hippocampus after GCI compared to controls (Fig. 23B). However, the anti-TREK1 antibody stained two bands of ~ 41 and 47 kDa; the latter appeared starting 3D after GCI (Fig. 23B), thus correlating with the onset of reactive gliosis as assessed by GFAP protein expression (Fig. 23C). The decrease in the amount of GFAP protein 6H and 1D after ischemia (Fig. 23C) might be caused by GFAP protein degradation, as described previously (Lukaszevicz et al., 2002; Acarin et al., 2007).

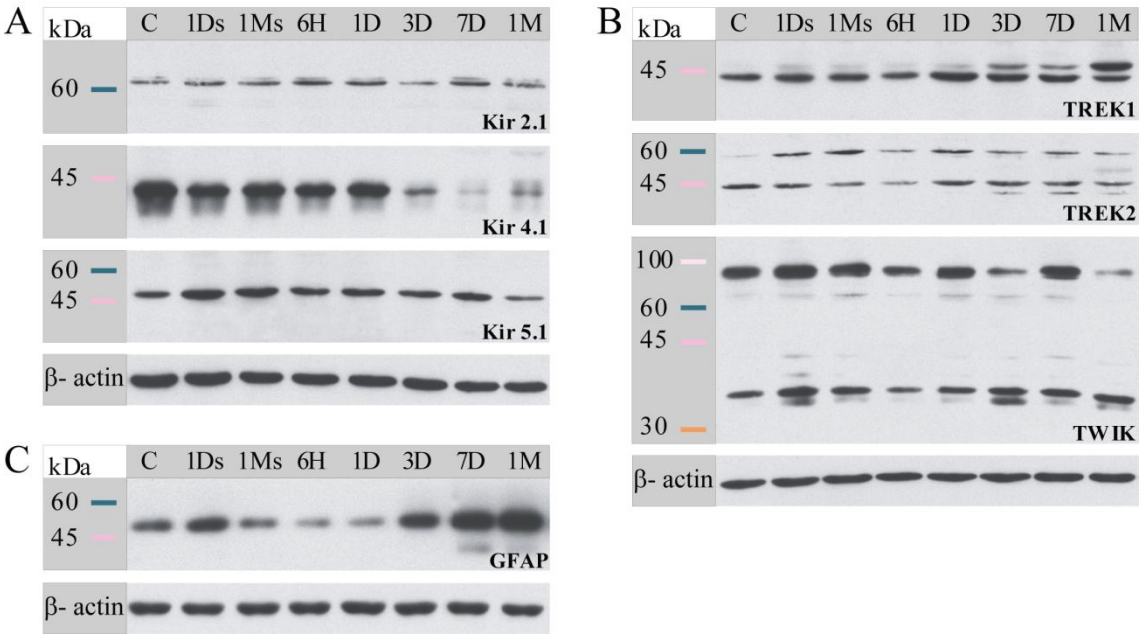

Fig. 23: Changes in the expression of Kir and K_{2P} channels in the CA1 region of the hippocampus after GCI. A: Kir2.1, Kir4.1 and Kir5.1 channel expression in the rat hippocampus in animals without surgery (C), in sham-operated animals (1Ds, 1Ms) and in animals 6 hours, 1 day, 3 days, 7 days and 1 month after ischemia, revealed by the Western blot technique. Kir4.1 channel expression shows a marked downregulation starting 3 days after GCI compared to controls. **B**: TREK1, TREK2 and TWIK1 expression in the rat hippocampus of non-operated animals (C), in sham-operated animals (1Ds, 1Ms) and in animals 6 hours, 1 day, 3 days, 7 days and 1 month after ischemia. The anti-TREK1 antibody stained two bands of ~ 41 and 47 kDa, the latter appeared starting 3D after GCI, representing another isoform of this channel. **C:** The expression of GFAP is downregulated 6 hours and 1 day after ischemia and upregulated starting 3 days after ischemia compared to non-operated (C) or sham-operated animals (1Ds, 1Ms).

To reveal in detail the cellular expression of the investigated K^+ ion channels, we performed immunohistochemical staining of the K^+ ion channels in the CA1 region of the hippocampus in control brain slices and those from rats subjected to GCI and different periods of reperfusion. Kir4.1 was expressed exclusively on GFAP-positive astrocytes (Fig. 24) during the whole studied timecourse after ischemia; however, we found its expression on the fine distal astrocytic processes only in controls and at early stages after ischemia (up to 1D) (Fig. 24; 1D inset), while later after ischemia we observed Kir4.1 staining mostly on the astrocyte cell bodies (Fig. 24; 1M inset). This observation correlates with the decreased Kir4.1 expression starting 3D after ischemia revealed by Western blot. In contrast to Kir4.1 channel expression, Kir2.1, Kir5.1 and

TREK1 were expressed in both neurons and astrocytes in the CA1 region of the hippocampus in controls and up to 7D after ischemia (Fig. 25, 26, 27). One month after GCI, when neurons were no longer present in the CA1 region of the hippocampus, we found the expression of these channel proteins almost exclusively in reactive astrocytes. Similar to the Kir4.1 channel, TWIK1 was also expressed exclusively in astrocytes in the CA1 region of the hippocampus during the whole studied timecourse after ischemia (Fig. 28). Since the total amount of Kir2.1 and Kir5.1 channel proteins does not change after ischemia, we might conclude that their relative expression increases in reactive astrocytes at later stages after ischemia (mostly at 1M). Moreover, the second isoform of the TREK1 channel, which appeared 3D after ischemia, might be expressed in reactive astrocytes. Similarly to other previously published data (Seifert et al., 2009), we found only negligible expression of TREK2 in hippocampal astrocytes (data not shown).

Fig. 24: (see the next page) Kir4.1 staining in the CA1 region of the hippocampus after GCI. The brain slices were stained with Kir4.1 antibody and an antibody directed against GFAP in controls and 6 hours, 1 day, 3 days, 7 days and 1 month after ischemia. Arrowheads show the fine Kir4.1-positive processes of astrocytes in controls and shortly after ischemia (6 hours, 1 day; see the inset). Such Kir4.1-positive dense processes are no longer present in astrocytes 1 month after ischemia (arrows; see the inset). (s.p. stratum pyramidale; s.r. – stratum radiatum)

Fig. 25: (see page 72) Kir2.1 staining in the CA1 region of the hippocampus after GCI. The brain slices were stained with Kir2.1 antibody and an antibody directed against GFAP in controls and 6 hours, 1 day, 3 days, 7 days and 1 month after ischemia. In controls and up to 7 days after ischemia, Kir2.1 is expressed in both GFAP-positive astrocytes and pyramidal neurons. One month after ischemia, only Kir2.1-positive astrocytes can be found in the CA1 region of the hippocampus. Arrows show Kir2.1/GFAP negative cells, presumably neurons, in the stratum radiatum. (s.p. stratum pyramidale; s.r. – stratum radiatum)

Fig. 26: (see page 73) Kir5.1 staining in the CA1 region of the hippocampus after GCI. The brain slices were stained with Kir5.1 antibody and an antibody directed against GFAP in controls and 6 hours, 1 day, 3 days, 7 days and 1 month after ischemia. Kir5.1 is expressed exclusively in pyramidal neurons in controls and 6 hours after ischemia; however, starting 1 day after ischemia, Kir5.1 expression can be found in GFAP-positive astrocytes in the vicinity of the pyramidal cell layer (arrowheads). (s.p. stratum pyramidale; s.r. – stratum radiatum)

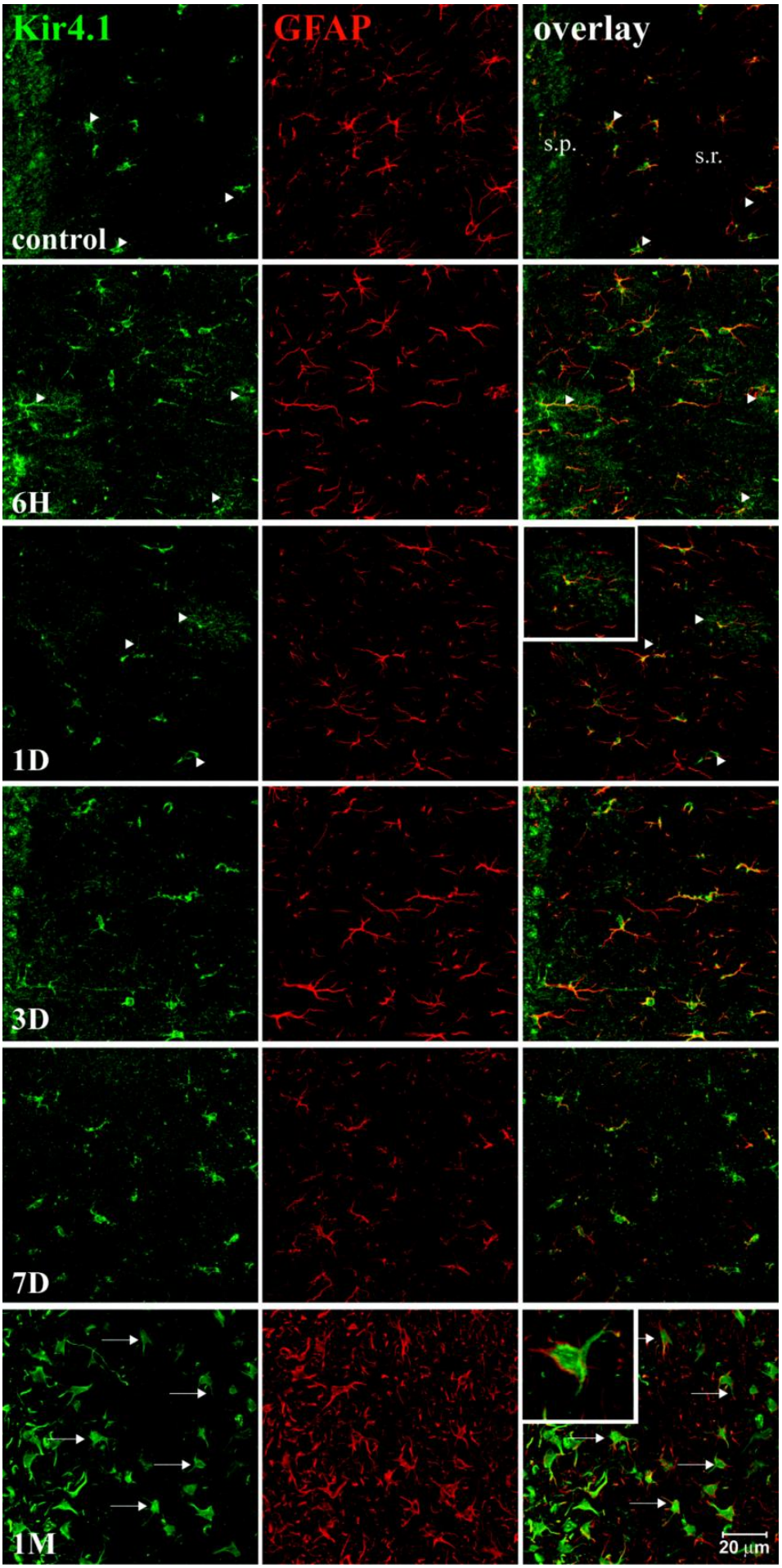
Kir4.1
GFAP
overlay
s.p.
s.r.
control
6H
1D
3D
7D
1M
20 μm

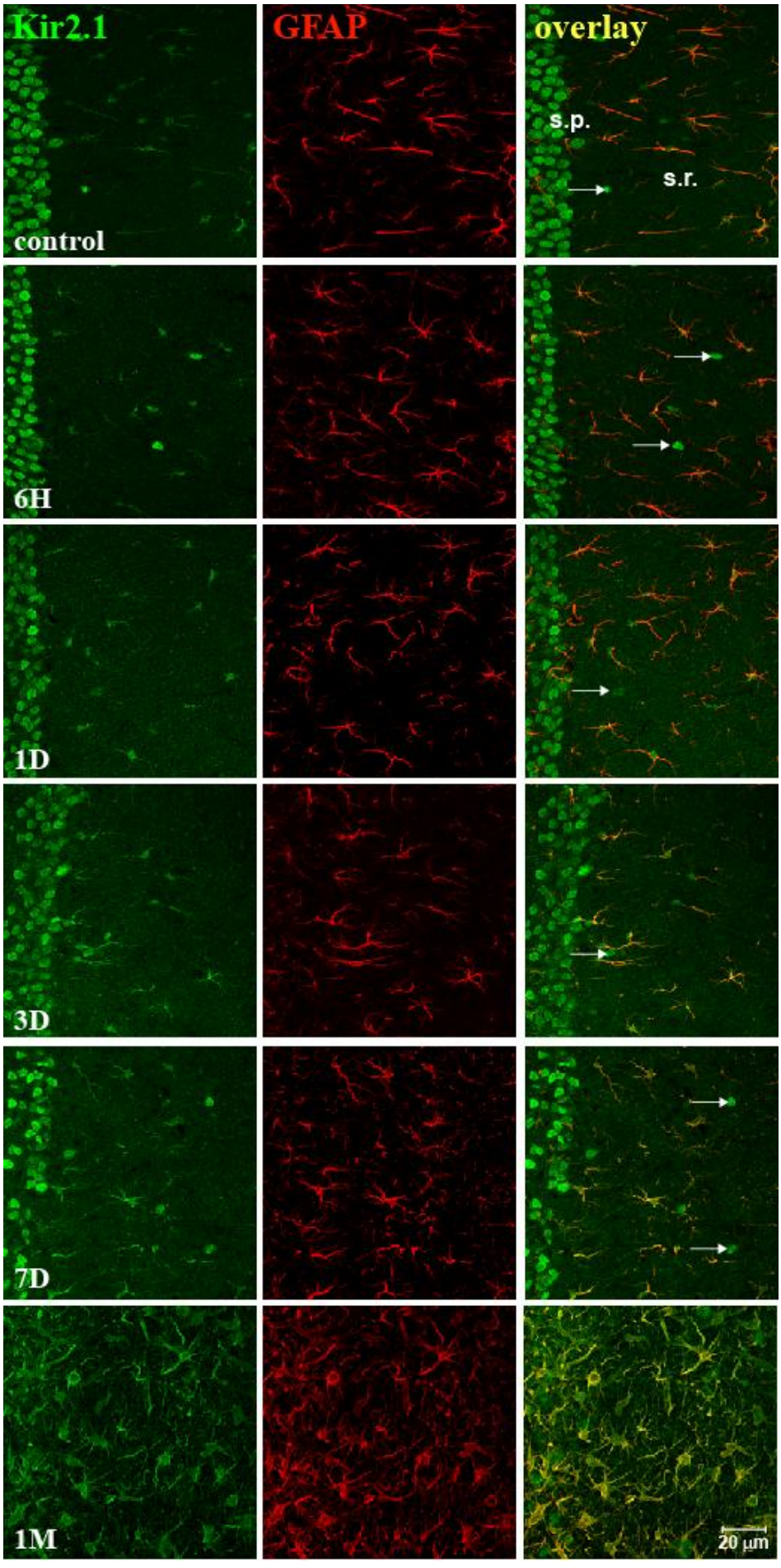
Kir2.1
GFAP
overlay
s.p.
s.r.
control
6H
1D
3D
7D
1M
20 µm

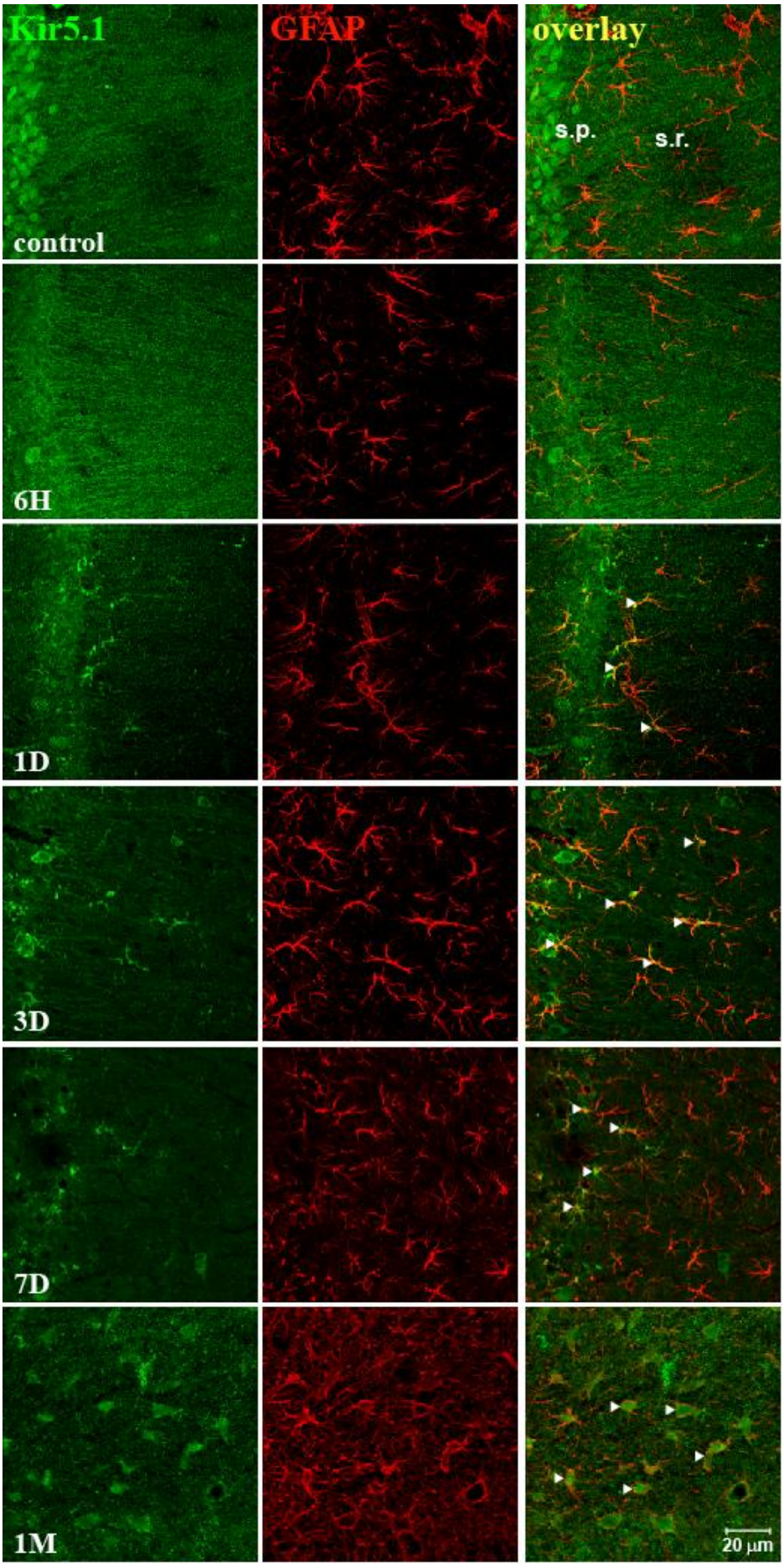
Kir5.1
GFAP
overlay
s.p.
s.r.
control
6H
1D
3D
7D
1M
20 µm

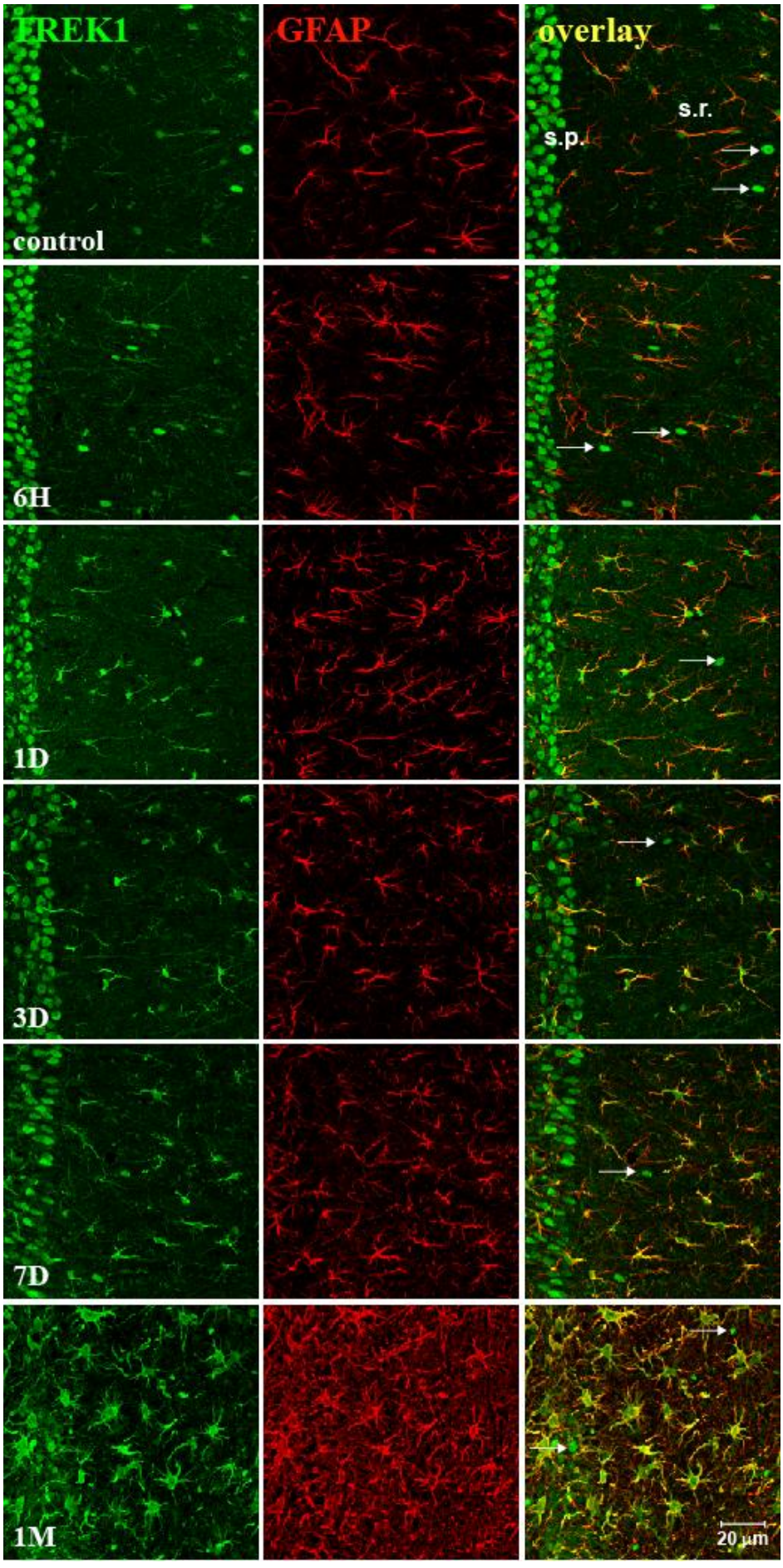
TREK1
GFAP
overlay
s.r.
s.p.
control
6H
1D
3D
7D
1M
20 μm

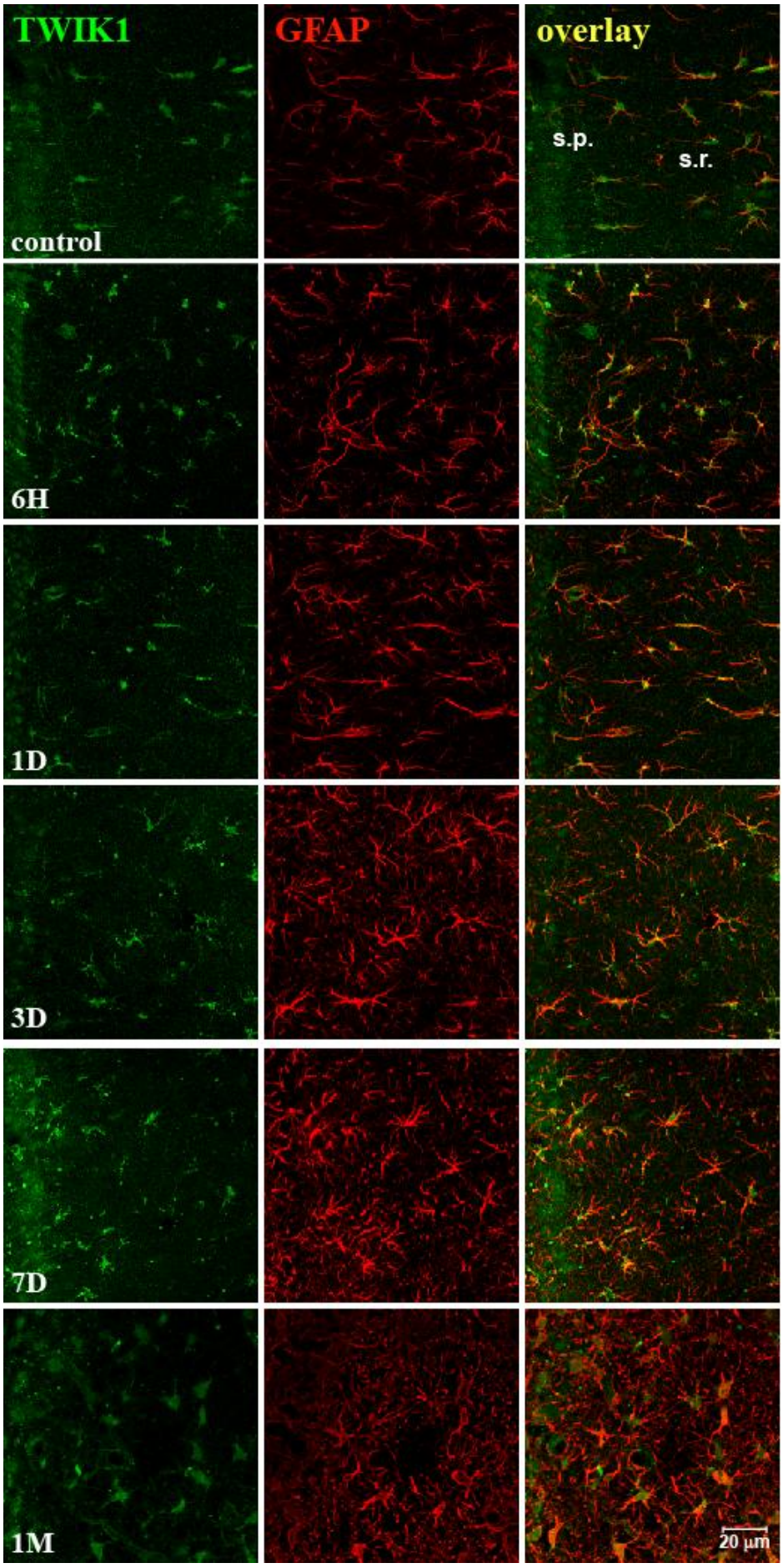
TWIK1
GFAP
overlay
s.p.
s.r.
control
6H
1D
3D
7D
1M
20 µm

Fig. 27: (see page 74) TREK1 staining in the CA1 region of the hippocampus after GCI. The brain slices were stained with TREK1 antibody and an antibody directed against GFAP in controls and 6 hours, 1 day, 3 days, 7 days and 1 month after ischemia. In controls and up to 7 days after ischemia, the TREK1 channel is expressed in both pyramidal neurons and astrocytes; however, 1 month after ischemia TREK1 expression remains almost exclusively in reactive astrocytes. Arrows show TREK1-positive neurons in the stratum radiatum. (s.p. stratum pyramidale; s.r. – stratum radiatum)

Fig. 28: (see page 75) TWIK1 staining in the CA1 region of the hippocampus after GCI. The brain slices were stained with TWIK1 antibody and an antibody directed against GFAP in controls and 6 hours, 1 day, 3 days, 7 days and 1 month after GCI. The TWIK1 channel is expressed exclusively in GFAP-positive astrocytes both in controls and at any studied timepoint after ischemia. (s.p. stratum pyramidale; s.r. – stratum radiatum)

4.2.3 Changes in the membrane properties of NG2 glia after GCI

Besides astrocytes, NG2 glia also participate in the formation of the glial scar. They show a high proliferation rate and might differentiate into other cell types including oligodendrocytes, astrocytes and neurons. Despite their promising effect in CNS tissue regeneration, their membrane properties after CNS ischemia have not yet been studied.

NG2 glia were morphologically recognizable, both in controls and after GCI, as small lucid cells (<10 μm) with rounded somata. Intracellular staining with a fluorescent dye showed that NG2 glia had several radially oriented primary and secondary processes, resembling the multi-process morphology typical of polydendrocytes (Fig. 29A) (Nishiyama et al., 2002). Immunohistochemical analysis confirmed their positivity for NG2 chondroitin sulfate proteoglycan (Fig. 29A). We never observed dye coupling between individual NG2 glial cells in controls or after GCI. Whole-cell patch-clamp recordings of hippocampal NG2 glia both in controls and after GCI revealed a current pattern typical for this glial cell population, i.e., they displayed time- and voltage-independent K^+ conductance together with K_{DR}, K_A and K_{IR} currents and, in a subset of cells, fast activating Na^+ inward currents (Fig. 29B) (Lin and Bergles, 2002; Chittajallu et al., 2004). Since we did not find any significant differences in any of the studied parameters in NG2 glia among the control animals (sham-operated rats with different reperfusion periods), the control NG2 glia were combined into a single control group for the statistical analysis.

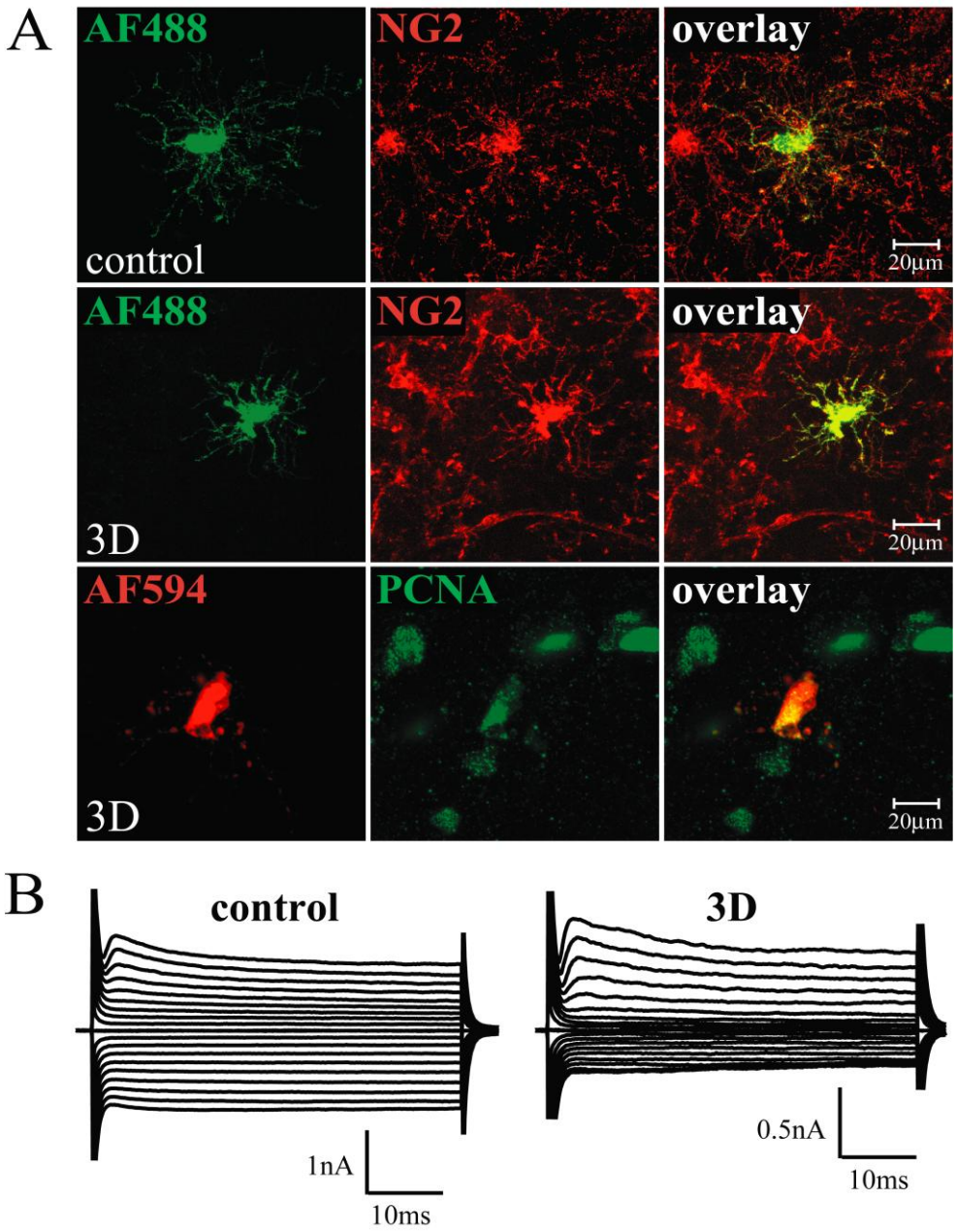

Fig. 29: NG2 glia morphology and current pattern after GCI. A: NG2 glia in control hippocampus (top) and 3 days (middle) after ischemia loaded with Alexa Fluor 488 hydrazid (AF488) during patch-clamp measurement, subsequently stained with an antibody directed against NG2 chondroitin sulfate proteoglycan. Note the "reactive morphology" of NG2 glia 3 days after ischemia, i.e., soma hypertrophy and the retraction of processes. NG2 glia 3 days after ischemia loaded with Alexa Fluor 594 hydrazid (AF594) during patch-clamp measurement and stained for a marker of proliferation, PCNA, post-recording (bottom). **B:** NG2 glia current pattern in controls and 3 days after ischemia. The NG2 glia membrane was depolarized from a holding potential of -70 mV to +20 mV and hyperpolarized to -160 mV (for the voltage protocol see the inset in Fig. 22). NG2 glia show a "complex" current pattern, i.e. time- and voltage-independent K^+ currents, K_{DR}, K_A and K_{IR} currents and fast activating Na^+ inward currents in some cells, both in controls and after ischemia. Note that control NG2 glia possess higher time- and voltage-independent conductance compared to NG2 glia 3 days after ischemia.

The average RMP of hippocampal NG2 glia in controls was -84.7 ± 1.1 mV (n=19), and GCI did not evoke any significant changes in their RMP during the time course of 2H, 6H, 1D and 3D after ischemia, compared to controls (Table 3). We found a significant increase in the NG2 glia R_M from 164.5 ± 15.8 MOhms (n=19) in controls to 320.9 ± 28.5 MOhms (n=21; p<0.001) 3D after GCI (Table 3). Moreover, the average C_M of NG2 glia 3D after ischemia was significantly lower (5.5 ± 0.6 pF; n=21) than that measured in controls (9.5 ± 1.0 pF; n=19; p<0.01) (Table 3). In contrast to astrocytes, later time points (7D and 1M) after GCI were not included in our study since we could not record a sufficient number of NG2 glial cells in the gliotic scar full of reactive astrocytes and microglia.

Table 3: Membrane properties of hippocampal NG2 glia in controls and after GCI

	RMP (mV)	R_M (MOhms)	C_M (pF)	n
CONTROLS	-84.7±1.1	164.5±15.8	9.5±1.0	19
2H	-88.5±1.2	253.9±32.8	6.2±0.8	12
6H	-86.6±2.3	219.7±21.5	8.3±1.0	15
1D	-80.7±2.0	153.5±24.1	10.4±1.4	10
3D	-78.9±2.6	320.9±28.5***	5.5±0.6**	21

RMP, resting membrane potential; R_M, membrane resistance; C_M, membrane capacitance. The values are presented as mean ± S.E.M. Statistical significance was calculated using one-way ANOVA with Dunnett's post-hoc test; ** p<0.01, very significant; *** p<0.001, extremely significant.

We observed a significant increase in both K_{DR} current amplitude and K_{DR} CD from 311.2 ± 45.0 pA (n=19) in controls to 536.2 ± 57.9 pA (n=21, p<0.01) 3D after GCI and from 39.4 ± 6.6 pA/pF (n=19) in controls to 123.7 ± 20.9 pA/pF (n=21, p<0.01) 3D after GCI, respectively (Fig. 30A, B). Furthermore, the K_A current amplitude was significantly increased from 730.5 ± 107.6 pA (n=19) in controls to 1335.0 ± 157.7 pA (n=12, p<0.01) 2H after GCI, and its CD was significantly increased from 91.8 ± 16.0 pA/pF (n=19) in controls to 237.8 ± 29.3 pA/pF (n=12, p<0.01) 2H after ischemia and to 246.2 ± 32.3 pA/pF (n=21, p<0.01) 3D after GCI (Fig. 30C, D). Since an increase in the outwardly rectifying K^+ currents has been shown to reflect the proliferative activity of OPCs (Knutson et al., 1997), we performed post-recording

staining of NG2 glia 3D after ischemia using an antibody against PCNA, a marker of proliferating cells. We found that 4 cells out of 4, displaying increased K_{DR} and K_A currents 3D after ischemia, were PCNA-positive (Fig. 29A). In addition, the K_{IR} current amplitude was significantly decreased from 867.3 ± 80.6 pA (n=19) in controls to 451.8 ± 46.8 pA (n=21, $p<0.01$) 3D after GCI; however, the quantification of K_{IR} CD revealed no significant differences in NG2 glia after GCI compared to controls. The average values of K_{IR} CD in controls and those 3D after ischemia were 97.8 ± 8.4 pA/pF (n=19) and 89.4 ± 7.6 pA/pF (n=21), respectively (Fig. 30E, F).

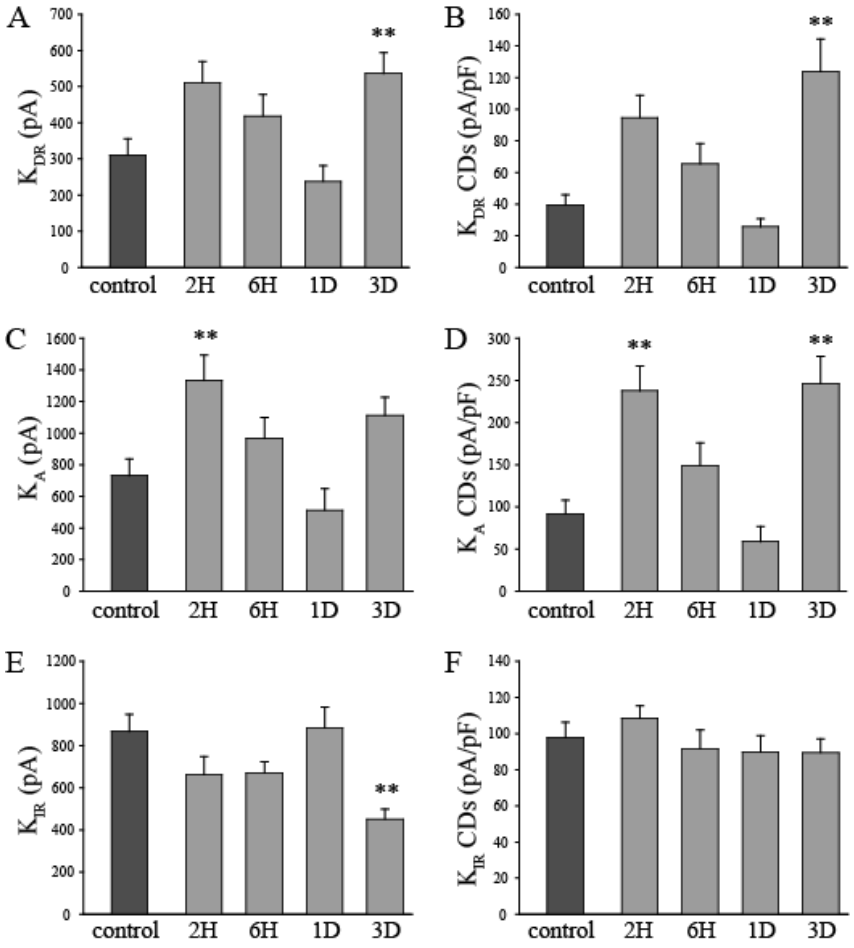

Fig. 30: Delayed outwardly rectifying-, A-type- and inward K^+ (K_{DR}, K_A and K_{IR}) currents in NG2 glia after GCI. A, C, E: The time-dependent changes in the current amplitudes of K_{DR}, K_A and K_{IR} currents after ischemia compared to controls. **B, D, F:** The time-dependent changes in the current densities of K_{DR}, K_A and K_{IR} currents after ischemia compared to controls. The numbers of measured cells are: n=19 for controls, n=12 for 2H, n=15 for 6H, n=10 for 1D and n=21 for 3D after ischemia. Statistical significance was calculated using one-way ANOVA followed by the Dunnett's post-hoc test; **$p<0.01$, very significant.

4.2.4 NG2 glia in the hippocampus proliferate and express nestin after GCI

Further, to assess the temporal pattern of hippocampal NG2 glia proliferation after GCI, we performed double immunostaining with a marker of proliferating cells, PCNA, and a marker of newly derived cells, nestin (Fig. 31A, B).

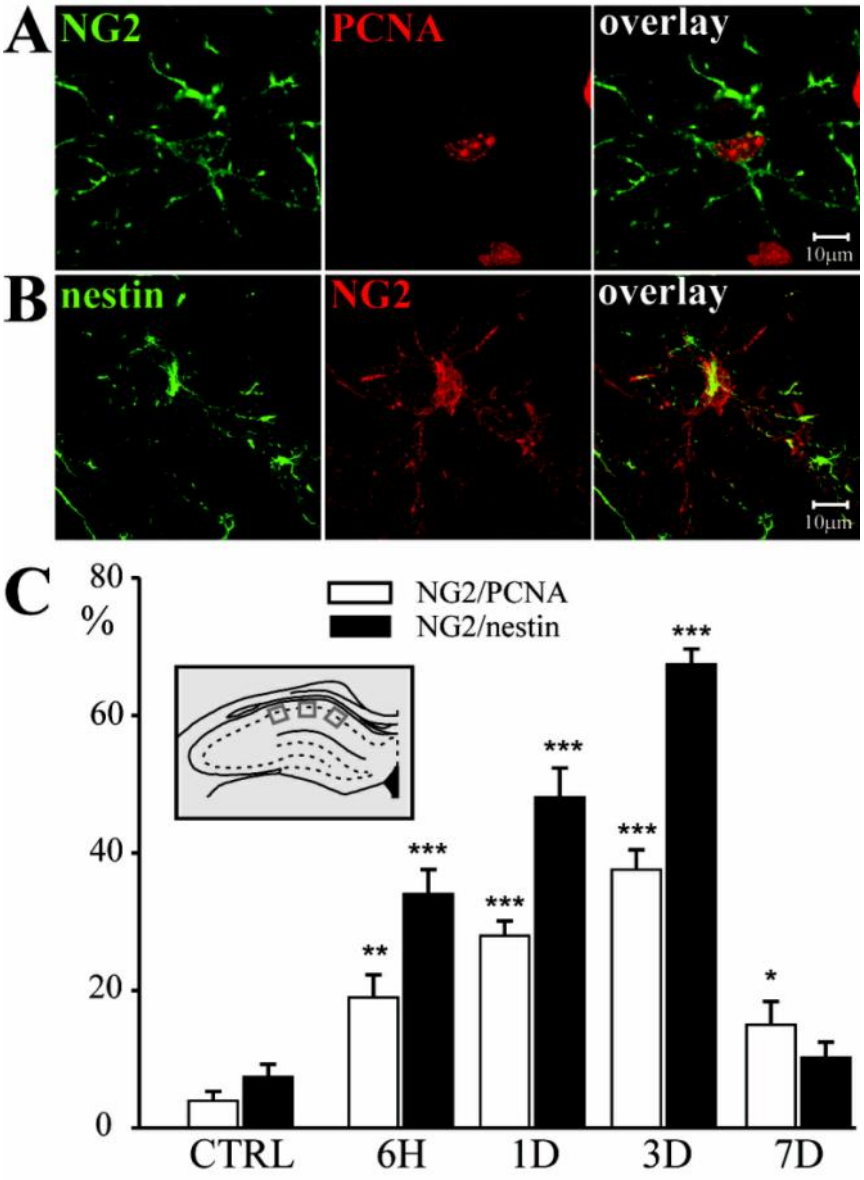

Fig. 31: Proliferation and nestin expression in NG2 glia after GCI. A, B: NG2 glia in the CA1 region of the hippocampus 3 days after ischemia stained for PCNA and nestin. **C**: The graph shows the time-dependent changes in the percentage of NG2 glia positively stained for a proliferation marker, PCNA, and for nestin during the studied time course after ischemia. The numbers of $NG2^+/PCNA^+$ and $NG2^+/nestin^+$ cells were quantified from stacks of images (225 x 225 x 20 µm; see the inset) taken in 6 zones from coronal hippocampal slices of both hemispheres (3 animals, 4 slices from each animal). The peak of NG2

glia proliferation 3 days after ischemia correlates with the peak of nestin expression in NG2 glia. Seven days after ischemia, the percentage of NG2 glia expressing PCNA and/or nestin returned almost to control values. Statistical significance was calculated using one-way ANOVA followed by the Dunnett's post-hoc test; *p<0.05, **p<0.01, ***p<0.001.

In control hippocampi, 3.9 ± 1.4% of NG2 glia were PCNA-positive, a value corresponding to the basal proliferation rate of NG2 glia under physiological conditions. We observed a significantly enhanced proliferation of hippocampal NG2 glia starting 6H after GCI (19.0 ± 3.3% of NG2/PCNA-positive cells; Fig. 31C) compared to controls ($p<0.01$). One day after ischemia, the percentage of proliferating NG2 glia increased to 28.0 ± 2.2% ($p<0.001$), and 3D after ischemia it reached its maximum of 37.6 ± 2.9% ($p<0.001$). The percentage of NG2/PCNA-positive cells declined 7D after ischemia, although it remained at a level significantly higher than in controls (15.0 ± 3.4%, $p<0.05$). Furthermore, we observed an increase in the number of NG2 glia expressing nestin after ischemia. In the CA1 region of control hippocampi, only 7.4 ± 1.8% of NG2 glia expressed nestin, while the percentage of NG2 glia expressing nestin increased to 34.0 ± 3.6% 6H after ischemia (Fig. 31C) and to 48.1 ± 4.3% 1D after ischemia. Similarly to the number of NG2/PCNA-positive cells, the number of nestin-positive NG2 glia reached its maximum of 67.4 ± 2.2% 3D after ischemia ($p<0.001$ for 6H, 1D and 3D compared to controls). Seven days after ischemia, the percentage of NG2/nestin-positive cells returned to control levels (10.2 ± 2.3%).

4.3 MEMBRANE PROPERTIES OF SPINAL CORD GLIAL CELLS AFTER EXPOSURE TO HIGH $[K^+]$

Ischemia or CNS tissue injury is accompanied by a substantial increase in $[K^+]_e$, which leads to the activation of astrocytes and the subsequent formation of a glial scar evident 3–7 days after the insult. To date, no comprehensive analyses of astrocyte membrane properties have been done *in situ* immediately after an insult that may trigger the processes leading to reactive astrogliosis, and the mechanisms underlying the initiation of astrogliosis are still poorly understood. CNS tissue incubation in high K^+ might thus be a useful model for studying astrocyte swelling and the early events of astrocytic

activation with respect to the astrocyte membrane properties and the activity of K^+ ion channels.

4.3.1 Effect of spinal cord exposure to 50 mM K^+ on resting levels of $[K^+]_e$ and pH_e

$[K^+]_e$ and pH_e in spinal cord lumbar segments, either non-incubated or following a 3 hour incubation in aCSF (control) or aCSF50, were measured using ion-selective microelectrodes. To check for possible ischemic effects resulting from a 3 hour incubation in aCSF, we first measured $[K^+]_e$ and pH_e in spinal cords that were not incubated and compared the results to those obtained in spinal cords incubated in aCSF. Incubation in aCSF caused no significant difference in $[K^+]_e$ or pH_e compared to spinal cords without incubation: $[K^+]_e$ was 4.10 mM and 4.11 mM and pH_e was 7.15 and 7.18, respectively. In spinal cords incubated in aCSF50, $[K^+]_e$ was 22.01 mM when measured 5 minutes after the end of the incubation, while 25 minutes later it had decreased almost to control values, 4.62 mM. Incubation in aCSF50 caused a decrease in pH_e to 7.0 (measured 5 minutes after the end of incubation) followed by an increase to 7.06 25 minutes later. These data indicate that $[K^+]_e$ returns to control values within 30 minutes after the end of the spinal cord's exposure to a high K^+ concentration, while pH_e remains shifted towards acidosis.

4.3.2 Immunohistochemistry and GFAP expression

Immunohistochemical staining revealed differences in GFAP immunoreactivity and the morphology of GFAP-positive cells between control spinal cords and those incubated in aCSF50 (Fig. 32A, B). The astrocytes from spinal cords incubated in aCSF50 showed increased GFAP immunoreactivity and a reactive astrocyte-like morphology, i.e. they had larger cell bodies and thicker and shorter processes compared to controls. Since these findings might indicate an increase in GFAP expression in astrocytes from spinal cords incubated in aCSF50, the GFAP content was examined by Western blotting. We found no differences in GFAP content between control spinal cords and those incubated in aCSF50 (Fig. 32C, D) or between non-incubated spinal cords and those incubated in either aCSF or aCSF50 (data not shown). We conclude that the increase in GFAP immunoreactivity and the changes in astrocyte morphology induced by a 3h incubation

of spinal cord segments in high K^+ are not a consequence of increased GFAP expression.

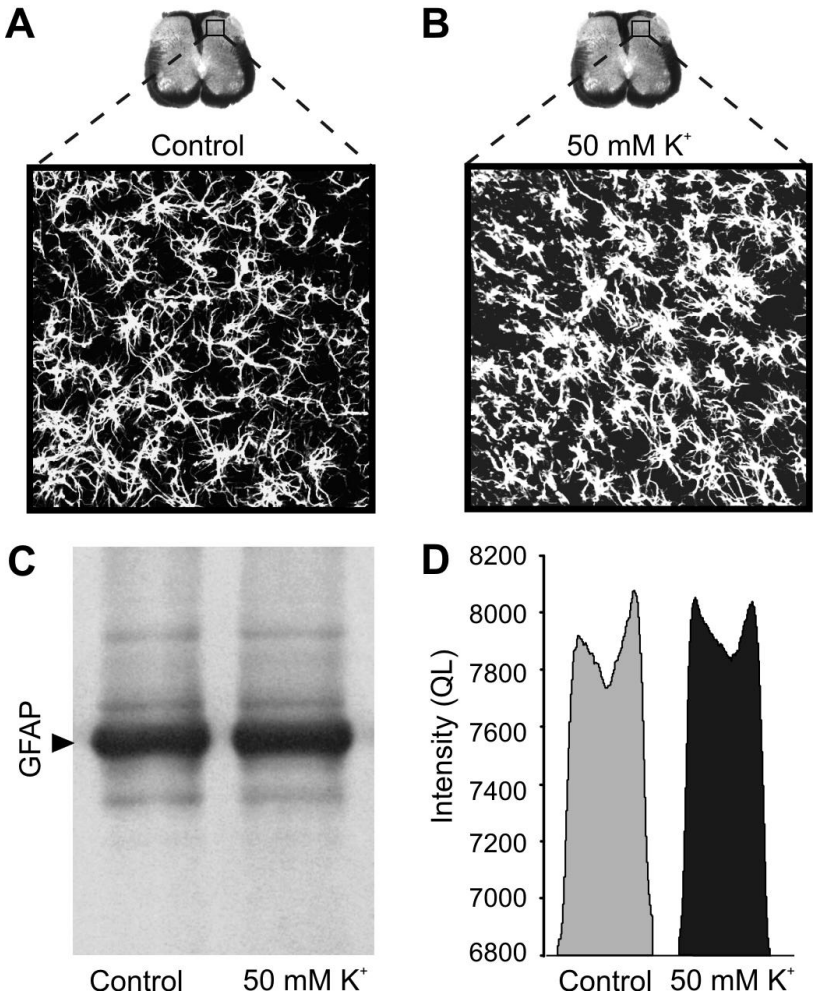

Fig. 32: GFAP immunoreactivity and GFAP content in the rat spinal cord after incubation in either aCSF or aCSF with 50 mM K^+. Spinal cord slices were stained for GFAP to visualize changes in the morphology of astrocytes following incubation in aCSF (control, **A**) or incubation in 50 mM K^+ (**B**). Note that in control tissue, astrocytes possess thinner and longer processes, whereas after incubation in 50 mM K^+, astrocytes have larger cell bodies and thicker and shorter processes. GFAP content in spinal cord segments was quantified by Western blotting (**C**, **D**). There was no increase in GFAP content after incubation in 50 mM K^+ compared to control samples.

4.3.3 Membrane properties of spinal cord astrocytes

Changes in the membrane properties of rat spinal cord astrocytes after incubation in aCSF or aCSF50 were studied using the patch-clamp method in the whole-cell

configuration, as described previously (Chvatal et al., 1995). The recorded cells were identified as astrocytes by the lack of an action potential during seal formation and during current clamp recording and by immunohistochemical staining specific for astrocytes. The following membrane parameters were compared: RMP, V_{rev}, R_M, C_M and the CDs of K_{DR}, K_A, K_{IR} and I_{Na} currents.

Based on passive membrane properties and the expression of voltage-dependent K^+ and Na^+ currents, three electrophysiologically distinct types of astrocytes were found in control spinal cords as well as in those incubated in aCSF50 (see Table 4 and Fig. 33). In controls, 25% of the recorded astrocytes exhibited a current pattern typical of complex astrocytes, i.e. the expression of K_{DR}, K_A, K_{IR} and I_{Na} currents (Fig. 33A, B), a high R_M and a low RMP (Kressin et al., 1995; Jabs et al., 1997). The relative number of complex astrocytes increased to 34% of all astrocytes after incubation in aCSF50. Nine out of 17 complex astrocytes measured in control slices and after incubation in aCSF50 were positive for GFAP, and 5 out of 11 were positive for S100β. A second group of astrocytes was characterized by a similar current pattern as that observed in complex astrocytes except for the undetectable expression of K_{IR} currents. Moreover, these cells had a ~4.7-fold higher R_M, were significantly more depolarized and had a lower C_M compared to complex astrocytes in control spinal cords (Fig. 33C, D). Similar membrane properties have been previously shown to be characteristic of astrocyte precursors or de-differentiating astrocytes after an insult (Kressin et al., 1995; Schroder et al., 1999). The relative number of astrocyte precursors decreased from 37% in control tissue to 28% after incubation in aCSF50. Ten out of 21 astrocyte precursors were positively stained for GFAP, and 3 out of 5 cells were positive for S100β. The third group of astrocytes (38% in control spinal cords) displayed a large time- and voltage-independent current component with additional K_{IR}, K_{DR} or K_A currents (passive astrocytes, Fig. 33E, F); their number remained unchanged (38%) after spinal cord incubation in aCSF50. In passive cells, 9 out of 18 cells were stained for GFAP, and 3 out of 6 cells were stained for S100β.

After spinal cord incubation in aCSF50, complex astrocytes were significantly depolarized; their R_M was increased and their C_M decreased when compared to controls (see Table 4). Moreover, their K_{DR}, K_A, K_{IR} and I_{Na} CDs were increased. In contrast, the membrane properties of astrocyte precursors in spinal cords incubated in aCSF50 were not significantly different from those in controls. We did not observe any TTX-insensitive I_{Na} currents in either complex astrocytes or astrocyte precursors, in contrast

to the results found in an *in vitro* model of reactive gliosis (MacFarlane and Sontheimer, 1998). In passive astrocytes, V_{rev} was shifted to more positive values and K_{DR} and K_A CDs were significantly decreased, whereas RMP, R_M, C_M, and K_{IR} CD were not affected by incubation in aCSF50.

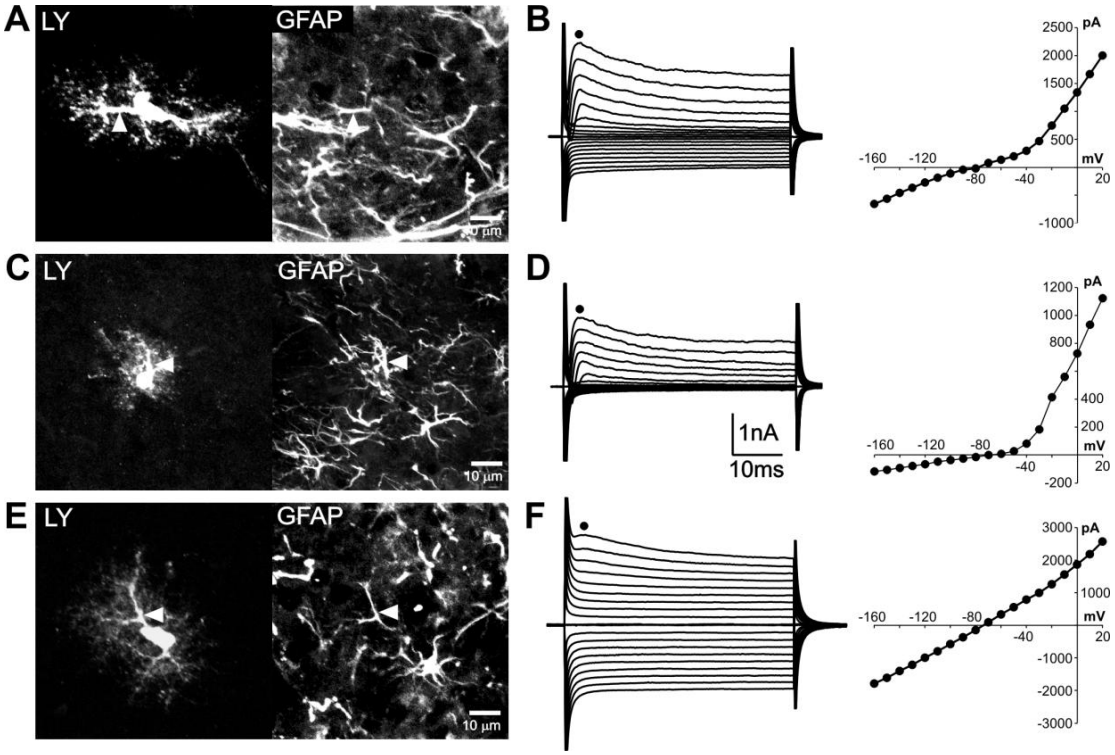

Fig. 33: Typical morphology, immunohistochemical identification, and current patterns of astrocytes in rat spinal cords. A, **C**, **E** Morphology based on LY staining (**left**) and GFAP-positive staining (**right**) of a complex astrocyte (**A**), astrocyte precursor (**C**), and passive astrocyte (**E**). Arrowheads indicate $LY^+/GFAP^+$ cell structures. **B**, **D**, **F** Currents evoked by membrane depolarization and hyperpolarization from -160 to +20 mV (**left**) and the I/V curves obtained from these currents taken 5 ms after the onset of the pulses (circles, **right**). Complex astrocytes (**B**) are characterized by the presence of delayed outwardly rectifying K^+ (K_{DR}), A-type K^+ (K_A), inwardly rectifying K^+ (K_{IR}), and Na^+ currents (I_{Na}); astrocyte precursors (**D**) are characterized by the presence of K_{DR}, K_A, and I_{Na}, but no K_{IR} and negligible passive conductance, while passive astrocytes (**F**) show mainly passive conductance and additional voltage-dependent K^+ currents.

Table 4: Membrane parameters of rat spinal cord astrocytes in control spinal cords and in spinal cords incubated in aCSF50.

Complex astrocytes		control	aCSF50
V_m	[mV]	-90.4 ± 2.3	-81.9 ± 1.5**
V_{rev}	[mV]	-88.2 ± 2.4	-79.2 ± 1.8**
R_M	[MΩ]	175.9 ± 47.9	427.2 ± 43.5***
C_m	[pF]	41.2 ± 6.9	11.8 ± 2.0***
K_{DR}/C_m	[pA/pF]	37.3 ± 13.4	99.5 ± 18.1*
K_A/C_m	[pA/pF]	70.6 ± 20.5	155.4 ± 26.9*
I_{Na}/C_m	[pA/pF]	19.9 ± 10.0	53.6 ± 10.8*
K_{IR}/C_m	[pA/pF]	3.8 ± 0.9	12.5 ± 2.1**
n		20	35

Astrocyte precursors		control	aCSF50
V_m	[mV]	-82.4 ± 1.9	-78.5 ± 2.3
V_{rev}	[mV]	-78.9 ± 2.4	-75.8 ± 2.6
R_M	[MΩ]	825.5 ± 94.0	836.3 ± 86.8
C_m	[pF]	10.0 ± 1.0	10.7 ± 2.2
K_{DR}/C_m	[pA/pF]	84.9 ± 9.3	106.6 ± 18.0
K_A/C_m	[pA/pF]	137.7 ± 15.4	176.9 ± 27.9
I_{Na}/C_m	[pA/pF]	54.1 ± 9.1	57.9 ± 14.8
n		30	29

Passive astrocytes		control	aCSF50
V_m	[mV]	-85.9 ± 1.1	-83.3 ± 1.2
V_{rev}	[mV]	-84.3 ± 1.4	-79.1 ± 1.3**
R_M	[MΩ]	61.2 ± 7.8	75.1 ± 10.3
C_m	[pF]	110.4 ± 17.6	128.4 ± 17.0
K_{DR}/C_m	[pA/pF]	7.9 ± 3.6	0*
K_A/C_m	[pA/pF]	16.6 ± 7.0	0.8 ± 0.4*
K_{IR}/C_m	[pA/pF]	1.1 ± 0.4	0.5 ± 0.2
n		31	39

I_{Na}/C_m in astrocyte precursors in control tissue and after incubation in ACF50 was determined from 16 and 14 cells, respectively. Statistical significance was evaluated as the difference between control spinal cord astrocytes and those incubated in ACF50 (unpaired, two-tailed *t* test). # represents that I_{Na}/C_m in complex astrocytes in control tissue and after incubation in ACF50 was determined from 12 and 13 cells, respectively. V_m membrane potential, V_{rev} reversal potential, R_M membrane resistance, C_m membrane capacitance, n number of cells *p<0.05; **p<0.01; ***p<0.001.

4.3.4 Astrocyte swelling evoked by hypotonic stress – electrophysiology

Our experiments show that exposure of spinal cord astrocytes to high K^+ leads to changes in their membrane properties. Since ion channels play an important role in cell volume regulation, we studied astrocyte swelling during secondary stress evoked by hypotonic solution in spinal cords pre-incubated in high K^+. Astrocyte membrane properties were determined every 2 minutes prior to and during a 20-minute application of hypotonic solution. The following parameters were analyzed: RMP, $V_{rev\ tail}$ and K^+ accumulation in the vicinity of the astrocyte membrane after a depolarizing prepulse (ΔK^+). Only passive astrocytes were considered as these cells possess predominantly high passive K^+ conductance and the values of $V_{rev\ tail}$ and ΔK^+ in complex astrocytes or in astrocyte precursors are affected by the activation of K_{DR} and K_A during the depolarizing prepulse (Chvatal et al., 1999).

During the application of hypotonic solution, RMP shifted to more negative values without any significant differences between astrocytes in control spinal cords and those pre-incubated in aCSF50 (Fig. 34A). However, $V_{rev\ tail}$ was shifted to more negative values only in astrocytes pre-incubated in aCSF50 (Fig. 34B). Thus, $[K^+]_e$ calculated from the Nernst equation revealed a smaller K^+ accumulation induced by a depolarizing prepulse in the vicinity of astrocytes pre-incubated in aCSF50 (Fig. 34C). In the control group, ΔK^+ increased to 142.1 ± 19.0% (n=25) of the initial values (taken to be 100%) after 20 minutes of perfusion with hypotonic solution, whereas in astrocytes pre-incubated in aCSF50, ΔK^+ decreased to 75.5 ± 17.5% (n=12) of the initial values. We conclude that under hypotonic stress, pre-incubation in high K^+ leads to a decrease in K^+ accumulation in the vicinity of the astrocyte membrane after a depolarizing prepulse, which might suggest an astrocyte volume decrease (Chvatal et al., 1999; Vargova et al., 2001).

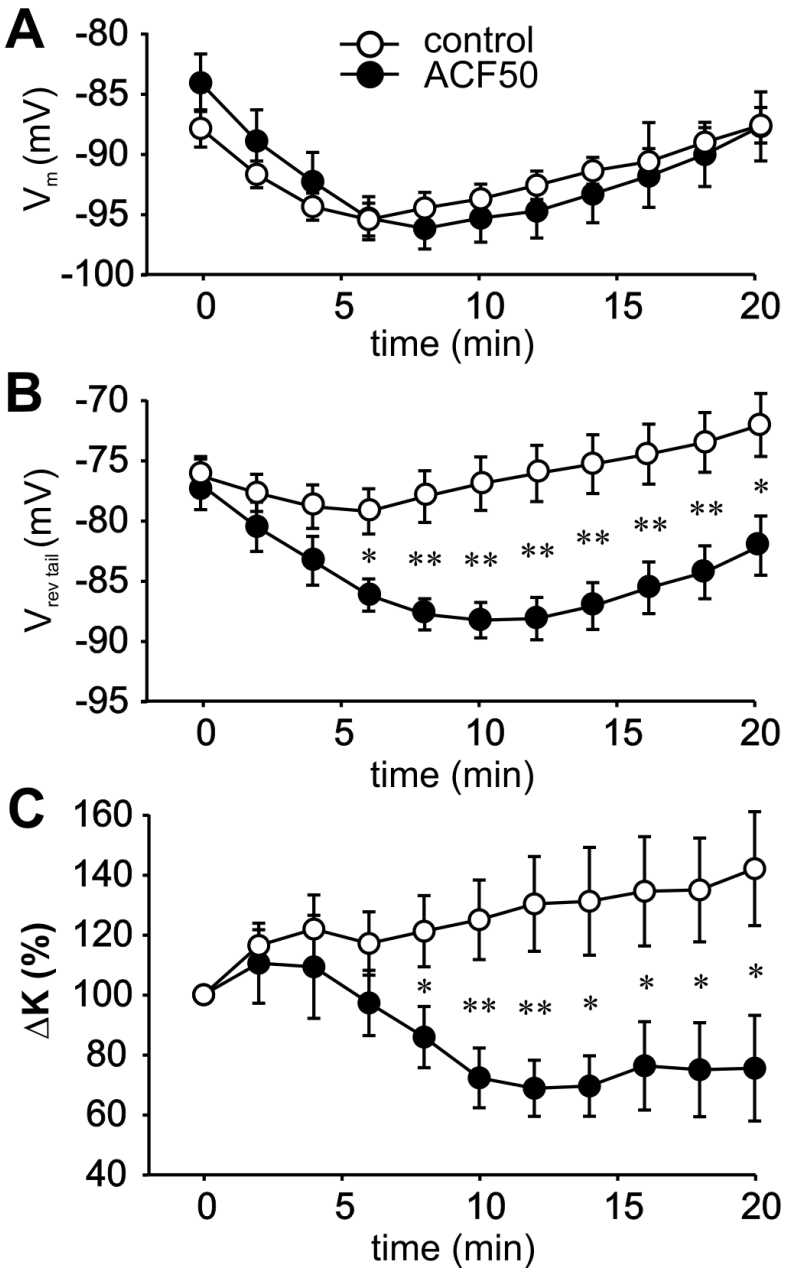

Fig. 34: Membrane properties and K^+ accumulation in astrocytes during hypotonic stress. Spinal cord astrocytes in control tissue (empty circles, n=25) and after preincubation in 50 mM K^+ (ACF50; filled circles, n=12) were perfused with hypotonic solution for 20 min. The membrane potential (V_m) and the reversal potential of the tail current ($V_{rev\ tail}$) were measured every 2 min (**A**, **B**). K^+ accumulation (ΔK^+) in the vicinity of the cell membrane was calculated from V_m and $V_{rev\ tail}$ and expressed as a percentage of the initial values (**C**). During hypotonic stress, in control astrocytes, ΔK^+ increased, whereas in astrocytes preincubated in 50 mM K^+, ΔK^+ decreased. Statistical significance was evaluated as the difference between spinal cords incubated in aCSF (control) and those incubated in 50 mM K^+ (**p < 0.01, *p < 0.05, unpaired, two-tailed *t* test).

4.3.5 Astrocyte swelling evoked by hypotonic stress - volume changes

Significant differences in K^+ accumulation around astrocytes after a depolarizing prepulse during perfusion with hypotonic solution might indicate changes in astrocyte volume regulation (Chvatal et al., 1999; Vargova et al., 2001). Thus, 3D confocal morphometry (see Methods) was used to examine the effect of high K^+ on astrocyte volume changes evoked by hypotonic stress. Previously, we have shown that spinal cord astrocytes in rats and mice display no significant inter-species differences in cell swelling or membrane properties when exposed to hypotonic stress (Anderova et al., 2001; Vargova et al., 2001; Chvatal et al., 2004). Therefore, we have taken advantage of the direct visualization of astrocytes in spinal cord slices from EGFP/GFAP mice to quantify the differences in volume changes between astrocytes in control tissue and those from spinal cords incubated in aCSF50. Because of photobleaching, only brightly fluorescent cells were chosen for 3D-confocal volume analysis. Patch-clamp measurements revealed that these cells display a passive current pattern (data not shown), which is consistent with the data of Matthias et al. (2003). Astrocyte volume was measured every 5 minutes prior to and during a 20 minute application of hypotonic solution.

In controls, astrocyte volume increased to 126.3 ± 3.8% (n=15) of the initial values (taken as 100%) 5 minutes after the beginning of perfusion with hypotonic solution, and it further increased to 133.9 ± 3.8% after an additional 15 minutes (Fig. 35). In contrast, in astrocytes pre-incubated in aCSF50, the cell volume increased to 120.3 ± 4.0% (n=15) after 5 minutes in hypotonic solution, and no further increase was observed. We conclude that spinal cord astrocytes pre-incubated in high K^+ swell rapidly during the first 5 minutes under hypotonic stress, but any further increase in their volume is significantly less than that seen in controls.

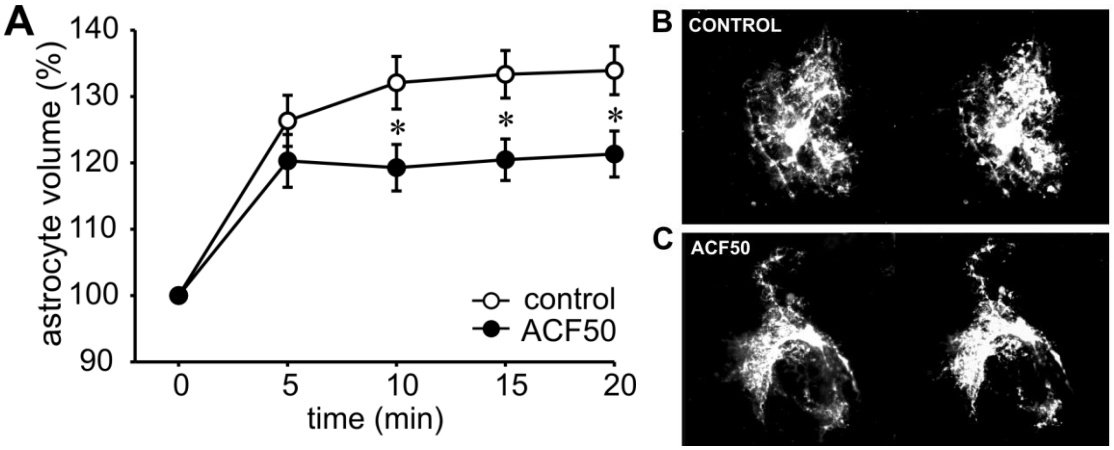

Fig. 35: Volume changes in astrocytes during hypotonic stress. Astrocytes from EGFP/GFAP mice in control spinal cord slices (empty circles, n=15) and after preincubation in 50 mM K^+ (ACF50; filled circles, n=15) were perfused with hypotonic solution for 20 min, and volume changes were measured using 3D confocal morphometry every 5 min and expressed as a percentage of the initial values (**A**). During hypotonic stress, the volume increase of control astrocytes was significantly greater compared to that of astrocytes preincubated in 50 mM K^+. Statistical significance was evaluated as the difference between control spinal cord astrocytes and those incubated in 50 mM K^+ (*$p < 0.05$, unpaired, two-tailed *t-test*). Typical morphology of an EGFP/GFAP astrocyte in control tissue (**B**) and after preincubation in 50 mM K^+ (**C**). Left panels in B and C show astrocyte volume before the application of hypotonic solution and the right panels show astrocyte volume after 20 min of hypotonic stress.

5. DISCUSSION

5.1 CELLULAR RESPONSE TO CNS INJURY

5.1.1 Development of reactive astrogliosis

Acute CNS injury is accompanied by a prompt reaction of all the cellular components in the nervous tissue. This is primarily characterized by rapid neuronal and oligodendrocyte loss, microglia and astrocyte activation and, as recently shown, the proliferation of NG2 glia.

For our experiments, we used a rat model of GCI leading to the development of reactive astrogliosis in the CA1 region of the hippocampus, to study the membrane properties of glial cells in the course of glial scar formation. At first, we attempted to characterize the cellular response in the CA1 region of the hippocampus to this type of injury. This was particularly important for subsequent correlation of the membrane properties of the specific glial cells with their activation, proliferation and/or apoptosis.

As has been demonstrated in previous studies, GCI triggers selective neuronal loss of pyramidal cells in the CA1 region of the hippocampus followed by cognitive deficits in learning and memory tasks, both in humans and in animal models (Petito et al., 1987; Ordy et al., 1993; Hartman et al., 2005). Neuronal death is accompanied by the rapid activation and proliferation of microglia (Pforte et al., 2005). Astrocytes in the affected region display morphological alterations typical of reactive astrogliosis, i.e. hypertrophy and the increased expression of GFAP together with *de novo* expression of nestin and vimentin (Ridet et al., 1997). Reactive astrogliosis formation is often reported to be accompanied by astrocyte proliferation (Miyake et al., 1988; Fawcett and Asher, 1999); however, we found only little evidence for astrocytic proliferation in the CA1 region of the hippocampus during reperfusion. Similar results showing that only about 5% of astrocytes proliferate after a CNS injury have been described in other studies (Magnus et al., 2008; Burns et al., 2009). The low proliferation rate of astrocytes is in contrast to their increased number starting 1 month after ischemia, suggesting that reactive astrocytes might differentiate from another cell type.

Interestingly, we found extensive proliferation of NG2 glia during the first three days after GCI. The proliferation of NG2 glia has been demonstrated in many CNS injury models (Rabchevsky et al., 2007; McTigue and Tripathi, 2008; Lytle et al.,

2009). Since the number of NG2 glial cells was not increased substantially after 7 days of reperfusion, we hypothesize that the newly derived NG2 glia do not survive or differentiate into another cell type. The intermediate filament nestin has been shown to be upregulated in dividing OPCs (Gallo and Armstrong, 1995). Most authors support the concept that NG2 glia give rise to oligodendrocytes after white matter injury, which is consistent with their primary function in the developing CNS, where they belong to the oligodendrocyte lineage. Others have suggested NG2 glia differentiation into reactive astrocytes. (Alonso, 2005; Magnus et al., 2008). Alonso (2005) described the expression of the intermediate filaments nestin and vimentin, specific for newly derived cells or reactive astrocytes, in NG2 glia after injury. This observation might signify an overlap of specific marker expression during the differentiation of NG2 glia into reactive astrocytes. We observed the highest numbers of NG2/nestin-positive cells 3 days after ischemia and, at the same time, GFAP/nestin-positive reactive astrocytes appeared at the lesion site. The source of the large number of reactive astrocytes in the glial scar is a matter of debate as astrocytes do not proliferate to a great extent during reactive gliosis formation (Burns et al., 2009) and, hence, they might be recruited from another cell type, such as NG2 glia. The recruitment of reactive astrocytes from NG2 glia has been shown recently by Zhao et al. (2009). Nevertheless, this hypothesis needs further corroboration by additional, preferentially fate mapping studies using transgenic animals.

5.1.2 Astrocyte apoptosis

Astrocytes have been shown to die by programmed cell death after ischemia both *in vitro* and *in vivo* (Yu et al., 2001; Giffard and Swanson, 2005). We have found that hippocampal astrocytes shortly after GCI express apoptotic markers, cleaved caspase-3 and cleaved PARP-1, and later after ischemia they stain positively for markers of cell death such as TUNEL, FJB or LC3, without showing any considerable decrease in their cell numbers. TUNEL-positive or LC3-positive astrocytes were detected 1 month after GCI. On the other hand, the only significant decrease in the number of astrocytes was found 6 hours after GCI, when a large population of astrocytes was cleaved caspase-3- and PARP-1-positive. At this time point, we were not able to identify TUNEL/GFAP-positive cells. Since astrocytes undergo a rapid reduction in GFAP immunoreactivity when exposed to ischemic conditions (Lukaszevicz et al., 2002), it is possible that the

observed decrease in the number of astrocytes 6 hours after GCI was due to the lack of GFAP immunoreactivity in a certain population of astrocytes, thus making them unable to be identified as apoptotic astrocytes. Contrasting with high caspase-3 immunoreactivity, only a small number of astrocytes was TUNEL-positive, which is in agreement with previously published data showing apoptosis only in a small number of astrocytes (Acarin et al., 2007).

The positivity of astrocytes after ischemia for the different apoptotic markers without any decrease in the number of astrocytes in the affected tissue might signify another functional role for the expression of programmed cell death markers in activated astroglia. Some reports have even shown a constitutive expression of caspase-3 in astrocytes (Noyan-Ashraf et al., 2005). Besides leading to cell death, activated caspases participate in non-apoptotic cellular events including cell proliferation, cell cycle regulation, and cellular differentiation (Schwerk and Schulze-Osthoff, 2003). In reactive astrocytes, the activation of caspases is important for astroglial cytoskeleton remodeling following cellular injury (Acarin et al., 2007). Moreover, the activation of caspase-3 has been shown to be a prerequisite for ischemic preconditioning in many cell types, including neurons and astrocytes (Garnier et al., 2003; McLaughlin et al., 2003).

5.2 IDENTIFICATION OF DISTINCT GLIAL CELL TYPES IN THE CNS

5.2.1 Expression of specific antigens

In our experiments, we used specific antigenic markers to identify the distinct glial cell types in control nervous tissue and in the nervous tissue after injury. This is a routinely used approach; however, it requires a critical appraisal. The most commonly used marker of mature astrocytes is GFAP. Nevertheless, the immunohistochemical staining of astrocytes with an anti-GFAP antibody may lead to confusing results since astrocytes with low GFAP expression might appear GFAP-negative, and post-recording staining of fluorescent dye-loaded cells after patch-clamp experiments is often unsuccessful, probably because of the inaccessibility of the antigen to the antibody. Similarly to our findings, other research groups have shown that only part of gray matter astrocytes stain for GFAP (Walz, 2000; Kimelberg, 2004). Another possible marker of mature astrocytes is S100β, which labels a larger astrocytic population.

NG2 glia can be clearly recognized by staining for NG2 chondroitin sulfate proteoglycan. This marker is both very specific and sensitive. Caution needs to be taken only in injured tissue, where NG2 chondroitin sulfate proteoglycan is also expressed in activated microglia (Gao et al., 2010). Activated microglia and NG2 glia might be distinguished by their specific morphology, i.e. NG2 glia have numerous fine processes extending far from their small cell bodies while activated microglia display an amoeboid morphology without any processes.

The problem of precise glial cell identification arises particularly in young animals where glial cells with a complex current pattern might represent both NG2 glia and astrocyte precursors. Thus, using multiple glial cell markers together with patch-clamp measurements and careful interpretation of the data might prevent erroneous results.

5.2.2 The electrophysiological criteria of glial cells

The basic electrophysiological properties of glial cells are their inability to conduct action potentials and a very negative RMP compared to neurons. Similarly to neurons, NG2 glia and astrocyte precursors display considerable fast-activating Na^+ currents. However, the current density of Na^+ currents in glial cells is much smaller than that in neurons, and thus glial cells are unable to fire repetitive action potentials.

The existence of new data concerning NG2 glial physiology has prompted a need to re-evaluate results describing the membrane properties of cells with a complex current pattern after CNS injury, as these results might have included both NG2 glia and astrocytes, especially in young animals. Glial cells with a complex current pattern in the developing brain (up to P21) comprise two cell populations – presumed astrocyte precursors and NG2 glia (Zhou et al., 2006; Vignali et al., 2009). Moreover, owing to the presence of weak EGFP expression in NG2-positive cells in transgenic mice expressing EGFP under the GFAP promoter, NG2 cells might have been referred to as complex astrocytes in some studies, yet the membrane properties of complex astrocytes are often consistent with those of NG2 glia (Matthias et al., 2003; Wallraff et al., 2004).

In our study describing the membrane properties of astrocytes and NG2 glia in the hippocampal CA1 region in adult rats subjected to GCI, astrocytes and NG2 glia could be unequivocally identified based on their morphology, membrane properties, coupling and immunohistochemical staining for GFAP or NG2, as described previously

(Wallraff et al., 2004). Actually, this is the first electrophysiological study concerning the membrane properties of glial cells after CNS injury in which these two cell types were carefully distinguished.

5.3 MEMBRANE PROPERTIES OF GLIAL CELLS AFTER ISCHEMIA

5.3.1 Membrane properties of astrocytes after GCI

We have found that hippocampal astrocytes depolarized starting 3 days after GCI, which correlates well with the onset of the decrease in Kir4.1 protein expression in the ischemic hippocampus. Since it has been previously shown that the astrocyte membrane potential is dependent on Kir4.1 expression (Neusch et al., 2006; Djukic et al., 2007), we may assume that the depolarization of reactive astrocytes is a direct consequence of the decreased Kir4.1 channel expression triggered by ischemia. The downregulation of Kir4.1 mRNA or protein expression has been already demonstrated in other CNS and retina injury models (Iandiev et al., 2006; Kaiser et al., 2006; Lichter-Konecki et al., 2008). While the Kir4.1 channel is the main mediator of K^+ buffering in astrocytes (Kofuji and Newman, 2004), its downregulation after a CNS injury might lead to impaired K^+ homeostasis in the affected tissue. Another important function of astrocytes is to modulate synaptic plasticity (Ben Achour and Pascual, 2010) and to maintain glutamate homeostasis under both physiological and pathological conditions (Domingues et al., 2010). Since glutamate uptake is affected by impaired K^+ homeostasis (Djukic et al., 2007), it is likely that astrocytes after ischemia might not be able to fulfill these functions. Kir4.1 channels have been shown to represent the predominant K^+ channels underlying the time- and voltage-independent K^+ conductance in astrocytes (Seifert et al., 2009). Hence, we would expect to find an increase in the membrane resistance in astrocytes correlating with the diminished Kir4.1 channel expression after ischemia. Indeed, we observed a significant increase in astrocyte membrane resistance only 7 days after ischemia, when Kir4.1 expression is lowest according to the Western blot data. On the other hand, this phenomenon was not observed 3 days or 1 month after GCI, when Kir4.1 channel expression is decreased as well.

Reactive astrocytes 1 month after GCI displayed stronger inwardly rectifying currents compared to control astrocytes as revealed by calculating the outward/inward current ratio and by constructing I/V plots of the astrocytic currents. We hypothesize that other K^+ channel subtypes might also contribute to the astrocyte K^+ conductance and to the maintenance of a highly negative RMP, such as Kir2.1, Kir5.1 and the K_{2P} channels TREK1 and TWIK1 (Seifert et al., 2009; Zhou et al., 2009). The stronger inwardly rectifying currents in reactive astrocytes 1 month after ischemia might be explained by the differential regulation of weakly and strongly rectifying Kir channel subunits as described previously for retinal Muller cells (Iandiev et al., 2006). Indeed, Kang et al. (2008) has shown an upregulation of Kir2.1 channels in CA1 and CA3 astrocytes after a kainic acid lesion. However, we found no changes in Kir2.1 channel expression in the hippocampus after ischemia. On the other hand, immunohistochemistry revealed the relatively higher expression of Kir2.1 in reactive astrocytes 1 month after ischemia, when neurons are no longer present in the CA1 region of the hippocampus. A similar result was also observed for the expression of the Kir5.1 channel. The lower expression of the weakly rectifying Kir4.1 channel combined with the higher expression of the strongly rectifying Kir2.1 and Kir5.1 channels might lead to the observed increase in the inward rectification of the currents in reactive astrocytes. Since TWIK1 mediates weakly inwardly rectifying currents and TREK1 conducts outwardly rectifying currents, the lower out/in current ratio in reactive astrocytes might be also caused by different TWIK1/TREK1 expression levels. Western blot analysis revealed the expression of two different isoforms of the TREK1 channel in the hippocampus starting 3 days after GCI. These two isoforms of ~41 and 47 kDa with distinct functional properties might arise from the alternative initiation of mRNA translation, as described previously (Thomas et al., 2008). The expression of the ~41 kDa isoform was detected in controls and also during the entire time course of reperfusion; however, the expression of the ~47 kDa protein started 3 days after GCI and reached its maximum 1 month after GCI, thus correlating with the onset of reactive gliosis, astrocyte depolarization and Kir4.1 downregulation. Thus, it is likely that the ~47 kDa protein subunit might be expressed in reactive astrocytes. Since Kir4.1 channel expression seems to be sensitive to ischemia, the persistent expression of other Kir and K_{2P} channels might act as a protective mechanism in reactive astrocytes and might at least partially maintain their physiological functions, including K^+ buffering. It has been shown that ischemia increases the expression level of TREK2 channels in cultured

cortical astrocytes (Kucheryavykh et al., 2009); nevertheless, our data show that TREK2 overexpression does not occur after ischemia *in vivo*. It remains to be determined to what extent the changes in Kir4.1 and other Kir or K_{2P} channel activity influence the RMP and time- and voltage-independent K^+ conductance in astrocytes under both physiological and pathological conditions.

Some authors have reported an increase in the number of "complex astrocytes" and a decrease in the number of "passive astrocytes" in gliotic tissue after injury (Schroder et al., 1999; Wang et al., 2008). Here, we show that in the glial scar evoked by GCI in the CA1 region of the adult rat hippocampus, both reactive astrocytes and NG2 glia basically maintain their physiological current profiles, i.e. reactive astrocytes display time- and voltage-independent K^+ conductance and NG2 glia have substantial K_{DR}, K_A and K_{IR} currents in addition to the time- and voltage-independent K^+ conductance. In addition, reactive astrocytes considerably outnumber NG2 glia in the glial scar.

The depolarization and increased inward currents in reactive astrocytes 1 month after GCI might possibly have another nature. The hyperpolarization-activated, time- and voltage-dependent, non-inactivating inward currents observed in hippocampal astrocytes after GCI strongly resemble the I_{ha} currents, permeable for both K^+ and Na^+ cations, described by Guatteo et al. (1996) in cortical astrocyte cultures. Moreover, despite the fact that downregulation of Kir4.1 protein expression might have caused depolarization in astrocytes starting 3 days after GCI, additional ion conductance, presumably for Na^+ or Cl^- ions, might contribute to the astrocyte depolarization as well. Concerning Cl^- channels, the ClC2 channel subtype is activated by hyperpolarization, displays slow activation and no time-dependent inactivation, and its expression in astrocytes has been already demonstrated by Makara et al. (2003).

Many speculations have appeared about the homogeneity of the population of protoplasmic astrocytes in the adult grey matter. For example, the membrane potential of mature astrocytes was shown to display high variability in some studies (McKhann et al., 1997; Bolton et al., 2006); however, in other studies the astrocytic population in the CNS grey matter showed much more homogenous properties (Mishima and Hirase, 2010). This is consistent with our data measured in astrocytes in the adult rat hippocampus where the astrocyte RMP displayed very low variability.

5.3.2. Membrane properties of NG2 glia after GCI

In NG2 glia, ischemia resulted in their marked proliferation accompanied by the expression of nestin. The greatest NG2 glia proliferation was observed 3 days after ischemia, which coincided with an enhancement of the K_{DR} and K_A currents, an increase in the membrane resistance and a decrease in the K_{IR} currents. Enhanced voltage-dependent outwardly rectifying K^+ currents have been previously shown to be functionally associated with cell proliferation in different cell types including astrocytes (MacFarlane and Sontheimer, 2000; Pardo, 2004). In addition, the modulation of K^+ currents plays an important role in cell cycle regulation and proliferation in cultured OPCs (Knutson et al., 1997). More specifically, the Kv1.3 and Kv1.5 subunits have been shown to influence cell cycle progression in OPCs (Chittajallu et al., 2002; Vautier et al., 2004). Other authors have demonstrated that Kv1.4 subunit expression is enhanced in proliferating OPCs or NG2 glia after injury (Edwards et al., 2002; Herrero-Herranz et al., 2007). In contrast, Lytle et al. (2006) found an increase in membrane capacitance, a decrease in K_{DR} and K_A current densities and an increase in K_{IR} current density in NG2 glia isolated from the spinal cord 3 days after a contusion injury. The discrepancy between their and our results might arise from differences between *in vitro* and *in situ* approaches. Indeed, recently the same authors (Lytle et al., 2009) have shown an increase in K_{DR} currents in proliferative NG2 glia *in situ* 3 days after a spinal cord contusion injury performed in transgenic mice expressing EGFP driven by the 2-3-cyclic nucleotide 3-phosphodiesterase (CNP) promoter. Thus, we may conclude that NG2 or OPC proliferation is accompanied by increased outwardly rectifying K^+ currents both *in vitro* and *in vivo*. On the other hand, the increase in K_A currents shortly after ischemia (2 hours) might be a direct functional effect of the acute ischemic conditions. The excessive efflux of K^+ through K_{DR} and K_A channels has also been described as a key early step in apoptosis (Yu, 2003; Zhao et al., 2006).

It is unknown which ion channel subtypes underlie the K^+ inward currents in NG2 glia. Recent data have demonstrated that Kir4.1 channels might also mediate the inwardly rectifying K^+ currents in NG2 glia in addition to astrocytes (Djukic et al., 2007; Tang et al., 2009). Thus, the increase in NG2 glia membrane resistance after ischemia might be attributable to the decrease of Kir4.1 channel expression. On the other hand, we did not observe a significant depolarization of NG2 glia after ischemia. Nevertheless, our immunohistochemical analyses did not demonstrate the expression of

any studied Kir or K_{2P} channels in hippocampal NG2 glia in controls or after ischemia (data not shown).

5.3.3 Membrane properties of astrocytes after exposure to high [K^+]

We examined changes in the membrane properties and cell volume regulation of spinal cord astrocytes after exposure to high K^+. We found that a 3-hour incubation in 50 mM K^+ induced changes in both astrocyte morphology and GFAP immunoreactivity, but not in GFAP expression. The membrane properties of complex astrocytes were the most affected by incubation in high K^+ compared to passive astrocytes or astrocyte precursors (see Table 4). Furthermore, the quantification of volume changes during hypotonic stress based on K^+ accumulation and 3D morphometry showed differences in the volume regulation of spinal cord astrocytes preincubated in high K^+ compared to control astrocytes; that is, astrocytes pre-exposed to high K^+ exhibited less swelling.

Cell swelling and astrogliosis accompanied by impaired extracellular diffusion in the CNS tissue have been found after exposure of isolated rat spinal cord segments to an elevated K^+ concentration (Sykova et al., 1999). We observed changes in astrocyte morphology and an increase in GFAP immunoreactivity in rat spinal cords exposed to high K^+ as well; however, this increase was not the result of the overexpression of GFAP typical of astrogliosis. As has been demonstrated, an increase in GFAP immunostaining can be evoked in mature astrocyte cultures by exposing the cells to an acidic medium, which induces proteolytic degradation of the GFAP (Lee et al., 2000). At a lower pH, GFAP forms unusual ribbon-like filaments wider than the normal size of 10 nm (Inagaki et al., 1994). These data indicate that the initial rapid increase in GFAP staining following CNS injury may be the result of the exposure of specific antigenic haptens to GFAP antibodies, caused either by proteolytic degradation of the protein or by changes in its conformation. Our data show that incubation in 50 mM K^+ decreases the pH_e in the spinal cord; thus, the increased GFAP immunoreactivity might be caused by factors similar to those mentioned above. Moreover, GFAP staining revealed that the morphology of astrocytes incubated in high K^+ differed from that of control astrocytes and exhibited typical reactive astrocyte-like morphology, i.e., large cell bodies and thick and short processes, which might also result from GFAP conformational changes.

Based on the passive membrane properties and voltage-dependent K^+ and Na^+ channel expression, we divided spinal cord astrocytes into three groups: complex

astrocytes, astrocyte precursors, and passive astrocytes, as similarly described by others (Chvatal et al., 1995; Jabs et al., 1997; D'Ambrosio et al., 1999; Anderova et al., 2004). Because it has been shown that passive K^+ currents and K_{IR} currents are upregulated in astrocytes during postnatal maturation and, thus, a higher R_M might be related to the properties of astrocyte precursors (Kressin et al., 1995), we termed the astrocytes with a high R_M and undetectable K_{IR} currents "precursors". Moreover, astrocyte precursors did not change their membrane properties after exposure to high K^+, whereas complex astrocytes were the most affected. Another classification of glial cells based on their current patterns, GluR or GluT expression and staining for NG2 proteoglycan or GFAP has been proposed for the mouse hippocampus by Matthias et al. (2003). In contrast to their study, we have shown that complex astrocytes were stained for astrocyte markers such as GFAP and S100β. However, some of the complex astrocytes in our study might belong to the population of "NG2 glia" described by Matthias et al. (2003). Our finding that complex astrocytes are the type most affected by pathological conditions is in agreement with other studies (Jabs et al., 1997; D'Ambrosio et al., 1999). A shift of the RMP and V_{rev} to more positive values might be the result of a persistent ionic unbalance in the tissue; however, $[K^+]_e$ returned to control values within 30 min after the end of the spinal cords' incubation in 50 mM K^+. The depolarization of complex astrocytes might also be a result of altered relative Cl^-/K^+ permeability, which would shift the membrane potential to the equilibrium potential of Cl^-, i.e., to more positive values in our experiments. An increase in Cl^- conductance in astrocytes has been shown during swelling (Lascola and Kraig, 1996) and in decreased pH_e (Ferroni et al., 2000), which is the case in spinal cords incubated in elevated K^+. However, we did not further investigate this phenomenon. Similar to our observations, MacFarlane and Sontheimer (1997) showed a depolarization and a C_M decrease in astrocytes after acute injury, while an R_M increase was shown by Pannicke et al. (2000) and Bordey et al. (2001). Because outwardly rectifying K^+ currents have been suggested to be involved in RMP maintenance and K^+ homeostasis (Sontheimer, 1994; Pannicke et al., 2000) and Na^+ channels have been proposed to maintain Na^+/K^+ATPase and Na^+/glutamate transporter function in glia (Verkhratsky and Steinhauser, 2000), major changes in K^+ and Na^+ currents could be expected immediately after injury, when resting $[K^+]_e$ is increased. We observed an increase in K_{DR}, K_A, and I_{Na} CDs after incubation in high K^+. A similar result was found *in vitro* in proliferative astrocytes 4 hours after injury by MacFarlane and Sontheimer (1997), but excessive K^+ efflux by K_{DR} and K_A and the resulting

intracellular K^+ depletion have also been described as key early steps in apoptosis (Yu, 2003). In contrast to data presented by others (D'Ambrosio et al., 1999; Hinterkeuser et al., 2000; Koller et al., 2000), but in agreement with yet other data (Perillan et al., 1999; Bordey et al., 2000; Anderova et al., 2004), we have found K_{IR} current upregulation in complex astrocytes after exposure to high K^+. The increase in CDs might be a consequence of the much smaller C_M caused by the incubation of complex astrocytes in elevated K^+; however, this raises the question of whether ion channel expression and/or ion channel properties such as gating, kinetics, or unitary conductance are also affected. In contrast to complex astrocytes, passive astrocytes from spinal cords incubated in high K^+ exhibited a marked decrease in K_{DR} and K_A currents, while the membrane properties of astrocyte precursors were not significantly different from those in control tissue.

Because ion channels play a role in volume regulation in astrocytes, the ability of astrocytes preincubated in high K^+ to adjust their volume in response to hypotonic stress was examined. We found decreased K^+ accumulation around the cell membrane, suggesting cell shrinkage, which is in agreement with the smaller degree of swelling revealed by 3D morphometry in astrocytes preincubated in high K^+ compared to controls. Besides the astrocyte volume changes, it is possible that a decrease in ΔK^+ accumulation might reflect changes in the properties of the extracellular space or ion channel densities. Anderova et al. (2001) demonstrated a lower K^+ accumulation in the vicinity of the cell membrane after a depolarizing prepulse and slower swelling in $GFAP^{-/-}$ astrocytes. Because GFAP has been shown to play a role in astrocyte volume changes (Anderova et al., 2001; Pekny and Nilsson, 2005), a possible explanation for the smaller volume changes seen in astrocytes preincubated in high K^+ might be functional changes in GFAP, e.g., conformational changes, protein phosphorylation/dephosphorylation, or assembly/disassembly of protein subunits (Inagaki et al., 1994; Lee et al., 2000).

We conclude that exposure to high K^+, which is an early event accompanying many pathological states ultimately leading to astrogliosis, causes not only morphological changes in astrocytes, but also changes in their membrane properties and cell volume regulation. Such alterations in astrocyte properties may affect ion homeostasis and the diffusion of neuroactive substances in the CNS tissue during the early phases of pathological states and may also influence tissue regeneration.

5.3.4 Comparison of glial cell membrane properties after acute and chronic CNS ischemic injury

The basic membrane properties of passive astrocytes in an acute model of nervous tissue ischemia (spinal cord incubation in high K^+) and in the acute phases of reperfusion after GCI (up to 1 day) were comparable, i.e. we found no or just minor changes in their RMP, R_M and C_M. After GCI, we observed the first marked changes of astrocyte membrane properties, i.e. significant depolarization, starting 3 days after the injury. These results are consistent with the data from other laboratories, which also reported no changes in the membrane properties of passive astrocytes after CNS injury (Jabs et al., 1997; Schroder et al., 1999). However, only a small number of electrophysiological studies on astrocytes after CNS injury have been performed at late stages after the injury, and thus our study is the first to include astrocyte membrane properties in both the acute and late phases after ischemia, which makes our data also more comprehensive. A previous work conducted in our laboratory (Anderova et al., 2004) showed the presence of K_{DR} currents in astrocytes with prominent time- and voltage-independent currents 7 days after a mechanical cortical injury (stab wound). We did not observe this type of membrane current pattern in passive hippocampal astrocytes at any timepoint after GCI. This controversy might be explained by the fact that the specific nature of the injury might greatly influence the membrane properties of astrocytes. Moreover, the age of the animals might play a role as well; however, both models of CNS injury (GCI and stab wound) were performed in rats after the end of gliogenesis. In conclusion, it is obvious that mature astrocytes show considerable changes in their membrane properties starting only several days after a CNS injury. Moreover, these changes are accompanied by alterations in astrocyte morphology (transition to the reactive state) and by changes in the expression of GFAP and the Kir4.1 channel subunit.

Interestingly, we found comparable changes in the membrane properties of complex astrocytes in an acute ischemic CNS injury model and in NG2 glia in the acute phases of reperfusion after GCI. These two cell types with a complex current pattern, complex astrocytes and NG2 glia, show the greatest changes in their membrane properties after CNS injury. This phenomenon might have two explanations. First, some complex astrocytes measured in the rat spinal cord might belong to the NG2 glia population and thus might have similar properties as those of hippocampal NG2 glia.

Moreover, the membrane properties of hippocampal NG2 glia after ischemia are consistent with some of the data describing the membrane properties of complex astrocytes after CNS injury in other previous studies (D'Ambrosio et al., 1999; Bordey et al., 2001), and thus it is possible that glial cells with a complex current pattern might have included both NG2 glia and astrocytes, especially in young animals. Since we used two astrocyte-specific antibodies, against GFAP and S100β, to identify astrocytes in our experiments, this possibility is not likely. Second, glial cells with similar membrane properties, i.e. with the complex current profile, might respond to CNS injury in an analogous way. Here, we might speculate on the common reaction of some specific ion currents/channels to injury, such as the downregulation of K_{IR} currents together with depolarization and an increase in R_M and the upregulation of outwardly rectifying K_{DR} and K_A currents. Indeed, several publications have reported a similar response to CNS injury in neurons as well (Chi and Xu, 2000; Deng et al., 2005). Nevertheless, in each cell type, the functional effect of such changes in their membrane properties might be different, although always presumably leading to a kind of cell-protective mechanism against the injury.

Another group of astrocytes distinguished in the young rat spinal cord, the astrocyte precursors, could not be found in the adult rat hippocampal tissue after GCI, and hence we cannot compare the changes in their membrane properties in an acute and chronic CNS injury model.

5.4 THE FUNCTION OF SPECIFIC ION CHANNELS IN GLIAL CELLS AFTER CNS INJURY

5.4.1 The role of Kir channels in glial cells after CNS injury

The primary role of Kir channels in astrocytes is to set their negative RMP and high resting K^+ conductance, establishing the prerequisites for the K^+ spatial buffering mechanism. The specific Kir channel subtype expressed in astrocytes is the Kir4.1 (Poopalasundaram et al., 2000). In our study, we have found that Kir4.1 channel expression decreased in the hippocampal tissue starting 3 days after GCI. This fact might have great functional consequences including an impairment of the K^+ buffering and glutamate clearing capacity of reactive astrocytes in the gliotic tissue.

Consequently, such tissue might be prone to generate seizure activity. On the other hand, the expression of other K^+ channels expressed in astrocytes was not substantially altered in the hippocampal tissue after ischemia, and thus reactive astrocytes might still retain their ability to buffer K^+. The nervous tissue's buffering capacity might already be decreased earlier after ischemia, before the downregulation of Kir4.1 expression, because of channel mislocation, as described in proliferative vitreoretinopathy by Ulbricht et al. (2008).

Kir4.1 expression in astrocytes is developmentally regulated, i.e. its expression increases with postnatal age (Bordey and Sontheimer, 1997). The specific signals regulating Kir4.1 channel expression are unknown, but we might hypothesize that Kir4.1 expression is dependent on increasing neuronal activity during CNS development. Similarly, decreased neuronal activity in the CNS tissue after ischemia might lead to a decrease in Kir4.1 channel expression in astrocytes. This hypothesis; however, needs to be confirmed by further experiments. Moreover, the functional consequences during nervous tissue damage after ischemia are not well understood; astrocytes may loose their supportive functions and, as a result, neurons die, or the neuronal loss may lead to the functional impairment of astrocytes. For better understanding of the processes leading to the development of reactive gliosis, a deeper knowledge of the mechanisms regulating Kir channel expression in astrocytes is needed.

Some data from previous studies indicate different roles for distinct Kir channel subunits in astrocytes. In retinal Muller cells, the strongly rectifying Kir2.1 channels mediate the influx of K^+ at sites of neuronal activity, and the weakly inwardly rectifying Kir4.1 channels mediate the K^+ efflux at blood vessels (Kofuji et al., 2002). Similar mechanism might function in other CNS regions. Thus, it is surprising that astrocytes after ischemia lose the expression of Kir4.1 but retain the expression of the Kir2.1 channel. In accordance with our study, Perillan et al. (2000) also found the expression of a strongly rectifying K^+ channel, Kir2.3, in reactive astrocytes. Since strongly rectifying Kir channels are less suited for K^+ buffering, this transition of Kir channel subunit expression might lead to a further decrease of the K^+ buffering capacity of the affected nervous tissue.

In our study, we observed an increase in the expression of Kir5.1 in hippocampal astrocytes after ischemia. Kir5.1 channel subunits make heteromers with other Kir channels, such as Kir4.1, and may profoundly change their functional

properties. The heteromeric channels are highly sensitive to intracellular pH and CO_2 (Cui et al., 2001) and may therefore be involved in the regulation of cellular acid-base homeostasis in the ischemic tissue (Tanemoto et al., 2000). Moreover, the Kir4.1/Kir5.1 heteromers are strongly rectifying channels.

It is still not known which Kir channels mediate the K_{IR} currents in NG2 glia. Hippocampal NG2 glia show substantial proliferation and, concurrently, a decrease in K_{IR} currents after ischemia. It is likely that the decrease in K_{IR} currents in NG2 glia might play a role in their proliferative activity. Similar observations were made in other cell types including astrocytes (MacFarlane and Sontheimer, 2000) and fibroblasts (Chilton et al., 2005). In addition, Higashimori and Sontheimer (2007) showed that Kir4.1 causes membrane hyperpolarization leading to growth attenuation, which in turn induces cell maturation characterized by a shift of the cells from G2/M into G0/G1, and thus Kir4.1 may control the growth of glial cells.

In conclusion, Kir channels in astrocytes are primarily involved in homeostatic functions, which might be impaired after CNS injury when the expression pattern of Kir channels is changed. In NG2 glia, decreased K_{IR} currents contribute to cell proliferation.

5.4.2 The role of K_{2P} channels in glial cells after CNS injury

K_{2P} channels have only recently been discovered, and their expression in astrocytes in *situ* belongs to rather novel findings. Therefore, their properties and functions have been studied more extensively in other cell types, including neurons. In neurons, K_{2P} channels play an important role in the sensitivity to volatile anesthetics and in many different pathologies, such as depression (Heurteaux et al., 2006; Honore, 2007). It is likely that K_{2P} channels are important for physiological functions in astrocytes as well. However, this hypothesis needs to be corroborated by further experiments.

The K_{2P} channel TASK-3 has been shown to influence apoptosis in neurons. Patel and Lazdunski (2004) demonstrated that blocking the efflux of K^+ through TASK3 channels leads to the better survival of cerebellar granule neurons in conditions of elevated $[K^+]_e$. K_{2P} channels also underlie K^+ efflux during the apoptotic volume decrease in mouse embryos (Trimarchi et al., 2002). Similar mechanisms might be involved in astrocyte cell death in the hippocampal tissue after ischemia.

Since TREK-1 channels are activated by polyunsaturated fatty acids, such as AA (AA content increases in ischemic tissue, leading to the opening of neuronal K_{2P}

channels and subsequent hyperpolarization (Patel and Honore, 2001)), these channels might be involved in neuroprotection. Moreover, TREK-1 channels are resistant to hypoxia (Buckler and Honore, 2005). Pasler et al. (2007) have shown that K_{2P} channels mediate K^+ release from neurons and possibly contribute to glial K^+ buffering. Kucheryavykh et al. (2009) demonstrated that the upregulation of TREK-2 channels may help to rescue astrocyte function and lower extracellular glutamate during ischemia. All of these findings, together with our results showing the persistent expression of TREK-1 and TWIK-1 channels in hippocampal astrocytes after ischemia, lead to the conclusion that K_{2P} channels might represent an important mechanism in cellular protection after CNS ischemia. It is also likely that modulation of their activity might be a novel promising tool in ischemia treatment.

5.4.3 The role of Kv channels in glial cells after CNS injury

We have found that both astrocyte precursors and NG2 glia increase K_{DR} and K_A currents, presumably based on the expression of Kv channels, in response to an ischemic injury. The activation of outwardly rectifying K^+ currents has been shown in many cell types during their proliferation. More specifically, the activity of Kv1.3 and Kv1.5 channel subunits has been shown to influence cell cycle progression in OPCs (Chittajallu et al., 2002; Vautier et al., 2004). In cultured astrocytes, the activity of outwardly rectifying K^+ channels is crucial for G1/S checkpoint progression (MacFarlane and Sontheimer, 2000).

The outwardly rectifying K^+ channels have been also implicated in the apoptotic process. From a morphological point of view, apoptosis and mitosis have a number of similar characteristics such as cytoskeletal changes, rounding up of the cell, nuclear envelope breakdown, and chromatin condensation. Excessive K^+ efflux and intracellular K^+ depletion have been found to be required for apoptotic cell shrinkage in many cell types, including neurons (Bortner et al., 1997; Wei et al., 2003). Nevertheless, in the CA1 region of the hippocampus after GCI, NG2 glia stain for proliferative markers such as PCNA, but do not show any staining or specific signs of cell death. Astrocytes, in contrast, show positivity for some apoptotic markers and for markers of delayed cell death and only a very low number of them proliferate, but they do not have any outwardly rectifying K^+ currents. In conclusion, Kv channels and/or the outwardly

rectifying K_{DR} and K_A currents probably play a role in NG2 glia proliferation after CNS injury.

5.5 GLIAL CELLS AFTER CNS ISCHEMIA – GENERAL CONSIDERATIONS AND POSSIBLE THERAPEUTIC APPROACHES

It has been speculated for a long time that the glial scar, generated as a common response to CNS injury, might separate the healthy tissue from the injured tissue and thus impede the progression of seizures and/or further injury. For this function, reactive astrocytes would need to maintain a functional K^+ buffering mechanism. However, based on new electrophysiological data, this hypothesis is unlikely, because it is now obvious that reactive astrocytes lose their expression of the specific ion channel, Kir4.1, which performs the basic functions for K^+ spatial buffering and glutamate uptake. On the other hand, the expression of other K^+ channels is still preserved in reactive astrocytes and their function has not yet been identified. The extent to which reactive astrocytes are able to maintain ionic and neurotransmitter homeostasis needs to be determined in further experiments.

One aspect of reactive astrogliosis that is still not understood is whether reactive astrocytes are "injured" cells with an impaired functional capacity, or whether they are "activated" and thus better suited for tissue protection and repair. Reactive astrocytes produce a wide range of immunomodulatory molecules, such as cytokines or growth factors, which may promote neurogenesis and functional recovery of the affected CNS tissue.

Most therapeutic approaches proposed for CNS injury treatment are based on neuroprotective mechanisms. New therapeutic approaches might arise from studies focused on mechanisms of cellular injury not only in neurons, but also in glial cells. The response to an injury is an integrated and complex reaction of the individual components of the nervous tissue, thus new concepts for stroke research emphasize the interactions between astrocytes, microglia, endothelial cells, vascular smooth muscle cells and neurons. The goal of most studies is to find an approach to promote neuronal survival or neuronal regeneration in the damaged area. Since astrocytes have the ability to maintain homeostasis under physiological conditions, they might be able to help neurons survive during hypoxia/ischemia. Moreover, astrocytes might promote

neurogenesis and gliogenesis. For finding effective treatment of CNS injury including ischemia, it is necessary to know in great detail the behavior and possible protective mechanisms in glial cells induced by CNS injury.

NG2 glia have been shown to give rise to oligodendrocytes in the white matter after CNS injury in many studies. However, their behavior in the grey matter following injury is much less well understood. From our data and based on other published data, we might only speculate that NG2 glia give rise to reactive astrocytes in the grey matter after CNS injury. To prove this hypothesis, a fate mapping study using transgenic animals that express, e.g., GFP under the control of the Cspg4 promoter, would be necessary.

NG2 glia might play an important function in tissue regeneration and recovery because they proliferate and may differentiate into other CNS cell types, including neurons. Thus, finding therapeutic approaches affecting NG2 glia differentiation might represent a promising tool for CNS injury treatment. Indeed, the last reported clinical study on spinal cord injury employs the transplantation of human embryonic stem cell-derived oligodendrocyte progenitor cells into the injured spinal cord of the patients (www.geron.com).

6. CONCLUSIONS

In our experiments, we used two models of CNS ischemic injury to study the membrane properties of astrocytes and NG2 glia in the acute and chronic stages of reperfusion. First, using immunohistochemistry, cell counting and Western blot analyses, we characterized the tissue damage caused by GCI and spinal cord incubation in a solution with high [K^+]. GCI resulted in neuronal loss and the generation of a glial scar in the CA1 region of the hippocampus within 7 days of reperfusion. We found that reactive astrocytes expressed apoptotic markers and only a small number of them proliferated. Despite their low proliferation, the number of astrocytes was significantly increased starting 1 month after ischemia. NG2 glia and microglia proliferated extensively starting 1 day after ischemia and, moreover, NG2 glia expressed a marker of newly derived cells, nestin. In spinal cords incubated in a solution with high [K^+], we found early morphological changes in astrocytes but no changes in GFAP expression, indicating that 3 hours incubation results in pre-gliotic changes in astrocytes.

The main findings of our experiments are as follows:

1. Astrocytes show an increase in their total cell volume one month after ischemia accompanied by cell soma enlargement and retraction of the processes, changes typical of cellular hypertrophy. NG2 glia display a reduction in their total cell volume and the volume of the processes starting 3 days after ischemia, suggesting morphological alterations of proliferating cells.
2. Astrocytes depolarize starting 3 days after ischemia and demonstrate an increase in the inward rectification of their whole cell currents 1 month after ischemia.
3. The Kir4.1 channel expression in the hippocampal tissue is downregulated starting 3 days after ischemia, while the expression of other K^+ channels, such as Kir2.1, Kir5.1 and TREK1, is strongly upregulated in reactive astrocytes after ischemia, which might result in a shift in the rectification profile of astrocytes.
4. NG2 glia show higher membrane resistance and lower membrane capacitance 3 days after ischemia. The decrease in the membrane capacitance coincides with the morphological changes in NG2 glia.

5. NG2 glia display a significant increase in the outwardly rectifying K_A and K_{DR} currents 2 hours and 3 days after ischemia, and a decrease in K_{IR} currents 3 days after ischemia, a typical current pattern of proliferating NG2 glia.
6. Complex astrocytes in the spinal cord after incubation in a solution with high $[K^+]$ show the largest changes in their membrane properties compared to other astrocyte subtypes, i.e. increased activity of the outwardly rectifying K_{DR} and K_A currents.
7. Spinal cord exposure to high $[K^+]$ results in altered volume regulation in astrocytes.

To conclude, the decrease of Kir4.1 channel expression in astrocytes after ischemia followed by depolarization might lead to an impairment of K^+ and glutamate homeostasis in the affected tissue. It is apparent that mature, passive astrocytes respond to an ischemic injury with a delay; the first changes in their membrane properties could be detected only after 3 days of reperfusion. On the other hand, complex astrocytes in the spinal cord as well as hippocampal NG2 glia display membrane properties typical of proliferating cells during the early phases after an ischemic injury, i.e. increased activity of the outwardly rectifying K_{DR} and K_A currents.

The significance of our work lies in its new insight into the research of glial membrane properties after CNS injury because we also took into account the newly-described expression of K_{2P} channels as potential players. Moreover, after many years and a number of studies employing different models of CNS injury, we present a comprehensive view about the behavior of glial cells after CNS injury, during both the acute and chronic phases of reperfusion. This is also the first study of the membrane properties of NG2 glia after ischemia.

7. REFERENCES

1. Acarin, L., Villapol, S., Faiz, M., Rohn, T. T., Castellano, B. and Gonzalez, B. (2007) Caspase-3 activation in astrocytes following postnatal excitotoxic damage correlates with cytoskeletal remodeling but not with cell death or proliferation. Glia 55, 954-65.
2. Adams, H., Adams, R., Del Zoppo, G. and Goldstein, L. B. (2005) Guidelines for the early management of patients with ischemic stroke: 2005 guidelines update a scientific statement from the Stroke Council of the American Heart Association/American Stroke Association. Stroke 36, 916-23.
3. Adermark, L. and Lovinger, D. M. (2008) Electrophysiological properties and gap junction coupling of striatal astrocytes. Neurochem Int 52, 1365-72.
4. Adhami, F., Schloemer, A. and Kuan, C. Y. (2007) The roles of autophagy in cerebral ischemia. Autophagy 3, 42-4.
5. Alonso, G. (2005) NG2 proteoglycan-expressing cells of the adult rat brain: possible involvement in the formation of glial scar astrocytes following stab wound. Glia 49, 318-38.
6. Amiry-Moghaddam, M., Williamson, A., Palomba, M., Eid, T., de Lanerolle, N. C., Nagelhus, E. A., Adams, M. E., Froehner, S. C., Agre, P. and Ottersen, O. P. (2003) Delayed K^+ clearance associated with aquaporin-4 mislocalization: phenotypic defects in brains of alpha-syntrophin-null mice. Proc Natl Acad Sci U S A 100, 13615-20.
7. Anderova, M., Antonova, T., Petrik, D., Neprasova, H., Chvatal, A. and Sykova, E. (2004) Voltage-dependent potassium currents in hypertrophied rat astrocytes after a cortical stab wound. Glia 48, 311-26.
8. Anderova, M., Kubinova, S., Mazel, T., Chvatal, A., Eliasson, C., Pekny, M. and Sykova, E. (2001) Effect of elevated K(+), hypotonic stress, and cortical spreading depression on astrocyte swelling in GFAP-deficient mice. Glia 35, 189-203.
9. Araque, A., Parpura, V., Sanzgiri, R. P. and Haydon, P. G. (1999) Tripartite synapses: glia, the unacknowledged partner. Trends Neurosci 22, 208-15.
10. Assuncao Guimaraes, C. and Linden, R. (2004) Programmed cell deaths. Apoptosis and alternative deathstyles. Eur J Biochem 271, 1638-50.
11. Bekar, L. K., Loewen, M. E., Cao, K., Sun, X., Leis, J., Wang, R., Forsyth, G. W. and Walz, W. (2005) Complex expression and localization of inactivating Kv channels in cultured hippocampal astrocytes. J Neurophysiol 93, 1699-709.
12. Ben Achour, S. and Pascual, O. (2010) Glia: The many ways to modulate synaptic plasticity. Neurochem Int
13. Benesova, J., Hock, M., Butenko, O., Prajerova, I., Anderova, M. and Chvatal, A. (2009) Quantification of astrocyte volume changes during ischemia *in situ* reveals two populations of astrocytes in the cortex of GFAP/EGFP mice. J Neurosci Res 87, 96-111.
14. Bergles, D. E., Roberts, J. D., Somogyi, P. and Jahr, C. E. (2000) Glutamatergic synapses on oligodendrocyte precursor cells in the hippocampus. Nature 405, 187-91.

15. Bezzi, P., Gundersen, V., Galbete, J. L., Seifert, G., Steinhauser, C., Pilati, E. and Volterra, A. (2004) Astrocytes contain a vesicular compartment that is competent for regulated exocytosis of glutamate. Nat Neurosci 7, 613-20.
16. Bichet, D., Haass, F. A. and Jan, L. Y. (2003) Merging functional studies with structures of inward-rectifier K(+) channels. Nat Rev Neurosci 4, 957-67.
17. Block, F. (1999) Global ischemia and behavioural deficits. Prog Neurobiol 58, 279-95.
18. Bolton, S., Greenwood, K., Hamilton, N. and Butt, A. M. (2006) Regulation of the astrocyte resting membrane potential by cyclic AMP and protein kinase A. Glia 54, 316-28.
19. Bondarenko, A. and Chesler, M. (2001) Rapid astrocyte death induced by transient hypoxia, acidosis, and extracellular ion shifts. Glia 34, 134-42.
20. Bordey, A., Hablitz, J. J. and Sontheimer, H. (2000) Reactive astrocytes show enhanced inwardly rectifying K^+ currents *in situ*. Neuroreport 11, 3151-5.
21. Bordey, A., Lyons, S. A., Hablitz, J. J. and Sontheimer, H. (2001) Electrophysiological characteristics of reactive astrocytes in experimental cortical dysplasia. J Neurophysiol 85, 1719-31.
22. Bordey, A. and Sontheimer, H. (1997) Postnatal development of ionic currents in rat hippocampal astrocytes *in situ*. J Neurophysiol 78, 461-77.
23. Bordey, A. and Sontheimer, H. (1998a) Passive glial cells, fact or artifact? J Membr Biol 166, 213-22.
24. Bordey, A. and Sontheimer, H. (1998b) Properties of human glial cells associated with epileptic seizure foci. Epilepsy Res 32, 286-303.
25. Bordey, A. and Sontheimer, H. (2000) Ion channel expression by astrocytes *in situ*: comparison of different CNS regions. Glia 30, 27-38.
26. Bortner, C. D., Hughes, F. M., Jr. and Cidlowski, J. A. (1997) A primary role for K^+ and Na^+ efflux in the activation of apoptosis. J Biol Chem 272, 32436-42.
27. Bredesen, D. E., Rao, R. V. and Mehlen, P. (2006) Cell death in the nervous system. Nature 443, 796-802.
28. Buckler, K. J. and Honore, E. (2005) The lipid-activated two-pore domain K^+ channel TREK-1 is resistant to hypoxia: implication for ischaemic neuroprotection. J Physiol 562, 213-22.
29. Burg, E. D., Remillard, C. V. and Yuan, J. X. (2006) K^+ channels in apoptosis. J Membr Biol 209, 3-20.
30. Burns, K. A., Murphy, B., Danzer, S. C. and Kuan, C. Y. (2009) Developmental and post-injury cortical gliogenesis: a genetic fate-mapping study with Nestin-CreER mice. Glia 57, 1115-29.
31. Bush, T. G., Puvanachandra, N., Horner, C. H., Polito, A., Ostenfeld, T., Svendsen, C. N., Mucke, L., Johnson, M. H. and Sofroniew, M. V. (1999) Leukocyte infiltration, neuronal degeneration, and neurite outgrowth after ablation of scar-forming, reactive astrocytes in adult transgenic mice. Neuron 23, 297-308.
32. Bushong, E. A., Martone, M. E., Jones, Y. Z. and Ellisman, M. H. (2002) Protoplasmic astrocytes in CA1 stratum radiatum occupy separate anatomical domains. J Neurosci 22, 183-92.
33. Butt, A. M. and Kalsi, A. (2006) Inwardly rectifying potassium channels (Kir) in central nervous system glia: a special role for Kir4.1 in glial functions. J Cell Mol Med 10, 33-44.

34. Butt, A. M., Kiff, J., Hubbard, P. and Berry, M. (2002) Synantocytes: new functions for novel NG2 expressing glia. J Neurocytol 31, 551-65.
35. Cahoy, J. D., Emery, B., Kaushal, A., Foo, L. C., Zamanian, J. L., Christopherson, K. S., Xing, Y., Lubischer, J. L., Krieg, P. A., Krupenko, S. A., Thompson, W. J. and Barres, B. A. (2008) A transcriptome database for astrocytes, neurons, and oligodendrocytes: a new resource for understanding brain development and function. J Neurosci 28, 264-78.
36. Chen, M., Dong, Y. and Simard, J. M. (2003) Functional coupling between sulfonylurea receptor type 1 and a nonselective cation channel in reactive astrocytes from adult rat brain. J Neurosci 23, 8568-77.
37. Chen, M. and Simard, J. M. (2001) Cell swelling and a nonselective cation channel regulated by internal Ca^{2+} and ATP in native reactive astrocytes from adult rat brain. J Neurosci 21, 6512-21.
38. Chever, O., Djukic, B., McCarthy, K. D. and Amzica, F. (2010) Implication of Kir4.1 channel in excess potassium clearance: an *in vivo* study on anesthetized glial-conditional Kir4.1 knock-out mice. J Neurosci 30, 15769-77.
39. Chi, X. X. and Xu, Z. C. (2000) Differential changes of potassium currents in CA1 pyramidal neurons after transient forebrain ischemia. J Neurophysiol 84, 2834-43.
40. Chilton, L., Ohya, S., Freed, D., George, E., Drobic, V., Shibukawa, Y., Maccannell, K. A., Imaizumi, Y., Clark, R. B., Dixon, I. M. and Giles, W. R. (2005) K^+ currents regulate the resting membrane potential, proliferation, and contractile responses in ventricular fibroblasts and myofibroblasts. Am J Physiol Heart Circ Physiol 288, H2931-9.
41. Chittajallu, R., Aguirre, A. and Gallo, V. (2004) NG2-positive cells in the mouse white and grey matter display distinct physiological properties. J Physiol 561, 109-22.
42. Chittajallu, R., Chen, Y., Wang, H., Yuan, X., Ghiani, C. A., Heckman, T., McBain, C. J. and Gallo, V. (2002) Regulation of Kv1 subunit expression in oligodendrocyte progenitor cells and their role in G1/S phase progression of the cell cycle. Proc Natl Acad Sci U S A 99, 2350-5.
43. Chvatal, A., Anderova, M., Hock, M., Prajerova, I., Neprasova, H., Chvatal, V., Kirchhoff, F. and Sykova, E. (2007a) Three-dimensional confocal morphometry reveals structural changes in astrocyte morphology *in situ*. J Neurosci Res 85, 260-71.
44. Chvatal, A., Anderova, M. and Kirchhoff, F. (2007b) Three-dimensional confocal morphometry - a new approach for studying dynamic changes in cell morphology in brain slices. J Anat 210, 671-83.
45. Chvatal, A., Anderova, M. and Sykova, E. (2004) Analysis of K^+ accumulation reveals privileged extracellular region in the vicinity of glial cells *in situ*. J Neurosci Res 78, 668-82.
46. Chvatal, A., Anderova, M., Ziak, D. and Sykova, E. (1999) Glial depolarization evokes a larger potassium accumulation around oligodendrocytes than around astrocytes in gray matter of rat spinal cord slices. J Neurosci Res 56, 493-505.
47. Chvatal, A., Pastor, A., Mauch, M., Sykova, E. and Kettenmann, H. (1995) Distinct populations of identified glial cells in the developing rat spinal cord slice: ion channel properties and cell morphology. Eur J Neurosci 7, 129-42.
48. Cornell-Bell, A. H., Finkbeiner, S. M., Cooper, M. S. and Smith, S. J. (1990) Glutamate induces calcium waves in cultured astrocytes: long-range glial signaling. Science 247, 470-3.

49. Cui, N., Giwa, L. R., Xu, H., Rojas, A., Abdulkadir, L. and Jiang, C. (2001) Modulation of the heteromeric Kir4.1-Kir5.1 channels by P(CO(2)) at physiological levels. J Cell Physiol 189, 229-36.
50. Daikhin, Y. and Yudkoff, M. (2000) Compartmentation of brain glutamate metabolism in neurons and glia. J Nutr 130, 1026S-31S.
51. D'Ambrosio, R., Gordon, D. S. and Winn, H. R. (2002) Differential role of KIR channel and Na(+)/K(+)-pump in the regulation of extracellular K(+) in rat hippocampus. J Neurophysiol 87, 87-102.
52. D'Ambrosio, R., Maris, D. O., Grady, M. S., Winn, H. R. and Janigro, D. (1999) Impaired K(+) homeostasis and altered electrophysiological properties of post-traumatic hippocampal glia. J Neurosci 19, 8152-62.
53. Dawson, M. R., Polito, A., Levine, J. M. and Reynolds, R. (2003) NG2-expressing glial progenitor cells: an abundant and widespread population of cycling cells in the adult rat CNS. Mol Cell Neurosci 24, 476-88.
54. De Biase, L. M., Nishiyama, A. and Bergles, D. E. (2010) Excitability and synaptic communication within the oligodendrocyte lineage. J Neurosci 30, 3600-11.
55. Deng, P., Pang, Z. P., Zhang, Y. and Xu, Z. C. (2005) Increase of delayed rectifier potassium currents in large aspiny neurons in the neostriatum following transient forebrain ischemia. Neuroscience 131, 135-46.
56. Dijkhuizen, R. M., Knollema, S., van der Worp, H. B., Ter Horst, G. J., De Wildt, D. J., Berkelbach van der Sprenkel, J. W., Tulleken, K. A. and Nicolay, K. (1998) Dynamics of cerebral tissue injury and perfusion after temporary hypoxia-ischemia in the rat: evidence for region-specific sensitivity and delayed damage. Stroke 29, 695-704.
57. Dirnagl, U. (2006) Bench to bedside: the quest for quality in experimental stroke research. J Cereb Blood Flow Metab 26, 1465-78.
58. Dirnagl, U., Iadecola, C. and Moskowitz, M. A. (1999) Pathobiology of ischaemic stroke: an integrated view. Trends Neurosci 22, 391-7.
59. Djukic, B., Casper, K. B., Philpot, B. D., Chin, L. S. and McCarthy, K. D. (2007) Conditional knock-out of Kir4.1 leads to glial membrane depolarization, inhibition of potassium and glutamate uptake, and enhanced short-term synaptic potentiation. J Neurosci 27, 11354-65.
60. Domingues, A. M., Taylor, M. and Fern, R. (2010) Glia as transmitter sources and sensors in health and disease. Neurochem Int
61. Doyle, K. P., Simon, R. P. and Stenzel-Poore, M. P. (2008) Mechanisms of ischemic brain damage. Neuropharmacology 55, 310-8.
62. Edwards, F. A., Konnerth, A., Sakmann, B. and Takahashi, T. (1989) A thin slice preparation for patch clamp recordings from neurones of the mammalian central nervous system. Pflugers Arch 414, 600-12.
63. Edwards, L., Nashmi, R., Jones, O., Backx, P., Ackerley, C., Becker, L. and Fehlings, M. G. (2002) Upregulation of Kv 1.4 protein and gene expression after chronic spinal cord injury. J Comp Neurol 443, 154-67.
64. Eng, L. F., Ghirnikar, R. S. and Lee, Y. L. (2000) Glial fibrillary acidic protein: GFAP-thirty-one years (1969-2000). Neurochem Res 25, 1439-51.

65. Es-Salah-Lamoureux, Z., Steele, D. F. and Fedida, D. (2010) Research into the therapeutic roles of two-pore-domain potassium channels. Trends Pharmacol Sci 31, 587-95.
66. Faulkner, J. R., Herrmann, J. E., Woo, M. J., Tansey, K. E., Doan, N. B. and Sofroniew, M. V. (2004) Reactive astrocytes protect tissue and preserve function after spinal cord injury. J Neurosci 24, 2143-55.
67. Fawcett, J. W. and Asher, R. A. (1999) The glial scar and central nervous system repair. Brain Res Bull 49, 377-91.
68. Ferroni, S., Nobile, M., Caprini, M. and Rapisarda, C. (2000) pH modulation of an inward rectifier chloride current in cultured rat cortical astrocytes. Neuroscience 100, 431-8.
69. Ferroni, S., Valente, P., Caprini, M., Nobile, M., Schubert, P. and Rapisarda, C. (2003) Arachidonic acid activates an open rectifier potassium channel in cultured rat cortical astrocytes. J Neurosci Res 72, 363-72.
70. Feustel, P. J., Jin, Y. and Kimelberg, H. K. (2004) Volume-regulated anion channels are the predominant contributors to release of excitatory amino acids in the ischemic cortical penumbra. Stroke 35, 1164-8.
71. Fiacco, T. A. and McCarthy, K. D. (2006) Astrocyte calcium elevations: properties, propagation, and effects on brain signaling. Glia 54, 676-90.
72. Fidler, P. S., Schuette, K., Asher, R. A., Dobbertin, A., Thornton, S. R., Calle-Patino, Y., Muir, E., Levine, J. M., Geller, H. M., Rogers, J. H., Faissner, A. and Fawcett, J. W. (1999) Comparing astrocytic cell lines that are inhibitory or permissive for axon growth: the major axon-inhibitory proteoglycan is NG2. J Neurosci 19, 8778-88.
73. Frisen, J., Johansson, C. B., Torok, C., Risling, M. and Lendahl, U. (1995) Rapid, widespread, and longlasting induction of nestin contributes to the generation of glial scar tissue after CNS injury. J Cell Biol 131, 453-64.
74. Gadea, A., Schinelli, S. and Gallo, V. (2008) Endothelin-1 regulates astrocyte proliferation and reactive gliosis via a JNK/c-Jun signaling pathway. J Neurosci 28, 2394-408.
75. Gallo, V. and Armstrong, R. C. (1995) Developmental and growth factor-induced regulation of nestin in oligodendrocyte lineage cells. J Neurosci 15, 394-406.
76. Ganat, Y. M., Silbereis, J., Cave, C., Ngu, H., Anderson, G. M., Ohkubo, Y., Ment, L. R. and Vaccarino, F. M. (2006) Early postnatal astroglial cells produce multilineage precursors and neural stem cells *in vivo*. J Neurosci 26, 8609-21.
77. Gao, Q., Lu, J., Huo, Y., Baby, N., Ling, E. A. and Dheen, S. T. (2010) NG2, a member of chondroitin sulfate proteoglycans family mediates the inflammatory response of activated microglia. Neuroscience 165, 386-94.
78. Garnier, P., Ying, W. and Swanson, R. A. (2003) Ischemic preconditioning by caspase cleavage of poly(ADP-ribose) polymerase-1. J Neurosci 23, 7967-73.
79. Ge, W. P., Yang, X. J., Zhang, Z., Wang, H. K., Shen, W., Deng, Q. D. and Duan, S. (2006) Long-term potentiation of neuron-glia synapses mediated by Ca^{2+}-permeable AMPA receptors. Science 312, 1533-7.

80. Ge, W. P., Zhou, W., Luo, Q., Jan, L. Y. and Jan, Y. N. (2009) Dividing glial cells maintain differentiated properties including complex morphology and functional synapses. Proc Natl Acad Sci U S A 106, 328-33.
81. Giffard, R. G. and Swanson, R. A. (2005) Ischemia-induced programmed cell death in astrocytes. Glia 50, 299-306.
82. Gnatenco, C., Han, J., Snyder, A. K. and Kim, D. (2002) Functional expression of TREK-2 K^+ channel in cultured rat brain astrocytes. Brain Res 931, 56-67.
83. Goldstein, S. A., Bockenhauer, D., O'Kelly, I. and Zilberberg, N. (2001) Potassium leak channels and the KCNK family of two-P-domain subunits. Nat Rev Neurosci 2, 175-84.
84. Gordon, G. R., Choi, H. B., Rungta, R. L., Ellis-Davies, G. C. and MacVicar, B. A. (2008) Brain metabolism dictates the polarity of astrocyte control over arterioles. Nature 456, 745-9.
85. Gordon, G. R., Mulligan, S. J. and MacVicar, B. A. (2007) Astrocyte control of the cerebrovasculature. Glia 55, 1214-21.
86. Griffin, S., Clark, J. B. and Canevari, L. (2005) Astrocyte-neurone communication following oxygen-glucose deprivation. J Neurochem 95, 1015-22.
87. Guatteo, E., Stanness, K. A. and Janigro, D. (1996) Hyperpolarization-activated ion currents in cultured rat cortical and spinal cord astrocytes. Glia 16, 196-209.
88. Guo, F., Maeda, Y., Ma, J., Xu, J., Horiuchi, M., Miers, L., Vaccarino, F. and Pleasure, D. (2010) Pyramidal neurons are generated from oligodendroglial progenitor cells in adult piriform cortex. J Neurosci 30, 12036-49.
89. Gutman, G. A., Chandy, K. G., Grissmer, S., Lazdunski, M., McKinnon, D., Pardo, L. A., Robertson, G. A., Rudy, B., Sanguinetti, M. C., Stuhmer, W. and Wang, X. (2005) International Union of Pharmacology. LIII. Nomenclature and molecular relationships of voltage-gated potassium channels. Pharmacol Rev 57, 473-508.
90. Hamill, O. P., Marty, A., Neher, E., Sakmann, B. and Sigworth, F. J. (1981) Improved patch-clamp techniques for high-resolution current recording from cells and cell-free membrane patches. Pflugers Arch 391, 85-100.
91. Hamilton, N. B. and Attwell, D. (2010) Do astrocytes really exocytose neurotransmitters? Nat Rev Neurosci 11, 227-38.
92. Hartman, R. E., Lee, J. M., Zipfel, G. J. and Wozniak, D. F. (2005) Characterizing learning deficits and hippocampal neuron loss following transient global cerebral ischemia in rats. Brain Res 1043, 48-56.
93. Haydon, P. G. (2001) GLIA: listening and talking to the synapse. Nat Rev Neurosci 2, 185-93.
94. Herrero-Herranz, E., Pardo, L. A., Bunt, G., Gold, R., Stuhmer, W. and Linker, R. A. (2007) Re-expression of a developmentally restricted potassium channel in autoimmune demyelination: Kv1.4 is implicated in oligodendroglial proliferation. Am J Pathol 171, 589-98.
95. Herrmann, J. E., Imura, T., Song, B., Qi, J., Ao, Y., Nguyen, T. K., Korsak, R. A., Takeda, K., Akira, S. and Sofroniew, M. V. (2008) STAT3 is a critical regulator of astrogliosis and scar formation after spinal cord injury. J Neurosci 28, 7231-43.

96. Heurteaux, C., Guy, N., Laigle, C., Blondeau, N., Duprat, F., Mazzuca, M., Lang-Lazdunski, L., Widmann, C., Zanzouri, M., Romey, G. and Lazdunski, M. (2004) TREK-1, a K^+ channel involved in neuroprotection and general anesthesia. Embo J 23, 2684-95.
97. Heurteaux, C., Lucas, G., Guy, N., El Yacoubi, M., Thummler, S., Peng, X. D., Noble, F., Blondeau, N., Widmann, C., Borsotto, M., Gobbi, G., Vaugeois, J. M., Debonnel, G. and Lazdunski, M. (2006) Deletion of the background potassium channel TREK-1 results in a depression-resistant phenotype. Nat Neurosci 9, 1134-41.
98. Hibino, H., Fujita, A., Iwai, K., Yamada, M. and Kurachi, Y. (2004) Differential assembly of inwardly rectifying K^+ channel subunits, Kir4.1 and Kir5.1, in brain astrocytes. J Biol Chem 279, 44065-73.
99. Hibino, H., Inanobe, A., Furutani, K., Murakami, S., Findlay, I. and Kurachi, Y. (2010) Inwardly rectifying potassium channels: their structure, function, and physiological roles. Physiol Rev 90, 291-366.
100. Higashimori, H. and Sontheimer, H. (2007) Role of Kir4.1 channels in growth control of glia. Glia 55, 1668-79.
101. Hinterkeuser, S., Schroder, W., Hager, G., Seifert, G., Blumcke, I., Elger, C. E., Schramm, J. and Steinhauser, C. (2000) Astrocytes in the hippocampus of patients with temporal lobe epilepsy display changes in potassium conductances. Eur J Neurosci 12, 2087-96.
102. Honore, E. (2007) The neuronal background K2P channels: focus on TREK1. Nat Rev Neurosci 8, 251-61.
103. Hossmann, K. A. (2008) Cerebral ischemia: models, methods and outcomes. Neuropharmacology 55, 257-70.
104. Houades, V., Koulakoff, A., Ezan, P., Seif, I. and Giaume, C. (2008) Gap junction-mediated astrocytic networks in the mouse barrel cortex. J Neurosci 28, 5207-17.
105. Iandiev, I., Tenckhoff, S., Pannicke, T., Biedermann, B., Hollborn, M., Wiedemann, P., Reichenbach, A. and Bringmann, A. (2006) Differential regulation of Kir4.1 and Kir2.1 expression in the ischemic rat retina. Neurosci Lett 396, 97-101.
106. Inagaki, M., Nakamura, Y., Takeda, M., Nishimura, T. and Inagaki, N. (1994) Glial fibrillary acidic protein: dynamic property and regulation by phosphorylation. Brain Pathol 4, 239-43.
107. Inyushin, M., Kucheryavykh, L. Y., Kucheryavykh, Y. V., Nichols, C. G., Buono, R. J., Ferraro, T. N., Skatchkov, S. N. and Eaton, M. J. (2010) Potassium channel activity and glutamate uptake are impaired in astrocytes of seizure-susceptible DBA/2 mice. Epilepsia 51, 1707-13.
108. Jabs, R., Paterson, I. A. and Walz, W. (1997) Qualitative analysis of membrane currents in glial cells from normal and gliotic tissue *in situ*: down-regulation of Na^+ current and lack of P2 purinergic responses. Neuroscience 81, 847-60.
109. Kaiser, M., Maletzki, I., Hulsmann, S., Holtmann, B., Schulz-Schaeffer, W., Kirchhoff, F., Bahr, M. and Neusch, C. (2006) Progressive loss of a glial potassium channel (KCNJ10) in the spinal cord of the SOD1 (G93A) transgenic mouse model of amyotrophic lateral sclerosis. J Neurochem 99, 900-12.
110. Kang, S. J., Cho, S. H., Park, K., Yi, J., Yoo, S. J. and Shin, K. S. (2008) Expression of Kir2.1 channels in astrocytes under pathophysiological conditions. Mol Cells 25, 124-30.

111. Karadottir, R., Hamilton, N. B., Bakiri, Y. and Attwell, D. (2008) Spiking and nonspiking classes of oligodendrocyte precursor glia in CNS white matter. Nat Neurosci 11, 450-6.
112. Kawamura, S., Yasui, N., Shirasawa, M. and Fukasawa, H. (1991) Rat middle cerebral artery occlusion using an intraluminal thread technique. Acta Neurochir (Wien) 109, 126-32.
113. Keirstead, H. S., Levine, J. M. and Blakemore, W. F. (1998) Response of the oligodendrocyte progenitor cell population (defined by NG2 labelling) to demyelination of the adult spinal cord. Glia 22, 161-70.
114. Kettenmann, H. and Ransom, B. R. (2005) Neuroglia, Second Edition.
115. Kettenmann, H. and Verkhratsky, A. (2008) Neuroglia: the 150 years after. Trends Neurosci 31, 653-9.
116. Kiedrowski, L. (2007) NCX and NCKX operation in ischemic neurons. Ann N Y Acad Sci 1099, 383-95.
117. Kimelberg, H. K. (2004) The problem of astrocyte identity. Neurochem Int 45, 191-202.
118. Kimelberg, H. K. (2005) Astrocytic swelling in cerebral ischemia as a possible cause of injury and target for therapy. Glia 50, 389-97.
119. Kimelberg, H. K. (2007) Supportive or information-processing functions of the mature protoplasmic astrocyte in the mammalian CNS? A critical appraisal. Neuron Glia Biol 3, 181-189.
120. Kimelberg, H. K., Rutledge, E., Goderie, S. and Charniga, C. (1995) Astrocytic swelling due to hypotonic or high K^+ medium causes inhibition of glutamate and aspartate uptake and increases their release. J Cereb Blood Flow Metab 15, 409-16.
121. Kinouchi, R., Takeda, M., Yang, L., Wilhelmsson, U., Lundkvist, A., Pekny, M. and Chen, D. F. (2003) Robust neural integration from retinal transplants in mice deficient in GFAP and vimentin. Nat Neurosci 6, 863-8.
122. Knutson, P., Ghiani, C. A., Zhou, J. M., Gallo, V. and McBain, C. J. (1997) K^+ channel expression and cell proliferation are regulated by intracellular sodium and membrane depolarization in oligodendrocyte progenitor cells. J Neurosci 17, 2669-82.
123. Kofuji, P., Biedermann, B., Siddharthan, V., Raap, M., Iandiev, I., Milenkovic, I., Thomzig, A., Veh, R. W., Bringmann, A. and Reichenbach, A. (2002) Kir potassium channel subunit expression in retinal glial cells: implications for spatial potassium buffering. Glia 39, 292-303.
124. Kofuji, P. and Newman, E. A. (2004) Potassium buffering in the central nervous system. Neuroscience 129, 1045-56.
125. Koller, H., Schroeter, M., Jander, S., Stoll, G. and Siebler, M. (2000) Time course of inwardly rectifying K(+) current reduction in glial cells surrounding ischemic brain lesions. Brain Res 872, 194-8.
126. Kosugi, T. and Kawahara, K. (2006) Reversed actrocytic GLT-1 during ischemia is crucial to excitotoxic death of neurons, but contributes to the survival of astrocytes themselves. Neurochem Res 31, 933-43.
127. Kressin, K., Kuprijanova, E., Jabs, R., Seifert, G. and Steinhauser, C. (1995) Developmental regulation of Na^+ and K^+ conductances in glial cells of mouse hippocampal brain slices. Glia 15, 173-87.

128. Kubo, Y., Adelman, J. P., Clapham, D. E., Jan, L. Y., Karschin, A., Kurachi, Y., Lazdunski, M., Nichols, C. G., Seino, S. and Vandenberg, C. A. (2005) International Union of Pharmacology. LIV. Nomenclature and molecular relationships of inwardly rectifying potassium channels. Pharmacol Rev 57, 509-26.
129. Kucheryavykh, L. Y., Kucheryavykh, Y. V., Inyushin, M., Shuba, Y. M., Sanabria, P., Cubano, L. A., Skatchkov, S. N. and Eaton, M. J. (2009) Ischemia Increases TREK-2 Channel Expression in Astrocytes: Relevance to Glutamate Clearance. Open Neurosci J 3, 40-47.
130. Kucheryavykh, Y. V., Kucheryavykh, L. Y., Nichols, C. G., Maldonado, H. M., Baksi, K., Reichenbach, A., Skatchkov, S. N. and Eaton, M. J. (2007) Downregulation of Kir4.1 inward rectifying potassium channel subunits by RNAi impairs potassium transfer and glutamate uptake by cultured cortical astrocytes. Glia 55, 274-81.
131. Kuffler, S. W., Nicholls, J. G. and Orkand, R. K. (1966) Physiological properties of glial cells in the central nervous system of amphibia. J Neurophysiol 29, 768-87.
132. Kukley, M., Nishiyama, A. and Dietrich, D. (2010) The fate of synaptic input to NG2 glial cells: neurons specifically downregulate transmitter release onto differentiating oligodendroglial cells. J Neurosci 30, 8320-31.
133. Larsson, A., Wilhelmsson, U., Pekna, M. and Pekny, M. (2004) Increased cell proliferation and neurogenesis in the hippocampal dentate gyrus of old GFAP(-/-)Vim(-/-) mice. Neurochem Res 29, 2069-73.
134. Lascola, C. D. and Kraig, R. P. (1996) Whole-cell chloride currents in rat astrocytes accompany changes in cell morphology. J Neurosci 16, 2532-45.
135. Lee, Y. B., Du, S., Rhim, H., Lee, E. B., Markelonis, G. J. and Oh, T. H. (2000) Rapid increase in immunoreactivity to GFAP in astrocytes *in vitro* induced by acidic pH is mediated by calcium influx and calpain I. Brain Res 864, 220-9.
136. Levine, J. M. (1994) Increased expression of the NG2 chondroitin-sulfate proteoglycan after brain injury. J Neurosci 14, 4716-30.
137. Li, S., Mealing, G. A., Morley, P. and Stys, P. K. (1999) Novel injury mechanism in anoxia and trauma of spinal cord white matter: glutamate release via reverse Na^+-dependent glutamate transport. J Neurosci 19, RC16.
138. Lichter-Konecki, U., Mangin, J. M., Gordish-Dressman, H., Hoffman, E. P. and Gallo, V. (2008) Gene expression profiling of astrocytes from hyperammonemic mice reveals altered pathways for water and potassium homeostasis *in vivo*. Glia 56, 365-77.
139. Lin, S. C. and Bergles, D. E. (2002) Physiological characteristics of NG2-expressing glial cells. J Neurocytol 31, 537-49.
140. Lin, S. C. and Bergles, D. E. (2004) Synaptic signaling between GABAergic interneurons and oligodendrocyte precursor cells in the hippocampus. Nat Neurosci 7, 24-32.
141. Lin, S. C., Huck, J. H., Roberts, J. D., Macklin, W. B., Somogyi, P. and Bergles, D. E. (2005) Climbing fiber innervation of NG2-expressing glia in the mammalian cerebellum. Neuron 46, 773-85.
142. Lipton, P. (1999) Ischemic cell death in brain neurons. Physiol Rev 79, 1431-568.

143. Liu, B., Chen, H., Johns, T. G. and Neufeld, A. H. (2006) Epidermal growth factor receptor activation: an upstream signal for transition of quiescent astrocytes into reactive astrocytes after neural injury. J Neurosci 26, 7532-40.
144. Lo, E. H., Dalkara, T. and Moskowitz, M. A. (2003) Mechanisms, challenges and opportunities in stroke. Nat Rev Neurosci 4, 399-415.
145. Lukaszevicz, A. C., Sampaio, N., Guegan, C., Benchoua, A., Couriaud, C., Chevalier, E., Sola, B., Lacombe, P. and Onteniente, B. (2002) High sensitivity of protoplasmic cortical astroglia to focal ischemia. J Cereb Blood Flow Metab 22, 289-98.
146. Lytle, J. M., Chittajallu, R., Wrathall, J. R. and Gallo, V. (2009) NG2 cell response in the CNP-EGFP mouse after contusive spinal cord injury. Glia 57, 270-85.
147. Lytle, J. M., Vicini, S. and Wrathall, J. R. (2006) Phenotypic changes in $NG2^+$ cells after spinal cord injury. J Neurotrauma 23, 1726-38.
148. Lytle, J. M. and Wrathall, J. R. (2007) Glial cell loss, proliferation and replacement in the contused murine spinal cord. Eur J Neurosci 25, 1711-24.
149. MacFarlane, M. and Williams, A. C. (2004) Apoptosis and disease: a life or death decision. EMBO Rep 5, 674-8.
150. MacFarlane, S. N. and Sontheimer, H. (1997) Electrophysiological changes that accompany reactive gliosis *in vitro*. J Neurosci 17, 7316-29.
151. MacFarlane, S. N. and Sontheimer, H. (1998) Spinal cord astrocytes display a switch from TTX-sensitive to TTX-resistant sodium currents after injury-induced gliosis *in vitro*. J Neurophysiol 79, 2222-6.
152. MacFarlane, S. N. and Sontheimer, H. (2000) Changes in ion channel expression accompany cell cycle progression of spinal cord astrocytes. Glia 30, 39-48.
153. Magnus, T., Carmen, J., Deleon, J., Xue, H., Pardo, A. C., Lepore, A. C., Mattson, M. P., Rao, M. S. and Maragakis, N. J. (2008) Adult glial precursor proliferation in mutant SOD1G93A mice. Glia 56, 200-8.
154. Makara, J. K., Rappert, A., Matthias, K., Steinhauser, C., Spat, A. and Kettenmann, H. (2003) Astrocytes from mouse brain slices express ClC-2-mediated Cl- currents regulated during development and after injury. Mol Cell Neurosci 23, 521-30.
155. Matthias, K., Kirchhoff, F., Seifert, G., Huttmann, K., Matyash, M., Kettenmann, H. and Steinhauser, C. (2003) Segregated expression of AMPA-type glutamate receptors and glutamate transporters defines distinct astrocyte populations in the mouse hippocampus. J Neurosci 23, 1750-8.
156. McKhann, G. M., 2nd, D'Ambrosio, R. and Janigro, D. (1997) Heterogeneity of astrocyte resting membrane potentials and intercellular coupling revealed by whole-cell and gramicidin-perforated patch recordings from cultured neocortical and hippocampal slice astrocytes. J Neurosci 17, 6850-63.
157. McLaughlin, B., Hartnett, K. A., Erhardt, J. A., Legos, J. J., White, R. F., Barone, F. C. and Aizenman, E. (2003) Caspase 3 activation is essential for neuroprotection in preconditioning. Proc Natl Acad Sci U S A 100, 715-20.
158. McTigue, D. M. and Tripathi, R. B. (2008) The life, death, and replacement of oligodendrocytes in the adult CNS. J Neurochem 107, 1-19.

159. Meeks, J. P. and Mennerick, S. (2007) Astrocyte membrane responses and potassium accumulation during neuronal activity. Hippocampus 17, 1100-8.
160. Mishima, T. and Hirase, H. (2010) *In vivo* intracellular recording suggests that gray matter astrocytes in mature cerebral cortex and hippocampus are electrophysiologically homogeneous. J Neurosci 30, 3093-100.
161. Miyake, T., Hattori, T., Fukuda, M., Kitamura, T. and Fujita, S. (1988) Quantitative studies on proliferative changes of reactive astrocytes in mouse cerebral cortex. Brain Res 451, 133-8.
162. Mulligan, S. J. and MacVicar, B. A. (2004) Calcium transients in astrocyte endfeet cause cerebrovascular constrictions. Nature 431, 195-9.
163. Nagelhus, E. A., Mathiisen, T. M. and Ottersen, O. P. (2004) Aquaporin-4 in the central nervous system: cellular and subcellular distribution and coexpression with KIR4.1. Neuroscience 129, 905-13.
164. Nakka, V. P., Gusain, A., Mehta, S. L. and Raghubir, R. (2008) Molecular mechanisms of apoptosis in cerebral ischemia: multiple neuroprotective opportunities. Mol Neurobiol 37, 7-38.
165. Nedergaard, M. and Dirnagl, U. (2005) Role of glial cells in cerebral ischemia. Glia 50, 281-6.
166. Neusch, C., Papadopoulos, N., Muller, M., Maletzki, I., Winter, S. M., Hirrlinger, J., Handschuh, M., Bahr, M., Richter, D. W., Kirchhoff, F. and Hulsmann, S. (2006) Lack of the Kir4.1 channel subunit abolishes K^+ buffering properties of astrocytes in the ventral respiratory group: impact on extracellular K^+ regulation. J Neurophysiol 95, 1843-52.
167. Neusch, C., Rozengurt, N., Jacobs, R. E., Lester, H. A. and Kofuji, P. (2001) Kir4.1 potassium channel subunit is crucial for oligodendrocyte development and *in vivo* myelination. J Neurosci 21, 5429-38.
168. Nielsen, H. H., Ladeby, R., Drojdahl, N., Peterson, A. C. and Finsen, B. (2006) Axonal degeneration stimulates the formation of $NG2^+$ cells and oligodendrocytes in the mouse. Glia 54, 105-15.
169. Nishiyama, A., Komitova, M., Suzuki, R. and Zhu, X. (2009) Polydendrocytes (NG2 cells): multifunctional cells with lineage plasticity. Nat Rev Neurosci 10, 9-22.
170. Nishiyama, A., Watanabe, M., Yang, Z. and Bu, J. (2002) Identity, distribution, and development of polydendrocytes: NG2-expressing glial cells. J Neurocytol 31, 437-55.
171. Nishiyama, A., Yu, M., Drazba, J. A. and Tuohy, V. K. (1997) Normal and reactive $NG2^+$ glial cells are distinct from resting and activated microglia. J Neurosci Res 48, 299-312.
172. Nolte, C., Matyash, M., Pivneva, T., Schipke, C. G., Ohlemeyer, C., Hanisch, U. K., Kirchhoff, F. and Kettenmann, H. (2001) GFAP promoter-controlled EGFP-expressing transgenic mice: a tool to visualize astrocytes and astrogliosis in living brain tissue. Glia 33, 72-86.
173. Noyan-Ashraf, M. H., Brandizzi, F. and Juurlink, B. H. (2005) Constitutive nuclear localization of activated caspase 3 in subpopulations of the astroglial family of cells. Glia 49, 588-93.
174. Oberheim, N. A., Takano, T., Han, X., He, W., Lin, J. H., Wang, F., Xu, Q., Wyatt, J. D., Pilcher, W., Ojemann, J. G., Ransom, B. R., Goldman, S. A. and Nedergaard, M. (2009) Uniquely hominid features of adult human astrocytes. J Neurosci 29, 3276-87.
175. Oberheim, N. A., Wang, X., Goldman, S. and Nedergaard, M. (2006) Astrocytic complexity distinguishes the human brain. Trends Neurosci 29, 547-53.

176. Ogata, K. and Kosaka, T. (2002) Structural and quantitative analysis of astrocytes in the mouse hippocampus. Neuroscience 113, 221-33.
177. Olsen, M. L., Campbell, S. C., McFerrin, M. B., Floyd, C. L. and Sontheimer, H. (2010) Spinal cord injury causes a wide-spread, persistent loss of Kir4.1 and glutamate transporter 1: benefit of 17 beta-oestradiol treatment. Brain 133, 1013-25.
178. Ordy, J. M., Wengenack, T. M., Bialobok, P., Coleman, P. D., Rodier, P., Baggs, R. B., Dunlap, W. P. and Kates, B. (1993) Selective vulnerability and early progression of hippocampal CA1 pyramidal cell degeneration and GFAP-positive astrocyte reactivity in the rat four-vessel occlusion model of transient global ischemia. Exp Neurol 119, 128-39.
179. Orkand, R. K. (1986) Glial-interstitial fluid exchange. Ann N Y Acad Sci 481, 269-72.
180. Orkand, R. K., Nicholls, J. G. and Kuffler, S. W. (1966) Effect of nerve impulses on the membrane potential of glial cells in the central nervous system of amphibia. J Neurophysiol 29, 788-806.
181. Ouyang, Y. B., Voloboueva, L. A., Xu, L. J. and Giffard, R. G. (2007) Selective dysfunction of hippocampal CA1 astrocytes contributes to delayed neuronal damage after transient forebrain ischemia. J Neurosci 27, 4253-60.
182. Panickar, K. S. and Norenberg, M. D. (2005) Astrocytes in cerebral ischemic injury: morphological and general considerations. Glia 50, 287-98.
183. Pannicke, T., Faude, F., Reichenbach, A. and Reichelt, W. (2000) A function of delayed rectifier potassium channels in glial cells: maintenance of an auxiliary membrane potential under pathological conditions. Brain Res 862, 187-93.
184. Pannicke, T., Uckermann, O., Iandiev, I., Biedermann, B., Wiedemann, P., Perlman, I., Reichenbach, A. and Bringmann, A. (2005) Altered membrane physiology in Muller glial cells after transient ischemia of the rat retina. Glia 50, 1-11.
185. Pardo, L. A. (2004) Voltage-gated potassium channels in cell proliferation. Physiology (Bethesda) 19, 285-92.
186. Pasler, D., Gabriel, S. and Heinemann, U. (2007) Two-pore-domain potassium channels contribute to neuronal potassium release and glial potassium buffering in the rat hippocampus. Brain Res 1173, 14-26.
187. Pastor, A., Chvatal, A., Sykova, E. and Kettenmann, H. (1995) Glycine- and GABA-activated currents in identified glial cells of the developing rat spinal cord slice. Eur J Neurosci 7, 1188-98.
188. Patel, A. J. and Honore, E. (2001) Properties and modulation of mammalian 2P domain K^+ channels. Trends Neurosci 24, 339-46.
189. Patel, A. J. and Lazdunski, M. (2004) The 2P-domain K^+ channels: role in apoptosis and tumorigenesis. Pflugers Arch 448, 261-73.
190. Pekny, M., Eliasson, C., Siushansian, R., Ding, M., Dixon, S. J., Pekna, M., Wilson, J. X. and Hamberger, A. (1999) The impact of genetic removal of GFAP and/or vimentin on glutamine levels and transport of glucose and ascorbate in astrocytes. Neurochem Res 24, 1357-62.
191. Pekny, M. and Nilsson, M. (2005) Astrocyte activation and reactive gliosis. Glia 50, 427-34.
192. Pellerin, L. (2003) Lactate as a pivotal element in neuron-glia metabolic cooperation. Neurochem Int 43, 331-8.

193. Pellerin, L., Bouzier-Sore, A. K., Aubert, A., Serres, S., Merle, M., Costalat, R. and Magistretti, P. J. (2007) Activity-dependent regulation of energy metabolism by astrocytes: an update. Glia 55, 1251-62.
194. Perez-Pinzon, M. A., Tao, L. and Nicholson, C. (1995) Extracellular potassium, volume fraction, and tortuosity in rat hippocampal CA1, CA3, and cortical slices during ischemia. J Neurophysiol 74, 565-73.
195. Perillan, P. R., Li, X., Potts, E. A., Chen, M., Bredt, D. S. and Simard, J. M. (2000) Inward rectifier K(+) channel Kir2.3 (IRK3) in reactive astrocytes from adult rat brain. Glia 31, 181-92.
196. Perillan, P. R., Li, X. and Simard, J. M. (1999) K(+) inward rectifier currents in reactive astrocytes from adult rat brain. Glia 27, 213-25.
197. Petito, C. K., Feldmann, E., Pulsinelli, W. A. and Plum, F. (1987) Delayed hippocampal damage in humans following cardiorespiratory arrest. Neurology 37, 1281-6.
198. Petito, C. K. and Halaby, I. A. (1993) Relationship between ischemia and ischemic neuronal necrosis to astrocyte expression of glial fibrillary acidic protein. Int J Dev Neurosci 11, 239-47.
199. Pforte, C., Henrich-Noack, P., Baldauf, K. and Reymann, K. G. (2005) Increase in proliferation and gliogenesis but decrease of early neurogenesis in the rat forebrain shortly after transient global ischemia. Neuroscience 136, 1133-46.
200. Poopalasundaram, S., Knott, C., Shamotienko, O. G., Foran, P. G., Dolly, J. O., Ghiani, C. A., Gallo, V. and Wilkin, G. P. (2000) Glial heterogeneity in expression of the inwardly rectifying K(+) channel, Kir4.1, in adult rat CNS. Glia 30, 362-72.
201. Qiu, J., Cai, D. and Filbin, M. T. (2000) Glial inhibition of nerve regeneration in the mature mammalian CNS. Glia 29, 166-74.
202. Rabchevsky, A. G., Sullivan, P. G. and Scheff, S. W. (2007) Temporal-spatial dynamics in oligodendrocyte and glial progenitor cell numbers throughout ventrolateral white matter following contusion spinal cord injury. Glia 55, 831-43.
203. Rami, A., Langhagen, A. and Steiger, S. (2008) Focal cerebral ischemia induces upregulation of Beclin 1 and autophagy-like cell death. Neurobiol Dis 29, 132-41.
204. Raponi, E., Agenes, F., Delphin, C., Assard, N., Baudier, J., Legraverend, C. and Deloulme, J. C. (2007) S100B expression defines a state in which GFAP-expressing cells lose their neural stem cell potential and acquire a more mature developmental stage. Glia 55, 165-77.
205. Raps, S. P., Lai, J. C., Hertz, L. and Cooper, A. J. (1989) Glutathione is present in high concentrations in cultured astrocytes but not in cultured neurons. Brain Res 493, 398-401.
206. Reynolds, R., Dawson, M., Papadopoulos, D., Polito, A., Di Bello, I. C., Pham-Dinh, D. and Levine, J. (2002) The response of NG2-expressing oligodendrocyte progenitors to demyelination in MOG-EAE and MS. J Neurocytol 31, 523-36.
207. Ridet, J. L., Malhotra, S. K., Privat, A. and Gage, F. H. (1997) Reactive astrocytes: cellular and molecular cues to biological function. Trends Neurosci 20, 570-7.
208. Rivers, L. E., Young, K. M., Rizzi, M., Jamen, F., Psachoulia, K., Wade, A., Kessaris, N. and Richardson, W. D. (2008) PDGFRA/NG2 glia generate myelinating oligodendrocytes and piriform projection neurons in adult mice. Nat Neurosci 11, 1392-401.

209. Roitbak, T. and Sykova, E. (1999) Diffusion barriers evoked in the rat cortex by reactive astrogliosis. Glia 28, 40-8.
210. Rose, C. R., Waxman, S. G. and Ransom, B. R. (1998) Effects of glucose deprivation, chemical hypoxia, and simulated ischemia on Na^+ homeostasis in rat spinal cord astrocytes. J Neurosci 18, 3554-62.
211. Rouach, N., Koulakoff, A., Abudara, V., Willecke, K. and Giaume, C. (2008) Astroglial metabolic networks sustain hippocampal synaptic transmission. Science 322, 1551-5.
212. Roy, M. L., Saal, D., Perney, T., Sontheimer, H., Waxman, S. G. and Kaczmarek, L. K. (1996) Manipulation of the delayed rectifier Kv1.5 potassium channel in glial cells by antisense oligodeoxynucleotides. Glia 18, 177-84.
213. Schiffer, D., Giordana, M. T., Cavalla, P., Vigliani, M. C. and Attanasio, A. (1993) Immunohistochemistry of glial reaction after injury in the rat: double stainings and markers of cell proliferation. Int J Dev Neurosci 11, 269-80.
214. Schmidt-Kastner, R., Szymas, J. and Hossmann, K. A. (1990) Immunohistochemical study of glial reaction and serum-protein extravasation in relation to neuronal damage in rat hippocampus after ischemia. Neuroscience 38, 527-40.
215. Schools, G. P., Zhou, M. and Kimelberg, H. K. (2006) Development of gap junctions in hippocampal astrocytes: evidence that whole cell electrophysiological phenotype is an intrinsic property of the individual cell. J Neurophysiol 96, 1383-92.
216. Schroder, W., Hager, G., Kouprijanova, E., Weber, M., Schmitt, A. B., Seifert, G. and Steinhauser, C. (1999) Lesion-induced changes of electrophysiological properties in astrocytes of the rat dentate gyrus. Glia 28, 166-74.
217. Schroder, W., Seifert, G., Huttmann, K., Hinterkeuser, S. and Steinhauser, C. (2002) AMPA receptor-mediated modulation of inward rectifier K^+ channels in astrocytes of mouse hippocampus. Mol Cell Neurosci 19, 447-58.
218. Schwerk, C. and Schulze-Osthoff, K. (2003) Non-apoptotic functions of caspases in cellular proliferation and differentiation. Biochem Pharmacol 66, 1453-8.
219. Seifert, G., Huttmann, K., Binder, D. K., Hartmann, C., Wyczynski, A., Neusch, C. and Steinhauser, C. (2009) Analysis of astroglial K^+ channel expression in the developing hippocampus reveals a predominant role of the Kir4.1 subunit. J Neurosci 29, 7474-88.
220. Sherwood, C. C., Stimpson, C. D., Raghanti, M. A., Wildman, D. E., Uddin, M., Grossman, L. I., Goodman, M., Redmond, J. C., Bonar, C. J., Erwin, J. M. and Hof, P. R. (2006) Evolution of increased glia-neuron ratios in the human frontal cortex. Proc Natl Acad Sci U S A 103, 13606-11.
221. Silver, J. and Miller, J. H. (2004) Regeneration beyond the glial scar. Nat Rev Neurosci 5, 146-56.
222. Simard, J. M., Chen, M., Tarasov, K. V., Bhatta, S., Ivanova, S., Melnitchenko, L., Tsymbalyuk, N., West, G. A. and Gerzanich, V. (2006) Newly expressed SUR1-regulated NC(Ca-ATP) channel mediates cerebral edema after ischemic stroke. Nat Med 12, 433-40.
223. Skatchkov, S. N., Eaton, M. J., Shuba, Y. M., Kucheryavykh, Y. V., Derst, C., Veh, R. W., Wurm, A., Iandiev, I., Pannicke, T., Bringmann, A. and Reichenbach, A. (2006) Tandem-pore domain potassium channels are functionally expressed in retinal (Muller) glial cells. Glia 53, 266-76.

224. Sofroniew, M. V. (2005) Reactive astrocytes in neural repair and protection. Neuroscientist 11, 400-7.
225. Sontheimer, H. (1994) Voltage-dependent ion channels in glial cells. Glia 11, 156-72.
226. Stallcup, W. B. (1981) The NG2 antigen, a putative lineage marker: immunofluorescent localization in primary cultures of rat brain. Dev Biol 83, 154-65.
227. Steinhauser, C., Berger, T., Frotscher, M. and Kettenmann, H. (1992) Heterogeneity in the Membrane Current Pattern of Identified Glial Cells in the Hippocampal Slice. Eur J Neurosci 4, 472-484.
228. Steinhauser, C., Kressin, K., Kuprijanova, E., Weber, M. and Seifert, G. (1994) Properties of voltage-activated Na^+ and K^+ currents in mouse hippocampal glial cells *in situ* and after acute isolation from tissue slices. Pflugers Arch 428, 610-20.
229. Stewart, T. H., Eastman, C. L., Groblewski, P. A., Fender, J. S., Verley, D. R., Cook, D. G. and D'Ambrosio, R. (2010) Chronic dysfunction of astrocytic inwardly rectifying K^+ channels specific to the neocortical epileptic focus after fluid percussion injury in the rat. J Neurophysiol 104, 3345-60.
230. Sykova, E., Jendelova, P., Simonova, Z. and Chvatal, A. (1992) K^+ and pH homeostasis in the developing rat spinal cord is impaired by early postnatal X-irradiation. Brain Res 594, 19-30.
231. Sykova, E., Vargova, L., Prokopova, S. and Simonova, Z. (1999) Glial swelling and astrogliosis produce diffusion barriers in the rat spinal cord. Glia 25, 56-70.
232. Tanemoto, M., Kittaka, N., Inanobe, A. and Kurachi, Y. (2000) *In vivo* formation of a proton-sensitive K^+ channel by heteromeric subunit assembly of Kir5.1 with Kir4.1. J Physiol 525 Pt 3, 587-92.
233. Tang, X., Taniguchi, K. and Kofuji, P. (2009) Heterogeneity of Kir4.1 channel expression in glia revealed by mouse transgenesis. Glia 57, 1706-15.
234. Taylor, A. L. and Hewett, S. J. (2002) Potassium-evoked glutamate release liberates arachidonic acid from cortical neurons. J Biol Chem 277, 43881-7.
235. Theis, M., Sohl, G., Eiberger, J. and Willecke, K. (2005) Emerging complexities in identity and function of glial connexins. Trends Neurosci 28, 188-95.
236. Thomas, D., Plant, L. D., Wilkens, C. M., McCrossan, Z. A. and Goldstein, S. A. (2008) Alternative translation initiation in rat brain yields K2P2.1 potassium channels permeable to sodium. Neuron 58, 859-70.
237. Trendelenburg, G. and Dirnagl, U. (2005) Neuroprotective role of astrocytes in cerebral ischemia: focus on ischemic preconditioning. Glia 50, 307-20.
238. Trimarchi, J. R., Liu, L., Smith, P. J. and Keefe, D. L. (2002) Apoptosis recruits two-pore domain potassium channels used for homeostatic volume regulation. Am J Physiol Cell Physiol 282, C588-94.
239. Tripathi, R. and McTigue, D. M. (2007) Prominent oligodendrocyte genesis along the border of spinal contusion lesions. Glia 55, 698-711.
240. Tripathi, R. B., Rivers, L. E., Young, K. M., Jamen, F. and Richardson, W. D. (2010) NG2 glia generate new oligodendrocytes but few astrocytes in a murine experimental autoimmune encephalomyelitis model of demyelinating disease. J Neurosci 30, 16383-90.

241. Tse, F. W., Fraser, D. D., Duffy, S. and MacVicar, B. A. (1992) Voltage-activated K^+ currents in acutely isolated hippocampal astrocytes. J Neurosci 12, 1781-8.
242. Ulbricht, E., Pannicke, T., Hollborn, M., Raap, M., Goczalik, I., Iandiev, I., Hartig, W., Uhlmann, S., Wiedemann, P., Reichenbach, A., Bringmann, A. and Francke, M. (2008) Proliferative gliosis causes mislocation and inactivation of inwardly rectifying K(+) (Kir) channels in rabbit retinal glial cells. Exp Eye Res 86, 305-13.
243. Ullian, E. M., Christopherson, K. S. and Barres, B. A. (2004) Role for glia in synaptogenesis. Glia 47, 209-16.
244. Vargova, L., Chvatal, A., Anderova, M., Kubinova, S., Ziak, D. and Sykova, E. (2001) Effect of osmotic stress on potassium accumulation around glial cells and extracellular space volume in rat spinal cord slices. J Neurosci Res 65, 129-38.
245. Vautier, F., Belachew, S., Chittajallu, R. and Gallo, V. (2004) Shaker-type potassium channel subunits differentially control oligodendrocyte progenitor proliferation. Glia 48, 337-45.
246. Verkhratsky, A. (2006) Patching the glia reveals the functional organisation of the brain. Pflugers Arch 453, 411-20.
247. Verkhratsky, A. and Butt, A. M. (2007) Glial Neurobiology, A Textbook.
248. Verkhratsky, A. and Steinhauser, C. (2000) Ion channels in glial cells. Brain Res Brain Res Rev 32, 380-412.
249. Vignali, M., Benfenati, V., Caprini, M., Anderova, M., Nobile, M. and Ferroni, S. (2009) The endocannabinoid anandamide inhibits potassium conductance in rat cortical astrocytes. Glia 57, 791-806.
250. Wallraff, A., Kohling, R., Heinemann, U., Theis, M., Willecke, K. and Steinhauser, C. (2006) The impact of astrocytic gap junctional coupling on potassium buffering in the hippocampus. J Neurosci 26, 5438-47.
251. Wallraff, A., Odermatt, B., Willecke, K. and Steinhauser, C. (2004) Distinct types of astroglial cells in the hippocampus differ in gap junction coupling. Glia 48, 36-43.
252. Walz, W. (2000) Controversy surrounding the existence of discrete functional classes of astrocytes in adult gray matter. Glia 31, 95-103.
253. Wang, D. D. and Bordey, A. (2008) The astrocyte odyssey. Prog Neurobiol 86, 342-67.
254. Wang, L. P., Cheung, G., Kronenberg, G., Gertz, K., Ji, S., Kempermann, G., Endres, M. and Kettenmann, H. (2008) Mild brain ischemia induces unique physiological properties in striatal astrocytes. Glia 56, 925-34.
255. Wei, L., Yu, S. P., Gottron, F., Snider, B. J., Zipfel, G. J. and Choi, D. W. (2003) Potassium channel blockers attenuate hypoxia- and ischemia-induced neuronal death *in vitro* and *in vivo*. Stroke 34, 1281-6.
256. White, B. C., Sullivan, J. M., DeGracia, D. J., O'Neil, B. J., Neumar, R. W., Grossman, L. I., Rafols, J. A. and Krause, G. S. (2000) Brain ischemia and reperfusion: molecular mechanisms of neuronal injury. J Neurol Sci 179, 1-33.
257. Wilhelmsson, U., Bushong, E. A., Price, D. L., Smarr, B. L., Phung, V., Terada, M., Ellisman, M. H. and Pekny, M. (2006) Redefining the concept of reactive astrocytes as cells that remain within their unique domains upon reaction to injury. Proc Natl Acad Sci U S A 103, 17513-8.

258. Wilhelmsson, U., Li, L., Pekna, M., Berthold, C. H., Blom, S., Eliasson, C., Renner, O., Bushong, E., Ellisman, M., Morgan, T. E. and Pekny, M. (2004) Absence of glial fibrillary acidic protein and vimentin prevents hypertrophy of astrocytic processes and improves post-traumatic regeneration. J Neurosci 24, 5016-21.
259. Yang, Z., Suzuki, R., Daniels, S. B., Brunquell, C. B., Sala, C. J. and Nishiyama, A. (2006) NG2 glial cells provide a favorable substrate for growing axons. J Neurosci 26, 3829-39.
260. Yellen, G. (2002) The voltage-gated potassium channels and their relatives. Nature 419, 35-42.
261. Yu, A. C., Wong, H. K., Yung, H. W. and Lau, L. T. (2001) Ischemia-induced apoptosis in primary cultures of astrocytes. Glia 35, 121-30.
262. Yu, S. P. (2003) Regulation and critical role of potassium homeostasis in apoptosis. Prog Neurobiol 70, 363-86.
263. Zhao, J. W., Raha-Chowdhury, R., Fawcett, J. W. and Watts, C. (2009) Astrocytes and oligodendrocytes can be generated from $NG2^{+}$ progenitors after acute brain injury: intracellular localization of oligodendrocyte transcription factor 2 is associated with their fate choice. Eur J Neurosci 29, 1853-69.
264. Zhao, Y. M., Sun, L. N., Zhou, H. Y. and Wang, X. L. (2006) Voltage-dependent potassium channels are involved in glutamate-induced apoptosis of rat hippocampal neurons. Neurosci Lett 398, 22-7.
265. Zhou, M. and Kimelberg, H. K. (2000) Freshly isolated astrocytes from rat hippocampus show two distinct current patterns and different [K(+)](o) uptake capabilities. J Neurophysiol 84, 2746-57.
266. Zhou, M., Schools, G. P. and Kimelberg, H. K. (2006) Development of GLAST(+) astrocytes and NG2(+) glia in rat hippocampus CA1: mature astrocytes are electrophysiologically passive. J Neurophysiol 95, 134-43.
267. Zhou, M., Xu, G., Xie, M., Zhang, X., Schools, G. P., Ma, L., Kimelberg, H. K. and Chen, H. (2009) TWIK-1 and TREK-1 are potassium channels contributing significantly to astrocyte passive conductance in rat hippocampal slices. J Neurosci 29, 8551-64.
268. Zhu, X., Bergles, D. E. and Nishiyama, A. (2008) NG2 cells generate both oligodendrocytes and gray matter astrocytes. Development 135, 145-57.
269. Zoremba, N., Homola, A., Slais, K., Vorisek, I., Rossaint, R., Lehmenkuhler, A. and Sykova, E. (2008) Extracellular diffusion parameters in the rat somatosensory cortex during recovery from transient global ischemia/hypoxia. J Cereb Blood Flow Metab 28, 1665-73.

8. ATTACHMENTS

1. **Pivonkova H.**, Benesova J., Butenko O., Chvatal A. and Anderova M. (2010) Impact of Global Cerebral Ischemia on K^+ Channel Expression and Membrane Properties of Glial Cells in the Rat Hippocampus. *Neurochemistry International. Dec;57(7):783-94*, IF 3.54
2. **Neprasova H.**, Anderova M., Petrik D., Vargova L., Kubinova S., Chvatal A. and Sykova E. (2007) High extracellular K^+ evokes changes in voltage-dependent K^+ and Na^+ currents and volume regulation in astrocytes. *Pflugers Archiv – European Journal of Physiology. Mar;453(6):839-49*, IF 3.84
3. Anderova M., Vorisek I., **Pivonkova H.**, Benesova J.,Vargova L., Cicanic M., Chvatal A. and Sykova E. (2010) Cell death/proliferation and alterations in glial morphology contribute to changes in diffusivity in the rat hippocampus after hypoxia-ischemia. *Journal of Cerebral Blood Flow and Metabolism. Mar;31(3):894-907*, IF 5.46
4. Chvatal A., Anderova M., **Neprasova H.**, Prajerova I., Benesova J., Butenko O., Verkhratsky A (2008) Pathological Potential of Astroglia. *Physiol Res. 57 Suppl 3:S101-S110*, IF 1.65
5. Chvatal A., Anderova M., Hock M., Prajerova I., **Neprasova H.**, Chvatal V., Kirchhoff F. and Sykova E. (2007) Three-Dimensional Confocal Morphometry Reveals Structural Changes in Astrocyte Morphology *In Situ*. *J Neurosci Res. Feb 1;85(2):260-71*, IF 3.27
6. Anderova M., Kubinova S., Jelitai M., **Neprasova H.**, Glogarova K., Prajerova I., Urdzikova L., Chvatal A. and Sykova E. (2006) Transplantation of embryonic neuroectodermal progenitor cells into the site of a photochemical lesion: immunohistochemical and electrophysiological analysis. *J Neurobiol. Sep 1;66(10):1084-100*, IF 4.2
7. Anderova M., Antonova T., Petrik D., **Neprasova H.**, Chvatal A. and Sykova E. (2004) Voltage-dependent potassium currents in hypertrophied rat astrocytes after a cortical stab wound, *Glia. 48:311-326*, IF 4.7